AN ABSTRACT OF THE THESIS OF

AHMED SARHAN MOHAMMED for the degree of *Doctor of Philosophy* in *Electrical and Computer Engineering* presented on *Dec. 2, 1987.*

Title : *ANALYSIS AND MODELING OF ELECTRICALLY LONG MESFET AND COUPLED SCHOTTKY LINES*

Redacted for Privacy

Abstract approved : _____
Prof. Vijai K. Tripathi

The properties of linear active coupled lines consisting of electrically long GaAs MESFET structures are investigated for possible applications as traveling-wave broad-band amplifiers. In addition, the nonlinear coupled Schottky lines are studied for applications as voltage tunable circuit elements.

The analysis of the general active asymmetric coupled transmission lines in an inhomogeneous medium is presented. The scattering parameters of a four-port network based on the general normal mode analysis of coupled lines are derived in terms of the equivalent circuit elements associated with the long MESFET structure. These are then used to study the properties of the four-port device for applications as traveling-wave amplifiers.

One of the objectives of this study is to model the device by calculating the electrical parameters of the structure from its physical (geometrical and material) parameters. An accurate computer program based on up to date theoretical formulas and experimental results for calculating these circuit elements is developed. A method

based on the conformal mapping is developed to calculate the exact values of interelectrode capacitances for the two and three asymmetric coplanar strips. Empirical closed-form expressions are also obtained for these capacitances by using simple curve fitting procedures.

In order to help optimize the performance of the device in terms of its gain and bandwidth, a CAD program "TOUCHSTONE" is used. Various techniques to compensate for the difference in the capacitive and inductive loading of the gate and drain lines and to synchronize the phase velocity of the waves on both lines are investigated. It is found that a distributed inductance has to be added to the drain line to equalize the velocities and optimize the device's performance, i.e., the gain-bandwidth product. The termination impedances are also optimized. Typical devices with the optimized termination impedances and synchronized phase velocities give more than 3 dB power gain for frequencies up to 34 GHz.

The dependence of the Schottky junction capacitance under the gate on the applied voltage gives rise to the nonlinear behavior in the transmission lines. The coupled Schottky lines are analyzed by using a linearized and a nonlinear quasi-harmonic model. It is shown that such structures can be used as voltage tunable devices including directional couplers and electronic switches consisting of a long dual-gate type coplanar structure. Examples of voltage tunable couplers and a 15 GHz switch are included.

ANALYSIS AND MODELING OF ELECTRICALLY LONG MESFETS AND COUPLED SCHOTTKY LINES

by

Ahmed Sarhan Mohammed

A THESIS

submitted to

Oregon State University

in partial fulfillment of the requirements for the degree of

DOCTOR OF PHILOSOPHY

Completed : Dec. 2, 1987

Commencement : June 1988

APPROVED :

Redacted for Privacy

Professor of Electrical and Computer Engineering in charge of Major

Redacted for Privacy

Head of the Electrical and Computer Engineering Department

Redacted for Privacy

Dean of Graduate School

Date thesis is presented : December 2, 1987

Typed by : Ahmed Sarhan Mohammed

بسم الله الرحمن الرحيم

DEDICATION

TO

THE MEMORY OF MY FATHER

WITH GRATITUDE TO MY MOTHER

ACKNOWLEDGEMENTS

I express my sincere thanks to Dr. Vijai K. Tripathi, my major professor, for his help, time, advice, patience and continued encouragement during this academic experience. I am grateful to Dr. Gerald C. Alexander, Mr. Donald L. Amort, Dr. Sydney John T. Owen, Dr. Thomas K. Plant and Dr. Alan H. Robinson for serving on my graduate committee.

Appreciation is due to all of the department of Electrical and Computer Engineering faculty, staff and my fellow graduate students and colleagues, especially Mr. Byoungchul Ahn, Mr. Tagore Kollipara and Mr. Michael Thorburn for their valuable assistance.

I wish to express my thanks and gratitude to the people and Government of my country, IRAQ, who awarded me a scholarship to pursue this advanced education.

Finally, I would like to give special thanks for the support and encouragement of all my friends and family members who accompanied me in the united states and those who remained at my back home waiting eagerly for my return.

TABLE OF CONTENTS

LIST OF FIGURES

LIST OF TABLES

GLOSSARY

a — *Thickness of the GaAs MESFET active layer.*

a_o — *Depletion layer (under the gate) thickness.*

C_{12} — *The mutual coupling coefficient of the coupled lines.*

C_d — *The drain-to-ground plane capacitance.*

C_{dp} — *p-n (or Schottky) junction depletion layer capacitance.*

C_{ds} — *Drain-to-source interelectrode (fringing) capacitance.*

C_{elec} — *Self capacitance of an electrode (electrode-to-ground).*

C_{even} — *Interelectrode capacitance associated with even-mode excitation.*

C_{fb} — *Feedback (gate-to-drain) capacitance due to the extension of the depletion layer under the gate towards the drain.*

C_{gd} — *Gate-to-drain interelectrode capacitance (fringing cap.).*

C_{gs} — *Gate-to-source fringing capacitance.*

C_{in} — *Gate-to-channel capacitance across the depleted region.*

C_{in-o} — *Gate-to-channel capacitance when $V_{DS}=0$.*

C_m — *Mutual capacitance between any two lines (strips or electrodes).*

C_{mm} — *Self capacitance, includes the mutual capacitance.*

C_{odd} — *Interelectrode (fringing) capacitance associated with odd-mode excitation.*

C_{pad} — *Pad-to-ground capacitance.*

C_s — *Source-to-ground capacitance.*

C_{sw} — *Side-wall (gate-to-source) capacitance due to the extension of the depleted region under the gate towards the source.*

D_s — *Diffusion coefficient at saturation.*

D_x — *Debye length.*

E *The electric field.*

E_c *The characteristic value of the electric field. It depends on the shape of v(E) curve.*

E_p *The electric field at which the drift velocity reaches its maximum value.*

E_s *Domain sustaining field.*

E_v *The electric field of electron velocity saturation.*

$F(\vartheta,\theta)$ *Incomplete elliptic integral of the first kind.*

G *Conductance.*

g_m *Active device transconductance.*

h *Substrate thickness.*

$h(x)$ *Thickness of the depleted region under the MESFET's gate.*

h_o *Thickness of undepleted active layer at the source end.*

k_c *Capacitive coupling factor.*

k_l *Inductive coupling factor.*

$K(k)$ *Complete elliptic integral of the first kind and k is the modulus.*

$K'(k)$ *complete elliptic integral of the co-modulus k'.*

l *length.*

$l_{mn}(l_{mm})$: *Mutual (self) inductance between line n and line m.*

$L(L_1,L_2)$: *channel length (length of region I, II).*

MESFET *Metal-Semiconductor Field-Effect Transistor.*

MOSFET *Metal-Oxide-Semiconductor Field-Effect Transistor.*

n_{cr} *Characteristic doping density.*

N_D *Carrier (donor) doping concentration [doping level].*

$P_{1,2}$ *Power on line 1, 2*

P_D *The power dissipated by the device in the parasitic elements.*

q *The electronic charge.*

Q_{dom} *The charge of the high-field Gunn domain.*

Q_e *The charge of the extended depletion area beyond the gate towards the drain.*

Q_g *The charge in the depletion area under the gate.*

Q_{sw} *The charge depleted from the extended depletion area beyond the gate towards the source.*

r_d *Drain-line (electrode) metalization resistance.*

r_g *Gate-line (electrode) metalization resistance.*

r_s *Source electrode metalization resistance if it is not grounded.*

R_{ch} *Resistance of the active layer between the channel under the gate and the corresponding electrode (drain or source).*

$R_{ci}(R_{\pi i})$: *Drain-to-gate current ratio for the corresponding normal mode [c- or π-mode].*

R_{co} *Ohmic or contact resistance (for n^+-metal contact).*

$R_{cv}(R_{\pi v})$: *Drain-to-gate voltage ratio for the corresponding normal mode [c- or π-mode].*

R_d *Drain resistance, the parasitic resistance between the channel and the drain.*

R_{dom} *Resistance of the high-field Gunn domain.*

RF *Radio-frequency.*

R_{in} *Input (gate-to-channel) resistance.*

R_o *The MESFET's output resistance.*

R_s *The active layer parasitic resistance between the source and the channel.*

R_{th} *Thermal resistance.*

TWA *Traveling-Wave (cascaded) Amplifier.*

TWT *Traveling-Wave Transistor.*

v_k *The wave velocity on line k.*

v_1 *Light velocity in the free space.*

v_{sat} *The saturation velocity of electrons in the GaAs MESFET.*

V_{Bi} *Metal-to-semiconductor Schottky barrier built-in voltage.*

V_{dc} *DC-bias voltage.*

$V_{GS}(V_{DS})$: *Gate-to-source (drain-to-source) intrinsic voltage.*

V_{dsi} *The voltage drop across region i (i=1,2) under the gate.*

V_j *The voltage on line j; (j=1,2,... or gate,drain,...).*

V_{po} *The pinch-off voltage.*

W *The electrode (line) width.*

W_{th} *Threshold width characterizing the existence or absence of the Gunn domain.*

z_{jk} *The mutual (self) impedance.*

$Z_{cj}(Z_{\pi j})$: *Characteristic impedance associated with the corresponding normal mode.*

α *he attenuation constant of a wave.*

$\beta(\beta_o)$ *The phase constant of a wave (in free space).*

δ *The channel thickness in region II; saturated velocity region.*

$\epsilon, \epsilon_o, \epsilon_r$: *The permittivity of the material, of free space, dielectric constant of the material respectively.*

γ *The propagation constant of a wave.*

γ_c, γ_π *The propagation constant of a corresponding normal mode.*

ρ *Doping density* = qN_D.

ϕ *The electric potential.*

μ, μ_o *The carriers mobility.*

ω *The angular frequency.*

τ *Time constant or transit time.*

ANALYSIS AND MODELING OF ELECTRICALLY LONG MESFETS AND COUPLED SCHOTTKY LINES

CHAPTER 1

INTRODUCTION

In the conventional two-port amplifiers, the transconductance can be increased by cascading active devices which results in an increase in the amplifier gain. However, this is accompanied by an increase in the input and output capacitances which reduces the gain. Therefore, in general, there is a direct gain-bandwidth tradeoff. To overcome this problem, Percival invented the concept of distributed amplifiers [1]. Although initially conceived of in 1936, Percival's concept did not receive much attention until the early 1950's[2,3]. The idea is based on the separation of the input and output capacitances of the active devices (tubes or transistors) by inductors in such a way that artificial transmission lines are formed at the input and output of each active device. In doing so, the input and output impedances become independent of the sections and relatively insensitive to the frequency.

The principle of distributed amplification has been widely applied by cascading the active devices or simply distributing them uniformly along two strips of different characteristic impedances to form a four-port device which can be used as an amplifier. Among these devices used to realize such amplifiers are tubes[4], Si-bipolar devices[5], Si-MOSFETs[6], Si-MESFETs[7] and most recently GaAs-MESFETs[8,9].

Although this type of amplifier is called a traveling-wave amplifier for historical reasons, the other set of amplifiers, which is referred to in literature as traveling-wave transistors (or traveling-wave FETs), is a true distributed parameter traveling-wave device. An amplifier of the second group consists of a single electrically long device. Traveling-wave transistors have been a topic of continued interest in recent years[10-12], although the attention given to this type of amplifier is far less than that given to the distributed discrete device amplifiers. These traveling-wave MESFET devices have small size, light weight, low distortion and low operating voltage, and the demand for them has increased rapidly over the years primarily for applications as broadband amplifiers in both hybrid and monolithic form.

Since the device parameters are distributed uniformly in the direction of the wave propagation, which is transverse to the electron-drift direction, the device electrodes can be modeled as active lossy coupled transmission lines in an inhomogeneous medium. Therefore, the theory of coupled distributed parameters can be applied to study the properties of the device.

The objective of this thesis is to conduct a comprehensive study of the traveling-wave transistor by applying rigorous coupled distributed parameters theory including all possible loss and coupling terms.

The general theory of passive asymmetric coupled lines in an inhomogeneous medium has been developed by Tripathi[13]. In the first chapter, this theory is generalized to include the active coupling between the lines as characterized by the distributed MESFET's

transconductance.

For a common-source MESFET, the finite length structure represents a four-port network whose immittance and scattering parameters can be evaluated in terms of the two normal modes of propagation, namely the c- and π-mode. These normal mode properties of the system including the propagation constants, characteristic impedances and admittance are derived in terms of the equivalent self and mutual distributed parameters of the MESFET.

One of the objectives of this study is to model the device by calculating the electrical parameters of the GaAs MESFET from its physical parameters. Because of the complexity of the GaAS MESFET internally, there is no agreement on a single small-signal model which accurately describes the behavior of the device under all operating conditions. However, there are instead many different models; most of them are derived from scattering parameter measurements. We have developed an accurate computer program based on the work by Pucel[14], Shur[15], Willing[16], Fukui[17], Niedert and Scott[18] and others to calculate the electrical parameters from the geometrical and material parameters of the device. The calculation is based on the two-region model suggested by Shockley[19] and developed later by Grebene and Ghandi[20]. In this model, the active channel under the gate is divided into two regions, a constant carrier mobility region and a constant velocity region. Many effects are considered in the analysis including the presence of the Gunn domain, the carrier velocity saturation, the non-zero channel thickness in the velocity saturation region, the degradation of the carrier mobility due to the power

heating effect, and the substrate current. It is worthwhile to mention at this point that not all the electrical parameters are calculated fully by analytical means. Some of these parameters are adjusted by constants found from the experimental curve fitting.

Excluding the interelectrode capacitances, all the device electrical parameters can be calculated by using analytical formulas or empirical expressions. Such formulas and expressions are scattered through out the literature in some form or the other. However, there is no accurate method to calculate the interelectrode capacitances. In the most recent article[18], the capacitances were calculated by applying Smythe derivation[21], which gives exact results if it is applied for two asymmetric lines. But applying this method to the lines of interest while ignoring the presence of a third line between or adjacent to them results in a high percentage error. Unfortunately, the interelectrode capacitances have a significant and direct effect on the gain-bandwidth product of the amplifier. Therefore, the inadequacy in calculating the mutual capacitive coupling between the device electrodes results in inaccurate results. In fact, intensive work has been done in this area. For example, Wen suggested in 1969 the use of conformal mapping technique as an exact method to calculate the mutual capacitances of the coplanar waveguides[22]. Lin derived the formula for the case of symmetric two lines[23]. Davis et al.[24] included the effect of the substrate thickness but came up with a very complicated expression which is not easy to solve analytically. Others [25,26] included the effect of the metalization thickness. But to the best of our knowledge, there is no method to calculate the mutual

(interelectrode) capacitances of three coplanar lines. We used the conformal mapping technique to derive such a method to calculate the exact values of the mutual capacitances of the two and three asymmetric coplanar strips in terms of the structure geometry and the substrate dielectric constant. The presence of a third line between the two lines or adjacent to them disturbs the electric field and reduces the capacitance between the two lines under consideration. This shielding effect is also investigated. In addition, accurate closed-form expressions for the computer aided design (CAD) are formulated by using curve fitting procedure.

Having the accurate values of the interelectrode capacitances along with the self capacitances of the device electrodes, the inductance matrix can be evaluated. This step completes the calculations of all the GaAs MESFET's electrical parameters.

Since the capacitive and inductive loading of the gate and drain lines are different, the phase velocities of the waves propagating on these lines are also different. To add the drain current in phase along the line, the phase velocities must be synchronized. As mentioned earlier, the discrete active devices are either distributed uniformly along the input and output lines where the characteristic impedances are different, or cascaded via transmission lines of different lengths or characteristic impedances in order to synchronize the phase velocities. But for the case of traveling-wave transistors, the same technique can not be used and the elements required to synchronize the velocities have to be distributed uniformly along the lines. In the previous work, where the small-signal equivalent circuit

models used were simplified and many approximations were made, the compensation elements have been estimated analytically. It had been found that a capacitance must be added to the drain electrode and this was done by direct overlays[10,11] or novel image gate arrangements [12]. For the comprehensive device model, where all the electrical parameters are included, it is not that easy to calculate analytically the value of the elements required to synchronize the velocities. TOUCHSTONE, a computer optimizer, is used in our study to estimate the value and the nature (capacitive, inductive,...) of the compensation elements[27]. More importantly, TOUCHSTONE is used as a tool to validate the results obtained by utilizing the scattering parameters matrix of the four-port distributed parameter amplifier. In this simulation, sections of lumped elements are used to build an artificial MESFET in a manner similar to that used in simulating transmission lines by artificial lines. It is found that as the number of these sections is increased, the results of the simulated MESFET become closer and closer to the results found by using the scattering parameters. TOUCHSTONE is also used to estimate the termination impedances which play a significant role in the device performance (gain and bandwidth). Due to the coupling, it is impossible to match perfectly all the device terminals, especially over a wide range of frequencies. Amemiya[28] suggested the use of T- or π-sections to terminate both lines. But Amemiya's equations are limited to the non-lossy transmission lines and they are not applicable to the general case where the losses and active couplings are involved.

The analysis of structures for applications as traveling-wave

amplifiers in microwave frequencies range is based on the assumption that the signal applied to the input end of the gate electrode is small enough such that the variation in the Schottky capacitance is negligible. Therefore, the higher order harmonics are not important and the junction capacitance is modeled as a linear element. If, on the other hand, the signal amplitude is not too small, and the voltage dependence of the junction capacitance and other nonlinear electrical parameters were considered, the structure can be used as a harmonic generator[29,30]. The nonlinearity of Schottky capacitance can be utilized to study coupled Schottky lines for possible applications as voltage tunable devices such as electronic switches and directional couplers. We have extended our study to include the analysis and applications of coupled nonlinear lines such as Schottky lines in a long dual-gate MESFETs.

OUTLINE OF THE THESIS :

This thesis is composed of seven chapters including this one. In the second chapter, the general normal mode analysis of active coupled lines in an inhomogeneous medium is presented. The properties of the transmission line system including the normal mode propagation constants, the characteristic impedances (admittances) of the two lines and the voltage (current) ratios for the two modes of propagation are derived in terms of the self and mutual distributed shunt admittances and series impedances of the system.

In the third chapter, the small-signal model of a GaAs MESFET is described. The calculation of the electrical parameters of the device

by utilizing the geometrical and material parameters is presented in detail. To complete the calculation of the device electrical parameters, an exact calculation of the interelectrode capacitances for two and three coplanar strips is introduced in chapter 4. In addition, closed-form expressions which should be useful in the computer aided design of three-line structures are presented.

In the fifth chapter, the expressions for the distributed self and mutual line constants are derived and used in the general active coupled line theory developed in the second chapter to compute the scattering parameters and the power gain of the four-port device. The use of TOUCHSTONE to help model design and optimize the amplifiers is also outlined. The results of this study are included in this chapter.

Based on the effect of the voltage-dependence of the Schottky capacitance under gate line electrodes, the analysis of coupled nonlinear lines has been developed. The analysis is presented in the sixth chapter and is used to demonstrate the design of voltage tunable devices such as electronic switches and directional couplers. The analysis can be applied to long dual-gate MESFET structures. The sixth chapter includes examples of these applications.

The last chapter includes the concluding remarks and our suggestions for future study which might extend and/or improve same aspects of this study.

CHAPTER 2

ANALYSIS OF ACTIVE COUPLED TRANSMISSION LINES

2.1 : INTRODUCTION :

Many types of coupled distributed parameter circuits (symmetric or asymmetric, active or passive, lossy or lossless) have been used in various applications including couplers, filters, impedance transformers, oscillator circuits, slow-wave structures, and traveling-wave transistors [10,29-32]. The parameters characterizing coupled-line four-port networks (impedance, admittance, chain scattering, etc.) can be used in the analysis and design of these circuits. Zysman and Johnson [33], and Jones and Bolljahn [34] used these parameters to study two- and four-port circuits, which are used as filters and directional couplers. For the case of homogeneous media (coupled TEM lines [34,35]) and symmetrical structure in an inhomogeneous media [33,36], the four-port parameters are obtained in terms of the coupled line impedances (or admittances) and phase velocities for the even and odd modes of excitation. By definition, the even mode corresponds to the case where the lines have equal voltages and equal currents. The odd mode results when the voltages and currents are equal in magnitude but 180° out of phase. However, since the system to be analyzed here is asymmetric, active and in an inhomogeneous medium, the even and odd mode description is inadequate since the voltages and currents on the two lines are, in general, not equal in magnitude for the normal modes of the system and the waves propagate with unequal phase

velocities. The difference in phase velocities in various regions of the structure precludes a pure TEM wave propagation and the different phase velocities of the normal modes give rise to the interference resulting in a periodic exchange of energy between lines [36]. It is convenient to describe a coupled pair of lines in terms of normal modes of excitation which have been called co- or c-mode (donated by a subscript c) and anti- or π-mode (denoted by a subscript π). These normal mode parameters are derived in terms of the equivalent series- and shunt-distributed parameters such as impedances and admittances of the lines. The equivalent distributed parameter constants can be found for quasi-TEM as well as hybrid-higher order modes of propagation by solving the corresponding quasi-static or general frequency dependent boundary value problems. The quasi-TEM approximation yields excellent results up to several gigahertz for structures with transverse dimensions small as compared to the wavelength, and the analysis is much simpler.

The equivalent series and shunt, self and mutual immittances together with active linear dependent sources per unit length of the lines are used to obtain the network parameters of the four-port asymmetric active coupled-line by utilizing the modal characteristics of the two independent modes of excitation which propagate in the system.

This analysis is a generalized approach based on the method developed by Tripathi[13] for the study of general uniformly coupled distributed parameter structures. The four-port parameters derived are similar in form to those derived by Tripathi and degenerate to the same expressions if the active element(s) in the system are removed.

The results obtained here can be used to study the properties of many general coupled line systems including the linear ac-analysis of GaAs MESFET structures for applications as traveling-wave transistors.

2.2 : THE ANALYSIS :

2.2.1 : Coupled-Line Analysis :

The voltages and currents on the two uniformly coupled lines are given, in general, by the transmission line equations as :

$$\frac{-dv_1}{dx} = z_{11}\, i_1 + z_{12}\, i_2 \qquad (1\text{-a})$$

$$\frac{-dv_2}{dx} = z_{21}\, i_1 + z_{22}\, i_2 \qquad (1\text{-b})$$

$$\frac{-di_1}{dx} = y_{11}\, v_1 + y_{12}\, v_2 \qquad (1\text{-c})$$

$$\frac{-di_2}{dx} = y_{21}\, v_1 + y_{22}\, v_2 \qquad (1\text{-d})$$

Where z_{jj} and y_{jj} $(j=1,2)$ are the self series impedance and shunt admittance per unit length of line j in the presence of line k $(k=1,2;\ k\neq j)$; z_{jk} and y_{jk} are the mutual impedance and admittance per unit length respectively. In general $z_{jk} \neq z_{kj}$ and $y_{jk} \neq y_{kj}$.

In the above equations, it is assumed that the voltages and currents vary as exp(jωt). Differentiating equations (1-a) and (1-b) with respect to x and substituting (1-c) and (1-d), equations for voltages on the two lines are obtained as :

$$\frac{d^2v_1}{dx^2} = a_v v_1 + b_v v_2 \qquad (2\text{-a})$$

$$\frac{d^2v_2}{dx^2} = c_v v_1 + d_v v_2 \qquad (2\text{-b})$$

Where,

$$a_v = z_{11}y_{11} + z_{12}y_{21} \qquad (3\text{-a})$$

$$b_v = z_{11}y_{12} + z_{12}y_{22} \qquad (3\text{-b})$$

$$c_v = z_{21}y_{11} + z_{22}y_{21} \qquad (3\text{-c})$$

$$d_v = z_{21}y_{12} + z_{22}y_{22} \qquad (3\text{-d})$$

Since none of the coefficients in equation (3) varies with x, an exponential solution for the voltage of the form $v(x)=v_0e^{\gamma x}$ can be assumed. Substituting this form of v(x) into equation (2) gives,

$$(a_v - \gamma^2) v_1 + b_v v_2 = 0 \qquad (4\text{-a})$$

$$c_v v_1 + (d_v - \gamma^2) v_2 = 0 \qquad (4\text{-b})$$

This is an eigenvalue problem. The nontrivial solution can be obtained by equating the determinant of equation (4) to zero and solving the biquadratic equations as:

$$\begin{bmatrix} a_v - \gamma^2 & b_v \\ c_v & d_v - \gamma^2 \end{bmatrix} = 0 \qquad (5)$$

or,

$$\gamma_c = \pm\left[\frac{a_v + d_v}{2} + \frac{1}{2} \{ (a_v - d_v)^2 + 4b_vc_v\}^{\frac{1}{2}} \right]^{\frac{1}{2}} \qquad (6\text{-a})$$

$$\gamma_\pi = \pm\left[\frac{a_v + d_v}{2} - \frac{1}{2} \{ (a_v - d_v)^2 + 4b_vc_v\}^{\frac{1}{2}} \right]^{\frac{1}{2}} \qquad (6\text{-b})$$

Where γ_c and γ_π correspond to c-mode and π-mode propagation constants respectively.

From equation (4), the relationships between the voltages on the two lines for each of these four waves can be obtained as :

$$\frac{v_2}{v_1} = \frac{\gamma^2 - a_v}{b_v} = \frac{c_v}{\gamma^2 - d_v} \qquad (7)$$

Define,

$$R_{cv} \equiv \frac{v_2}{v_1} \qquad \text{for} \quad \gamma = \gamma_c \qquad : (\text{ c-mode })$$

$$R_{cv} = \frac{1}{2b_v}\left[(d_v - a_v) + \{ (a_v - d_v)^2 + 4b_v c_v\}^{\frac{1}{2}} \right] \qquad (8\text{-a})$$

and

$$R_{\pi v} \equiv \frac{v_2}{v_1} \qquad \text{for} \quad \gamma = \gamma_\pi \qquad : (\ \pi\text{-mode }) $$

$$R_{\pi v} = \frac{1}{2b_v}\left[(d_v - a_v) - \{ (a_v - d_v)^2 + 4b_v c_v\}^{\frac{1}{2}} \right] \qquad (8\text{-b})$$

The current on the two lines can be obtained from equations (1-a) and (1-b) in terms of voltages or directly by following the same steps as the ones used to solve for v_1 and v_2. The current mode ratios are found to be :

$$R_{ci} \equiv \frac{i_2}{i_1} \qquad \text{for} \quad \gamma = \gamma_c \qquad : (\text{ c-mode })$$

$$R_{ci} = \frac{1}{2b_i}\left[(d_i - a_i) + \{ (a_i - d_i)^2 + 4b_i c_i\}^{\frac{1}{2}} \right] \qquad (9)$$

and

$$R_{\pi i} \equiv \frac{i_2}{i_1} \qquad \text{for} \quad \gamma = \gamma_\pi \qquad : (\ \pi\text{-mode }) $$

$$R_{\pi i} = \frac{1}{2b_i}\left[(d_i - a_i) - \{ (a_i - d_i)^2 + 4b_i c_i\}^{\frac{1}{2}} \right] \qquad (10)$$

Where,

$$a_i = z_{11}y_{11} + z_{21}y_{12} \qquad (11\text{-a})$$

$$b_i = z_{12}y_{11} + z_{22}y_{12} \qquad (11\text{-b})$$

$$c_i = z_{11}y_{21} + z_{21}y_{22} \qquad (11\text{-c})$$

$$d_i = z_{12}y_{21} + z_{22}y_{22} \qquad (11\text{-d})$$

In general, $R_{ci} \neq R_{cv}$ and $R_{\pi i} \neq R_{\pi v}$. If the system is passive i.e., $z_{12} = z_{21}$ and $y_{12} = y_{21}$, then $R_{ci} = -1/R_{\pi v}$ and $R_{\pi i} = -1/R_{cv}$[13]. Moreover, if the coupled-line system is lossless, the voltages and currents ratios are, in general, positive for the c-mode and negative for the π-mode of excitation. For the case of identical lines, $R_{ci} = R_{cv} = 1$ and $R_{\pi i} = R_{\pi v} = -1$, and the c- and π-mode becomes even- and odd-mode, respectively[13].

The solution of the voltage on the two lines is the sum of the solutions of the four waves and is given by:

$$v_1 = A_1 e^{-\gamma_c x} + A_2 e^{\gamma_c x} + A_3 e^{-\gamma_\pi x} + A_4 e^{\gamma_\pi x} \qquad (12\text{-a})$$

and

$$v_2 = A_1 R_{cv} e^{-\gamma_c x} + A_2 R_{cv} e^{\gamma_c x} + A_3 R_{\pi v} e^{-\gamma_\pi x} + A_4 R_{\pi v} e^{\gamma_\pi x} \qquad (12\text{-b})$$

Where A_j $(j=1,\ldots,4)$ is the amplitude coefficient of the corresponding wave.

By substituting the voltage equations (12-a) and (12-b) into equations (1-a) and (1-b), the currents for all four waves can be determined as :

$$i_1 = A_1 Y_{c1} e^{-\gamma_c x} - A_2 Y_{c1} e^{\gamma_c x} + A_3 Y_{\pi 1} e^{-\gamma_\pi x} - A_4 Y_{\pi 1} e^{\gamma_\pi x} \qquad (13\text{-a})$$

and

$$i_2 = A_1 R_{cv} Y_{c2} e^{-\gamma_c x} - A_2 R_{cv} Y_{c2} e^{\gamma_c x} + A_3 R_{\pi v} Y_{\pi 2} e^{-\gamma_\pi x} - A_4 R_{\pi v} Y_{\pi 2} e^{\gamma_\pi x} \qquad (13\text{-b})$$

Where Y_{c1}, Y_{c2}, $Y_{\pi 1}$ and $Y_{\pi 2}$ are the characteristic admittances of line 1 and 2 for the c- and π-mode respectively. They are given by :

$$Y_{c1} = \gamma_c \frac{z_{22} - z_{12} R_{cv}}{z_{11}z_{22} - z_{12}z_{21}} \qquad (14\text{-a})$$

$$Y_{c2} = \frac{\gamma_c}{R_{cv}} \frac{z_{11} R_{cv} - z_{21}}{z_{11}z_{22} - z_{12}z_{21}} \qquad (14\text{-b})$$

$$Y_{\pi 1} = \gamma_\pi \frac{z_{22} - z_{12} R_{\pi v}}{z_{11}z_{22} - z_{12}z_{21}} \qquad (14\text{-c})$$

$$Y_{\pi 2} = \frac{\gamma_\pi}{R_{\pi v}} \frac{z_{11} R_{\pi v} - z_{21}}{z_{11}z_{22} - z_{12}z_{21}} \qquad (14\text{-d})$$

On the other hand, if the current equations are used, then the general solution of the currents associated with the four waves of the two coupled lines is :

$$i_1 = B_1 e^{-\gamma_c x} + B_2 e^{\gamma_c x} + B_3 e^{-\gamma_\pi x} + B_4 e^{\gamma_\pi x} \qquad (15\text{-a})$$

and

$$i_2 = B_1 R_{ci} e^{-\gamma_c x} + B_2 R_{ci} e^{\gamma_c x} + B_3 R_{\pi i} e^{-\gamma_\pi x} + B_4 R_{\pi i} e^{\gamma_\pi x} \qquad (15\text{-b})$$

Where B_j is the amplitude coefficient of wave j.

By substituting the current equations (15-a) and (15-b) into equations (1-c) and (1-d), the voltages for all four waves can be determined as :

$$v_1 = B_1 Z_{c1} e^{-\gamma_c x} - B_2 Z_{c1} e^{\gamma_c x} + B_3 Z_{\pi 1} e^{-\gamma_\pi x} - B_4 Z_{\pi 1} e^{\gamma_\pi x} \qquad (16\text{-a})$$

and

$$v_2 = B_1 R_{ci} Z_{c2} e^{-\gamma_c x} - B_2 R_{ci} Z_{c2} e^{\gamma_c x} + B_3 R_{\pi i} Z_{\pi 2} e^{-\gamma_\pi x} - B_4 R_{\pi i} Z_{\pi 2} e^{\gamma_\pi x} \qquad (16\text{-b})$$

Where Z_{c1}, Z_{c2}, $Z_{\pi 1}$ and $Z_{\pi 2}$ are the characteristic impedances of line 1 and 2 for the c- and π-mode respectively. They are given by :

$$Z_{c1} = \frac{1}{Y_{c1}} = \gamma_c \frac{y_{22} - y_{12} R_{ci}}{y_{11}y_{22} - y_{12}y_{21}} \qquad (17\text{-a})$$

$$Z_{c2} = \frac{1}{Y_{c2}} = \frac{\gamma_c}{R_{ci}} \frac{y_{11} R_{ci} - y_{21}}{y_{11}y_{22} - y_{12}y_{21}} \qquad (17\text{-b})$$

$$Z_{\pi 1} = \frac{1}{Y_{\pi 1}} = \gamma_\pi \frac{y_{22} - y_{12} R_{\pi i}}{y_{11}y_{22} - y_{12}y_{21}} \qquad (17\text{-c})$$

$$Z_{\pi 2} = \frac{1}{Y_{\pi 2}} = \frac{\gamma_\pi}{R_{\pi i}} \frac{y_{11} R_{\pi i} - y_{21}}{y_{11}y_{22} - y_{12}y_{21}} \qquad (17\text{-d})$$

By comparing equations (12) with (16) and (13) with (15), it is seen that:

$$\frac{R_{cv}}{R_{ci}} = \frac{Y_{c1}}{Y_{c2}} = \frac{Z_{c2}}{Z_{c1}} \qquad (18\text{-a})$$

and

$$\frac{R_{\pi v}}{R_{\pi i}} = \frac{Y_{\pi 1}}{Y_{\pi 2}} = \frac{Z_{\pi 2}}{Z_{\pi 1}} \qquad (18\text{-b})$$

These relationships are similar to those given in [13]. In general, the ratio of the characteristic impedances of the two lines is given by :

$$\frac{Z_{char.-1}}{Z_{char.-2}} = \left[\frac{R_{ci} R_{\pi i}}{R_{cv} R_{\pi v}} \right]^{\frac{1}{2}} \qquad (19\text{-a})$$

Where, $Z_{char.-j} = \sqrt{Z_{cj} Z_{\pi j}}$; $(j = 1,2)$ (19-b)

2.2.2 : Coupled-Line Four-Port :

The terminal four-port parameters (impedances, admittances, etc.) of the finite length coupled line structure shown in Fig.2-1 are found by solving for the port voltages in terms of currents or vice versa.

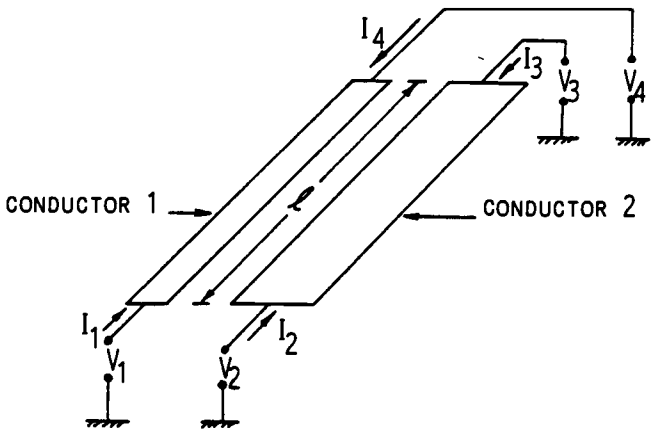

Fig. 2-1 : General asymmetric coupled transmission lines.

For example, equation (12) gives voltages at x=0 and x = l leading to:

$$\begin{bmatrix} V_1 \\ V_2 \\ V_3 \\ V_4 \end{bmatrix} = \begin{bmatrix} 1 & 1 & 1 & 1 \\ R_{cv} & R_{cv} & R_{\pi v} & R_{\pi v} \\ R_{cv}e^{-\gamma_c l} & R_{cv}e^{\gamma_c l} & R_{\pi v}e^{-\gamma_\pi l} & R_{\pi v}e^{\gamma_\pi l} \\ e^{-\gamma_c l} & e^{\gamma_c l} & e^{-\gamma_\pi l} & e^{\gamma_\pi l} \end{bmatrix} \begin{bmatrix} A_1 \\ A_2 \\ A_3 \\ A_4 \end{bmatrix}$$

or $[V]=[R^*]\times[A]$ *(20)*

Similarly, equation (13) gives the port currents as,

$$\begin{bmatrix} I_1 \\ I_2 \\ I_3 \\ I_4 \end{bmatrix} = \begin{bmatrix} Y_{c1} & -Y_{c1} & Y_{\pi 1} & -Y_{\pi 1} \\ R_{ci}Y_{c1} & -R_{ci}Y_{c1} & R_{\pi i}Y_{\pi 1} & -R_{\pi i}Y_{\pi 1} \\ -R_{ci}Y_{c1}e^{-\gamma_c l} & R_{ci}Y_{c1}e^{\gamma_c l} & -R_{\pi i}Y_{\pi 1}e^{-\gamma_\pi l} & R_{\pi i}Y_{\pi 1}e^{\gamma_\pi l} \\ -Y_{c1}e^{-\gamma_c l} & Y_{c1}e^{\gamma_c l} & -Y_{\pi 1}e^{-\gamma_\pi l} & Y_{\pi 1}e^{\gamma_\pi l} \end{bmatrix} \begin{bmatrix} A_1 \\ A_2 \\ A_3 \\ A_4 \end{bmatrix}$$

or $[I]=[Y^*]\times[A]$ *(21)*

To express the terminal voltages [V] in terms of terminal currents [I] or vice versa, the amplitude coefficients [A] are eliminated leading to:

$$[V]=[Z]\times[I], \quad \text{where:} \quad [Z]=[R^*]\times[Y^*]^{-1} \tag{22}$$

and

$$[I]=[Y]\times[V], \quad \text{where:} \quad [Y]=[Y^*]\times[R^*]^{-1} \tag{23}$$

The elements of the Z-matrix are found to be:

$$Z_{11}=Z_{44}=\frac{Z_{c1}\coth(\gamma_c l)}{(1-R_{ci}/R_{\pi i})}+\frac{Z_{\pi 1}\coth(\gamma_\pi l)}{(1-R_{\pi i}/R_{ci})} \tag{24-a}$$

$$Z_{12}=Z_{43}=\frac{-Z_{c1}\coth(\gamma_c l)}{R_{\pi i}(1-R_{ci}/R_{\pi i})}-\frac{Z_{\pi 1}\coth(\gamma_\pi l)}{R_{ci}(1-R_{\pi i}/R_{ci})} \tag{24-b}$$

$$Z_{13}=Z_{42}=\frac{-Z_{c1}}{R_{\pi i}(1-R_{ci}/R_{\pi i})\sinh(\gamma_c l)}-\frac{Z_{\pi 1}}{R_{ci}(1-R_{\pi i}/R_{ci})\sinh(\gamma_\pi l)} \tag{24-c}$$

$$Z_{14}=Z_{41}=\frac{Z_{c1}}{(1-R_{ci}/R_{\pi i})\sinh(\gamma_c l)}+\frac{Z_{\pi 1}}{(1-R_{\pi i}/R_{ci})\sinh(\gamma_\pi l)} \tag{24-d}$$

$$Z_{21}=Z_{34}=\frac{R_{cv}Z_{c1}\coth(\gamma_c l)}{(1-R_{ci}/R_{\pi i})}+\frac{R_{\pi v}Z_{\pi 1}\coth(\gamma_\pi l)}{(1-R_{\pi i}/R_{ci})} \tag{24-e}$$

$$Z_{22}=Z_{33}=\frac{-R_{cv}Z_{c1}\coth(\gamma_c l)}{R_{\pi i}(1-R_{ci}/R_{\pi i})}-\frac{R_{\pi v}Z_{\pi 1}\coth(\gamma_\pi l)}{R_{ci}(1-R_{\pi i}/R_{ci})} \tag{24-f}$$

$$Z_{23}=Z_{32}=\frac{-R_{cv}Z_{c1}}{R_{\pi i}(1-R_{ci}/R_{\pi i})\sinh(\gamma_c l)}-\frac{R_{\pi v}Z_{\pi 1}}{R_{ci}(1-R_{\pi i}/R_{ci})\sinh(\gamma_\pi l)} \tag{24-g}$$

$$Z_{24}=Z_{31}=\frac{R_{cv}Z_{c1}}{(1-R_{ci}/R_{\pi i})\sinh(\gamma_c l)}+\frac{R_{\pi v}Z_{\pi 1}}{(1-R_{\pi i}/R_{ci})\sinh(\gamma_\pi l)} \tag{24-h}$$

The elements of the Y-matrix are found to be:

$$Y_{11}=Y_{44}= \frac{Y_{c1}\coth(\gamma_c l)}{(1 - R_{cv} / R_{\pi v})} + \frac{Y_{\pi 1}\coth(\gamma_\pi l)}{(1 - R_{\pi v} / R_{cv})} \qquad (25\text{-}a)$$

$$Y_{12}=Y_{43}= \frac{- Y_{c1}\coth(\gamma_c l)}{R_{\pi v}(1 - R_{cv} / R_{\pi v})} - \frac{Y_{\pi 1}\coth(\gamma_\pi l)}{R_{cv}(1 - R_{\pi v} / R_{cv})} \qquad (25\text{-}b)$$

$$Y_{13}=Y_{42}= \frac{Y_{c1}}{R_{\pi v}(1-R_{cv}/R_{\pi v})\sinh(\gamma_c l)} + \frac{Y_{\pi 1}}{R_{cv}(1-R_{\pi v}/R_{cv})\sinh(\gamma_\pi l)} \qquad (25\text{-}c)$$

$$Y_{14}=Y_{41}= \frac{- Y_{c1}}{(1-R_{cv}/R_{\pi v})\sinh(\gamma_c l)} - \frac{Y_{\pi 1}}{(1-R_{\pi v}/R_{cv})\sinh(\gamma_\pi l)} \qquad (25\text{-}d)$$

$$Y_{21}=Y_{34}= \frac{R_{ci}Y_{c1}\coth(\gamma_c l)}{(1 - R_{cv} / R_{\pi v})} + \frac{R_{\pi i}Y_{\pi 1}\coth(\gamma_\pi l)}{(1 - R_{\pi v} / R_{cv})} \qquad (25\text{-}e)$$

$$Y_{22}=Y_{33}= \frac{- R_{ci}Y_{c1}\coth(\gamma_c l)}{R_{\pi v}(1 - R_{cv} / R_{\pi v})} - \frac{R_{\pi i}Y_{\pi 1}\coth(\gamma_\pi l)}{R_{cv}(1 - R_{\pi v} / R_{cv})} \qquad (25\text{-}f)$$

$$Y_{23}=Y_{32}= \frac{R_{ci}\, Y_{c1}}{R_{\pi v}(1-R_{cv}/R_{\pi v})\sinh(\gamma_c l)} + \frac{R_{\pi i}\, Y_{\pi 1}}{R_{cv}(1-R_{\pi v}/R_{cv})\sinh(\gamma_\pi l)} \qquad (25\text{-}g)$$

$$Y_{24}=Y_{31} = \frac{- R_{ci}\, Y_{c1}}{(1-R_{cv}/R_{\pi v})\sinh(\gamma_c l)} - \frac{R_{\pi i}\, Y_{\pi 1}}{(1-R_{\pi v}/R_{cv})\sinh(\gamma_\pi l)} \qquad (25\text{-}h)$$

The above immittance parameters or other network functions derived either from these parameters or directly from the expressions for voltages and currents can be used to study the properties of these four ports when the structure is terminated in desired impedances.

2.3 : CONCLUDING REMARKS :

The general analysis of active coupled transmission lines, which is presented in this chapter, can be used to study a GaAs MESFET structure as a traveling-wave transistor. In addition, the analysis is general and can be applied to other microwave circuits consisting of coupled distributed parameter structures.

The advantage of this analysis over the coupled-mode formulation [37] is that, the use of normal mode analysis leads to the four-port circuit matrices which can then be used to study all the transfer functions for different terminating impedances on both ends of the line.

The transmission structure properties are used to obtain the characteristics of the two normal modes of propagation. These characteristics, which include the immittances, the phase velocities and the voltage and current ratios on both lines associated with the two modes, are utilized to determine the 4×4 network matrices. The four-port parameters characterizing the coupled-line may be used in designing various microwave circuits including filters, couplers, oscillators, impedance matching networks, and traveling-wave transistors and amplifiers. The application of this analysis for the study of the traveling-wave transistor based on the scattering parameters is presented in chapter 5.

CHAPTER 3

GaAs MESFET SMALL-SIGNAL MODEL

3.1 : INTRODUCTION :

Device modeling is the cornerstone of any circuit design. Unfortunately, even today, unlike silicon devices, accurate and reliable GaAs device models are not available. The uncertainty in modeling the the equivalent small- (or large-) signal circuit of the GaAs MESFET (Metal-Semiconductor Field Effect Transistor) is reflected by the large number of different models in the literature [12,15,38-64]. This uncertainty sounds even stronger when the same author(s) use more than one model in one article in an attempt to improve the MESFET's model in order to match the measured data[65,66]. Many different models have been proposed and used by the same author(s) in recent years. For For example, see [67-69,70-72,73-74,75-76].

MESFETs are extremely complex internally and therefore, it is difficult to develop simple external models which accurately describe their behavior under all operating conditions based on the device physics.

The typical and most convenient approach of modeling GaAs FETs is based on the measurements of scattering parameters of the device at the bias of interest, the selection of a suitable small-signal model, and the optimization of the circuit element values by using a circuit simulator program such as SUPER-COMPACT and TOUCHSTONE to best fit the measured data. Many different models of this nature have been

reported (see for example [54,64,68-69,75,77-82]). Some authors have found that they need to introduce other elements or branches in their equivalent circuit model to get a better fit with the measured data, although these circuit elements may not have any physical explanation [50].

The above mentioned experimental modeling technique can not be easily used to predict the exact values of circuit elements, and therefore the circuit behavior, before manufacturing the circuit (or the device). This method is more useful as an analysis rather than synthesis tool. In addition, the model parameter values are usually obtained at a specific frequency and bias voltage. In summary, this technique does not necessarily provide accurate results, and the correlation between element values and the physical characteristics of the device is lost. For design purposes, it is important to have an analytical model where the small-signal parameters at any desired bias can be calculated from the physical device specifications efficiently, accurately and directly. Several analytical models have been proposed in recent years (see for example [14-15,17-18,56,63,65,66,70,73,74,83-88]). Gamand et al.[52] used SPICE2 to predict an analytical model, while Madjar and Rosenbaum[89] utilized the two-dimensional model of Yamaguchi and Kodera et al.[90] to produce analytical relationships for drain and gate currents as a function of drain-source and gate-source voltages and their derivatives. Willing et al.[16] considered the elements with essentially bias-independent values as linear elements and calculated them analytically. The nonlinear elements were determined from S-parameter measurements at different bias conditions.

Bandler and Zhang[76] used a new approach called "Monte-Carlo Sensitivity analysis" to determine the values of the elements of his model.

Our theoretical study of a distributed long device requires an analytical model such that the values of the equivalent circuit elements of GaAs MESFETs can be calculated by utilizing the geometrical and material parameters. Such a model is needed not only for this study but also for many other applications of GaAs monolithic circuits in both microwave and high speed digital applications. As a result, inexpensive, fairly accurate, and easy-to-run computer programs for calculating the equivalent circuit elements are needed. Neidert and Scott[18] wrote a FORTRAN program called FETREN in an attempt to satisfy this need. A new program written for this study called OSUFET is an improvement of FETREN. The features and limitations of this program are discussed in the following sections. A physical model has been chosen to account for many known physical effects in GaAs MESFETs. The calculation of all equivalent circuit elements based on the physical model is described in this chapter.

3.2 : THE FEATURES AND LIMITATIONS OF THE COMPUTER PROGRAM OSUFET :

OSUFET is a FORTRAN program , which is a modified version of FETREN by Neidert and Scott[18]. It is important to emphasize at this point that the problem with all analytical GaAs MESFET models proposed to date is that these models do not give results which agree well with the measured data over a wide range of bias voltages. Since the program is not an attempt to arbitrarily fit the measured data, its results are not perfect. This is because although new terms were

added in a logical and plausible way to permit adjustment of computed results to measured values, the program does not use arbitrary fitting constants. This results in improved agreement between the calculated and measured data over the full range of bias voltages (or over the full range of large signal "swing" conditions).

When the analytical theory is not applicable, as in the calculation of the input and feedback capacitances for the drain-to-source voltage between zero and half the pinch-off voltage, the interpolation has been introduced. This interpolation is made between the values calculated analytically where it is possible by utilizing the measured data.

The program is based on the two-region model suggested by Shockley[19] and developed by Grebene and Ghandi[20], and in more details by Pucel et al.[14]. In this approximation, the active channel is divided into two regions; one of constant carrier mobility and the other of saturated carrier velocity. The negative resistance region under the gate occupies a small space and this region is neglected. Since the calculations made in the transition between these two regions are not accurate, this approximation is one of the limitations of the program. Other approximations made are as follows: the doping concentrations are assumed to be constant through out the active layer and an abrupt junction is assumed. The overshoot effect of the velocity is ignored. One-dimensional analysis which does not include the potential variation in the longitudinal direction is used. Such an approximation, which is called a gradual channel approximation can be made if the gate length is much greater than the active layer

thickness. But often in microwave devices, the channel length is about equal to the active channel thickness. If this is the case, two-dimensional analysis may be used. But the program does not support such analysis.

In spite of these limitations, OSUFET gives meaningful results and can be used as a design tool for many applications.

FETREN calculates the intrinsic and parasitic circuit elements. It contains expressions to account for Gunn domain formation which has been ignored by the earlier models, temperature dependence of various parameters due to heating from the bias power, the effect of extension of the depletion region beyond the gate, and the non-zero channel thickness in the velocity saturation region. OSUFET contains, beside these expressions, routines to calculate the fringing capacitances between electrodes derived by using the conformal mapping technique, as well as the electrode inductances and resistances. Some modifications were made in calculating some of the circuit elements as shown in in the following sections.

3.3 : THEORETICAL REVIEW :

Many papers have been published about the general analysis of microwave GaAs MESFETs and their modeling. In the analysis presented here, a two-region model, which is suggested by Shockley[19], is adopted. This model is based on the assumption that the active channel under the gate can be divided into two regions; one, which is near the source, of constant carrier mobility, and the other, which is near the drain, of zero mobility i.e., saturated carrier velocity as

shown in Fig. 3-1. This model was expanded by Grebene and Ghandi[20], and by Pucel et al.[14].

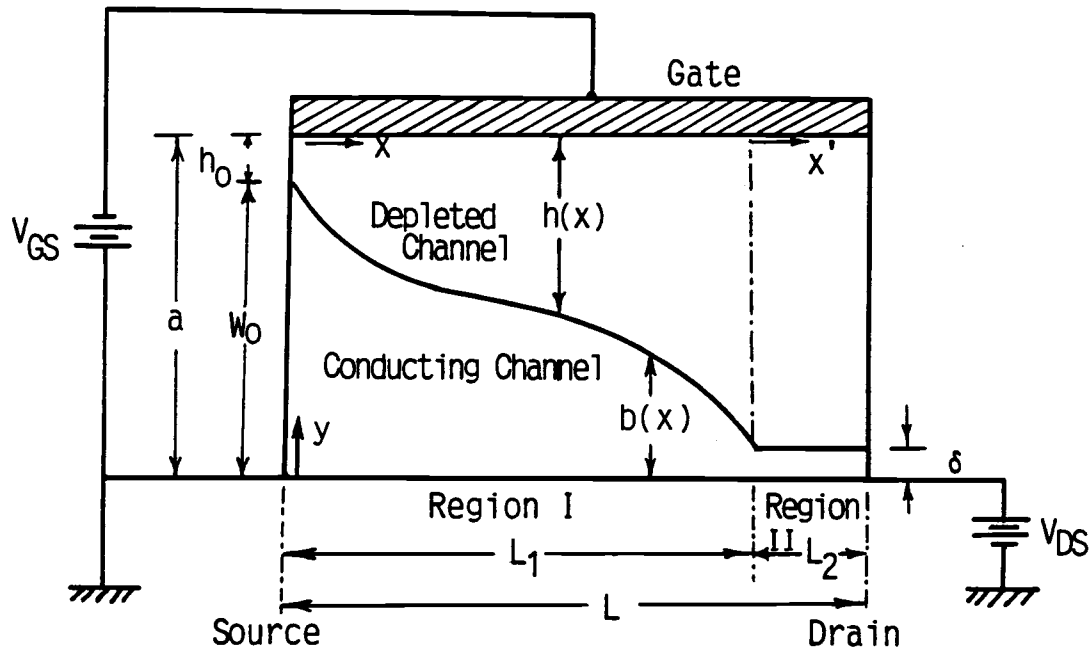

Fig.3-1-a: The assumed MESFET configuration for theoretical analysis. (After Grebene and Ghandi [20])

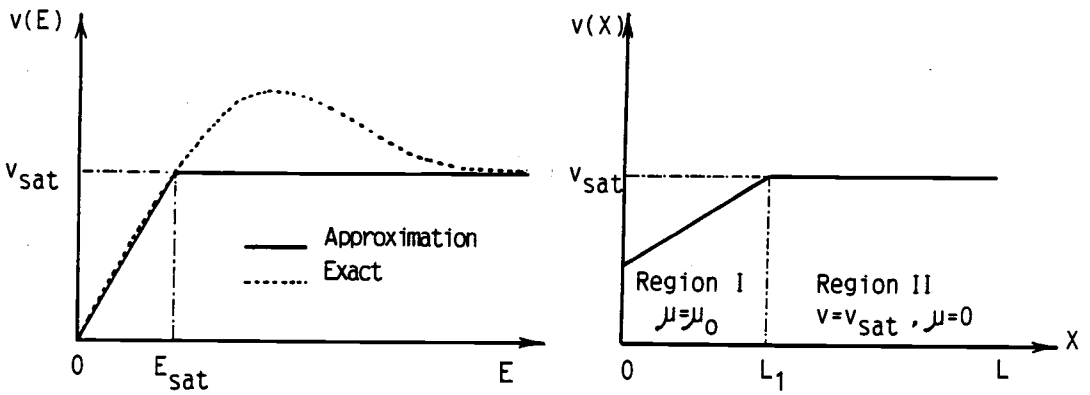

Fig.3-1-b: The actual and assumed carrier velocity dependence on the electric field and the assumed velocity along the channel.

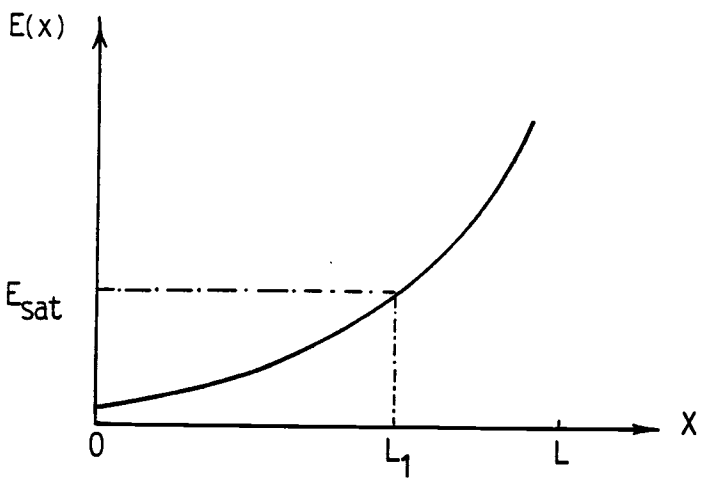

Fig.3-1-c: The electrical field along the channel.

3.3.1 : The Operating Point :

The operating point is determined by the longitudinal position of the boundary between region I and region II. The position of this boundary is determined by forcing the calculated voltage drops across the two regions and the parasitic resistances to be equal to the applied voltage, i.e.,

$$V_{applied} = V_{Rs} + V_{Rd} + V_{Ds\text{-}int.} \qquad (1)$$

Where,

$$V_{DS\text{-}int.} = V_{ds1} + V_{ds2} \qquad (2)$$

This is shown in Fig. 3-2.

This can be done by varying the longitudinal position of the boundary between the two regions such that the longitudinal electric field is large enough to produce velocity saturation. Therefore, the parasitic resistances must be calculated before any calculations can be made to determine the operating point.

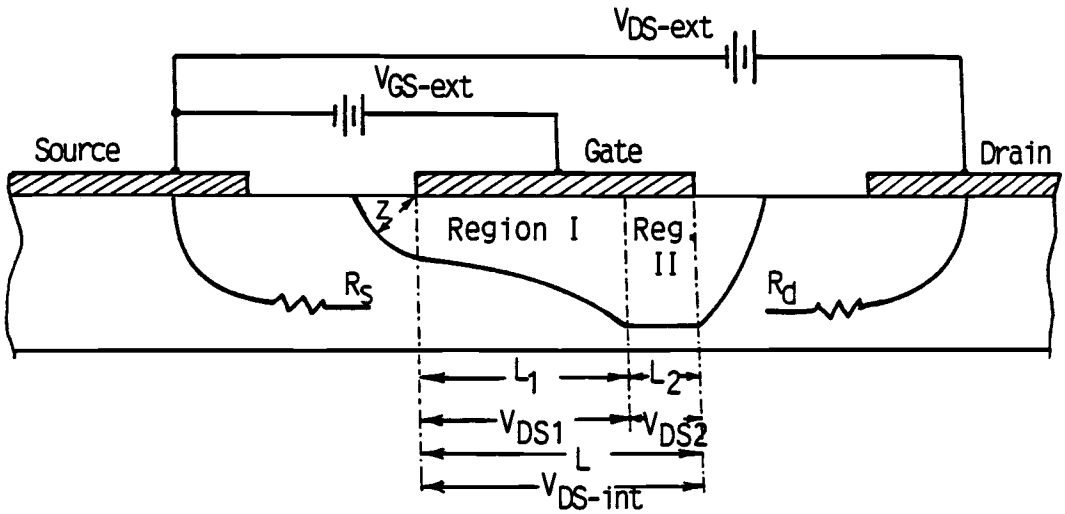

Fig. 3-2: The MESFET structure showing the internal and external voltages. (After Neidert and Scott[18])

In region I, assuming the gradual channel approximation, the potential variation in the vertical direction is much greater than that in the longitudinal direction, and the Poisson's equation for the abrupt depletion approximation is applicable. That is,

$$\nabla^2\phi = -\frac{\rho}{\epsilon} = -\frac{q\,N_D}{\epsilon_o\epsilon_r} \qquad (3)$$

Where ϕ is the potential, ϵ_r is the dielectric constant of the GaAS, ρ is the volume charge density, q is the electronic charge, and N_D is the doping density. The integration of this equation with appropriate boundary conditions yields:

$$\phi = -\frac{\rho}{\epsilon}\frac{y^2}{2} + \frac{\rho}{\epsilon}by + \left[\frac{\rho a^2}{2\epsilon} - \frac{\rho ab}{\epsilon}\right]$$

$$= \frac{\rho}{2\epsilon}\left[a^2 - y^2 + 2b(y - a)\right] \qquad (4)$$

Where, "a" is the total active layer thickness, "b" is the channel thickness as a function of longitudinal position[91].

By setting $y = b$, the potential along the boundary between the conducting channel and the depletion region is obtained as :

$$\phi_{y=b} = \frac{\rho a^2}{2\epsilon} \left[1 - \frac{b}{a} \right]^2 = V_{po} \left[1 - \frac{b}{a} \right]^2 \qquad (5)$$

Where $V_{po} = (qN_D a^2)/(2\epsilon)$ is the pinch-off voltage.

Applying Ohm's law, the current in the conducting channel is given by:

$$I_{ds1} = q\mu_o N_D b W \frac{\partial \phi}{\partial x} \qquad (6)$$

Where, μ_o is the carrier low field mobility, which is assumed constant in region I;

W is the total gate width; and

$\partial\phi/\partial x$ is the longitudinal electric field.

After an integration over region I length L_1 :

$$I_{ds1} = \frac{q\mu_o N_D W a}{L_1} (f_1) \qquad (7)$$

Where,

$$f_1 = p^2 - s^2 - \frac{2}{3} (p^3 - s^3) \qquad (8)$$

With,

$$p^2 = \frac{(V_{Bi} - V_{GS} + V_{ds1})}{V_{po}} , \qquad (9)$$

and $$s^2 = \frac{(V_{Bi} - V_{GS})}{V_{po}} \qquad (10)$$

V_{Bi} is the metal-to-semiconductor built-in voltage. V_{Bi} and V_{po} are taken as positive voltages.

V_{GS} and V_{DS} are the intrinsic gate-to-source and drain-to-source voltages, respectively.

V_{ds1} is the intrinsic drain-to-source voltage drop across region I.

The current in region II at the boundary between the two regions is given by :

$$I_{ds2} = q\mu_o N_D b_1 W E_s \qquad (11)$$

Where, E_s is the longitudinal field which is required to cause carrier velocity saturation; and

b_1 is the channel thickness at this point; it is given by :

$$b_1 = a - d_{max} = a - \left[\frac{2\epsilon}{qN_D} (V_{Bi} - V_{GS} + V_{ds1}) \right]^{\frac{1}{2}}$$

$$= a - \left[\frac{2\epsilon}{qN_D} \frac{V_{po}}{V_{po}} (V_{Bi} - V_{GS} + V_{ds1}) \right]^{\frac{1}{2}}$$

$$= a - ap = a(1 - p) \qquad (12)$$

Therefore, $I_{ds2} = q\mu_o N_D a W E_s (1-p)$ (13)

Current continuity between the two regions requires that I_{ds1} given by equation (7) and I_{ds2} given by equation (13), be equal; this gives :

$$L_1 = \frac{V_{po}\, f_1}{E_s (1 - p)} \qquad (14\text{-a})$$

$$L_2 = L - L_1 = L - \frac{V_{po}\, f_1}{(1 - P) E_s} \qquad (14\text{-b})$$

To find the voltage drop in region I, one can integrate the longitudinal electric field over the length of the region, L_1. Therefore,

$$V_{ds1} = \int_{x=0}^{x=L_1} E_{1ong.} dx = \int_{x=0}^{x=L_1} - \left[\frac{d\phi_I}{dx} \right] dx \qquad (15)$$

As shown in Pucel et al.[14],

$$V_{ds1} = V_{po} (p^2 - s^2) \qquad (16)$$

In region II, the potential distribution can be found by using the solution of the two-dimensional Laplace's equation, $\nabla^2\phi_{II} = 0$. However, the solutions are not easily found for any arbitrary planar MESFET's geometry. Shockley[19] proposed an approximation to simplify the problem by assuming that the physical shape of the drain conductor follows the shape of the equi-potential lines far away from the drain. Grebene and Ghandi[20] and Pucel et al.[14] adopted the same approximation. Since this is not the case in planar MESFETs, a constant CDR2 was included in the program to affect the amount of voltage drop in region II. Of course, the form of the analytical expression is maintained :

$$V_{ds2} = \int_{x=L_1}^{x=L} - [\frac{d\phi_{II}}{dx}]dx \qquad (17)$$

The approximated solution at $y = \delta$, is:

$$V_{ds2} = \frac{2(a-\delta)}{\pi} E_s \sinh[\frac{\pi(L-L_1)}{2(a-\delta)}] \qquad (18)$$

Note that "a" has been replaced by $(a-\delta)$ to account for the finite thickness of the conducting channel in region II. The total (internal) voltage drop across the intrinsic transistor is :

$$V_{DS\text{-}int} = V_{po}(p^2-s^2) + \frac{2E_s(a-\delta)}{\pi} \sinh[\frac{\pi}{2(a-\delta)} \{L - \frac{V_{po}f_1}{(1-p)E_s}\}] \qquad (19)$$

The measurable drain-to-source voltage is:

$$V_{DS\text{-}ext} = V_{DS\text{-}int} + I_{DS}(R_s + R_d) \qquad (20)$$

and the accessible gate-to-source voltage is:

$$V_{GS\text{-}ext} = V_{GS\text{-}int} + I_{DS} R_s \qquad (21)$$

The current is given by:

$$I_{DS} = q\mu_o N_D a W V_{po}[(d^2-s^2) - (2/3)(d^3-s^3)]/L \qquad (22)$$

Where,

$$d^2 = \left[\frac{V_{Bi} - V_{GS} + V_{DS}}{V_{po}} \right] \qquad (23)$$

Again, V_{GS} and V_{DS} are the internal voltages.

The operating point can be found by varying the position of the boundary between the two regions until the calculated V_{GS} and V_{DS}, in addition to the calculated voltage drops across the parasitic resistance R_s and R_d, become equal to the applied V_{GS} and V_{DS} respectively. Although OSUFET allows L_1 to overshoot and be temporarily larger than the total length L due to the iterative nature of the solution method, the final value of L_1, after convergence, is less than L. Otherwise this indicates that the bias levels were such that there is no region II, and the problem will be resolved completely by using the equations that are applicable for region I only.

3.3.2 : Current-Voltage Calculations :

The drain-source current calculated in equation (22) represents the major component of the actual total current, which is due to carrier flow in the undepleted device channel. The second component is the substrate current resulting from the electron injection into the adjacent substrate when a stationary Gunn domain exists in the channel. Eastman and Shur[92] found that the substrate current can be expressed as :

$$I_{sub} \propto W\ (\ N_D\ )^{\frac{1}{4}}\ (\ V_{DS\text{-}int}\ )^{\frac{1}{2}} \qquad (24)$$

However, Neidert and Scott[18] introduced a constant, AK, to achieve a strong agreement between the analytical expression given by equation (24) and the measured data. In OSUFET, the substrate current is given as :

$$I_{sub} = (AK)\ v_{sat}\ W\ [\ q\epsilon V_{DS\text{-}int}\ \sqrt{N_D\ n_{cr}}\ ]^{\frac{1}{2}} \qquad (25)$$

Where, n_{cr} is the characteristic value of the electron concentration [92].

The third component is the simple resistive leakage current across the top surface of the transistor due to surface defects, or through the substrate due to either its higher conductivity (higher than the desirable one) or the doping "tail"[18], as shown in Fig.3-3. Neidert and Scott suggested a fixed shunt resistance, RSHUNT, to model the effect of this component.

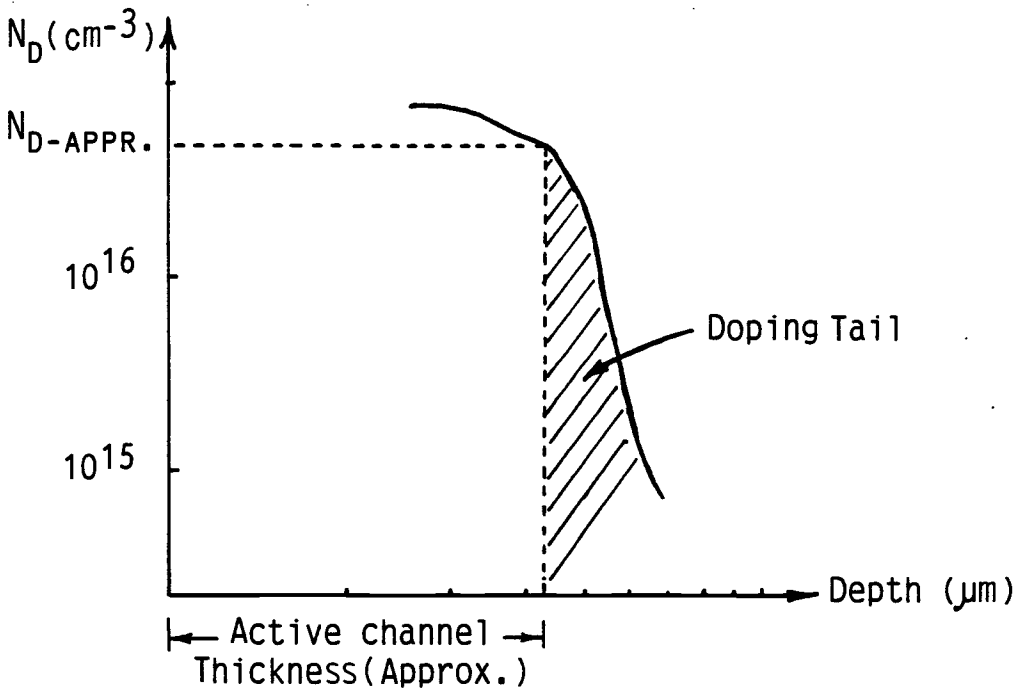

Fig. 3-3 : Doping profile showing the doping "tail". (After Neidert and Scott[18])

3.3.3 : Thickness of The Conducting Channel in Region II :

In region II, where the carrier velocity reaches its saturation value, a finite thickness of a conducting channel must exist to carry the current. This thickness is given by:

$$\delta = \frac{I_{DS}}{qN_D W v_{sat}} \qquad (26)$$

Where, v_{sat} is the assumed electron saturated velocity. Although, some authors [14,20] have hinted that this thickness may be disregarded in the solution of the potential equation in region II, it is found that it has a significant effect in the calculation of the device electrical parameters such as the output resistance.

3.3.4 : Calculation of Temperature Effects on a GaAs MESFET :

A good review of the calculation of the temperature effects on a GaAs MESFET based on the knowledge of thermal resistance of the device in actual operation, and the variation of the device's low field mobility with temperature is given by Neidert[18].

The low field mobility value is adjusted, for the temperature rise resulting from the bias power dissipation as :

$$\mu_o\ (T) = \mu_o(300°K)[(300 + R_{th}\ P_D)/300]^{-0.7} \qquad (27)$$

Where, R_{th} is the thermal resistance in C° per watt, and P_D is the total power being dissipated by the device. $P_D = V_{DS} I_{DS}$ (28)

3.3.5 : Transit Time :

The transit time in GaAs MESFETs is given by:

$$\tau = \tau_1 + \tau_2 = \frac{L_1}{v_{aveage}} + \frac{L_2}{v_{saturation}} \qquad (29)$$

Where,

$$v_{averge} = \mu_o E_{average} = \mu_o \frac{V_{ds1}}{L_1} , \qquad (30)$$

and, $V_{ds1} = V_{po}(p^2 - s^2)$ as mentioned before.

If there is no region II, then $L_2 = \tau_2 = 0$ and :

$$V_{ds1} = V_{po}(d^2 - s^2). \qquad (31)$$

3.4 : SMALL-SIGNAL PARAMETERS :

The small-signal model and its physical origin are shown in Fig. 3-4. The electrical parameters are calculated as follows :

3.4.1 : The Transconductance :

When the bias level is high enough to create velocity saturation region under the gate, the transconductance can be calculated from the equation derived by Statz et al.[85] as :

$$g_m = - \left. \frac{\partial I_{DS}}{\partial V_{GS}} \right|_{V_{DS} = constant} = \frac{aq\mu_o N_D W E_s}{V_{po}} f_g \qquad (32)$$

Where,

$$f_g = \frac{\cosh[\pi L_2/\{2(a-\delta)\}][1-s] - (1-p)}{\cosh[\pi L_2/\{2(a-\delta)\}][2p(1-p) + E_s L_1/V_{po}] - 2p(1-P)} \qquad (33)$$

In this equation, the channel thickness "a" is replaced by $(a-\delta)$ to account for the finite undepleted channel thickness in region II, which is neglected by Statz et al.

If region II does not exist, equation(33) reduces to :

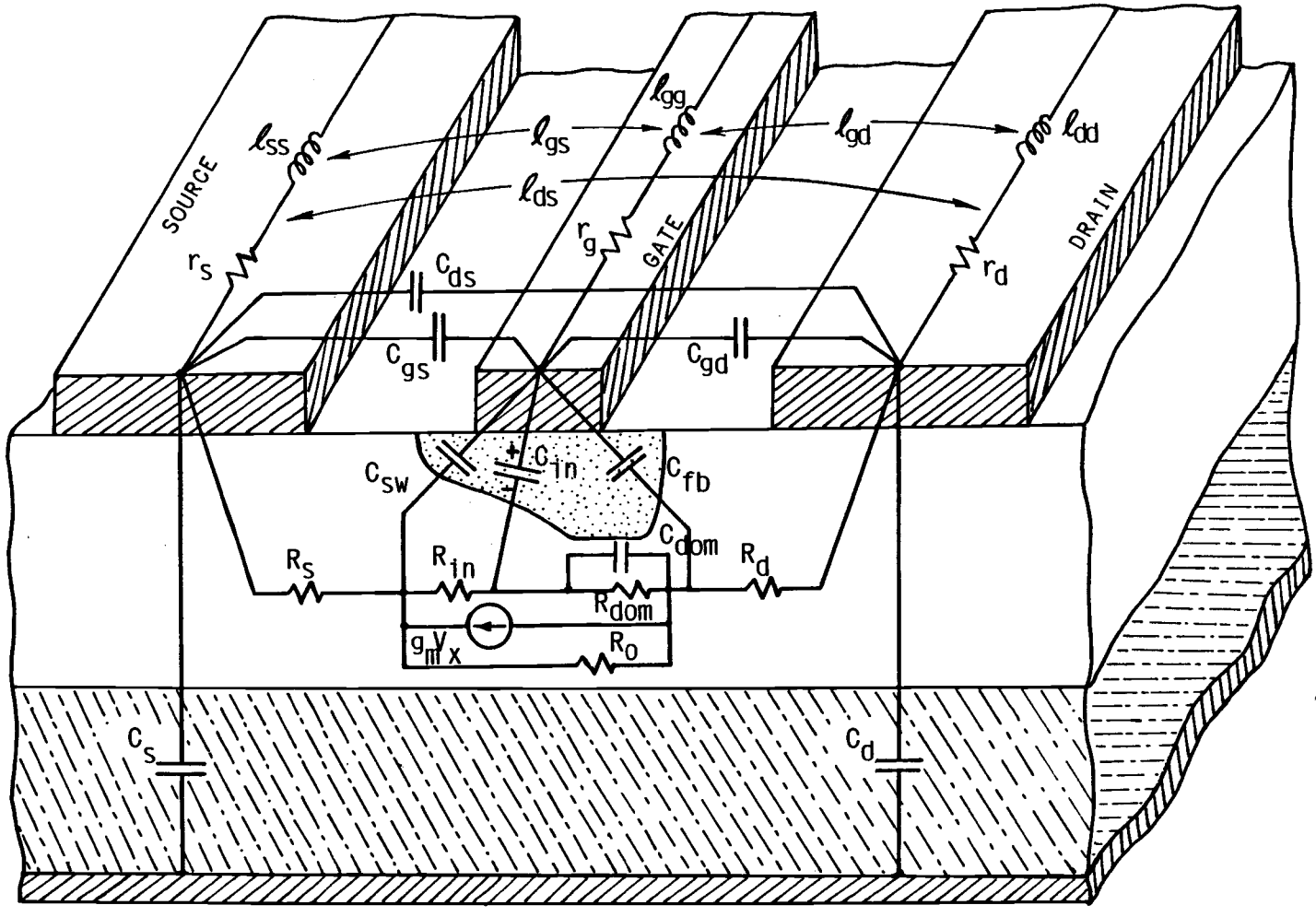

Fig. 3-4-a: The physical origin of the circuit elements of the GaAs MESFET.

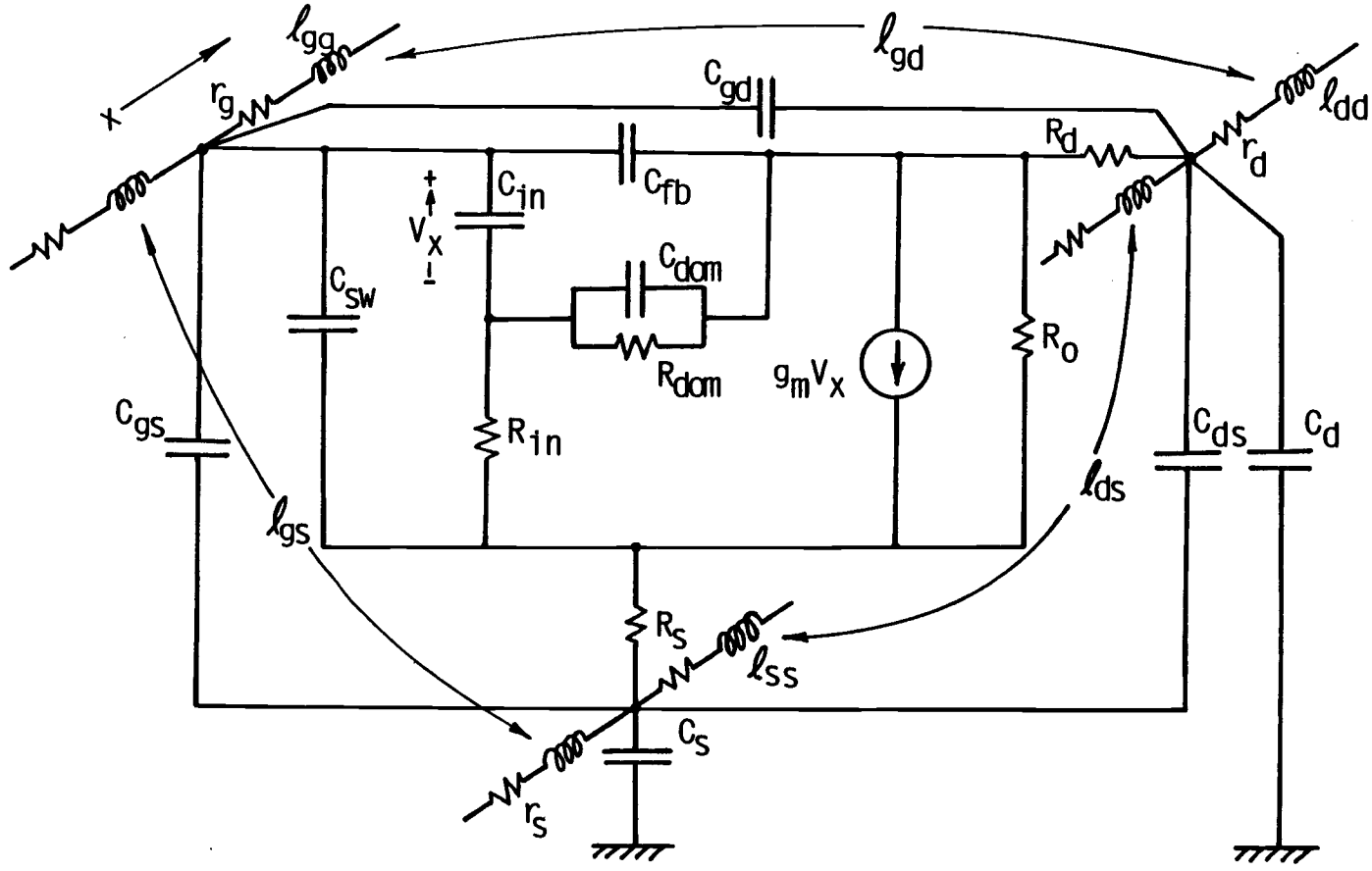

Fig. 3-4-b: Equivalent circuit representation of the GaAs MESFET.

$$f_g = \frac{V_{po}(d-s)}{LE_s} \quad , \qquad (34)$$

and equation (32) becomes :

$$g_m = q\mu_o N_D a W(d-s)/L \qquad (35)$$

The transconductance, g_m, is a nonlinear element. It is a function of the bias voltage as demonstrated by the small-signal scattering-parameter measurements made by Willing et al.[16].

3.4.2 : The Input Resistance :

Even today, it is not clear how to calculate the input or the gate-to-channel resistance, R_{in}. Willing et al.[16] measured R_{in} and the input capacitance, C_{in}, verses V_{DS} with different V_{GS} values for a particular transistor by using small-signal S-parameters. These measurements demonstrate the nonlinear nature of these elements.

For a drain voltage between 1 and 4 volts, it is assumed that the high field at the drain end of the gate is near the threshold that characterizes the Gunn domain formation and this range is difficult to model. For drain voltage higher than 3 volts, there is a proportional relationship between the input conductance and capacitance. That is the product of the input resistance and capacitance is about equal to the transit time. The input resistance is given as :

$$R_{in} = \frac{\tau}{R_{in\text{-}fit} \times C_{in}} \qquad (36)$$

Where $R_{in\text{-}fit}$ is a fitting constant used to fit the measured data.

OSUFET generates two values for R_{in}; one value is obtained by ignoring the presence (effect) of the Gunn domain, where $R_{in\text{-}fit}$ is

set to one, and the second value accounts for the presence of the Gunn domain.

3.4.3 : The Output Resistance :

The output resistance consists of three resistances in parallel, the intrinsic output resistance, the resistance associated with the leakage current, and the resistance associated with the substrate injection current due to the presence of the Gunn domain.

The intrinsic output resistance is defined as :

$$R_o = \left.\frac{\partial V_{DS}}{\partial I_{DS}}\right|_{V_{GS}= \text{ constant}} \qquad (37)$$

Statz et al.[85] derived the analytic expression as :

$$R_o = \frac{2pV_{po}}{q\mu_o N_D E_s aW}\left[\cosh\left(\frac{\pi L_2}{2a}\right) - 1\right] + \frac{L_1 \cosh(\pi L_2/2a)}{q\mu_o N_D aW(1-p)} \qquad (38)$$

But as mentioned before, Statz et al. neglected the conducting channel thickness in region II. Neidert and Scott[18] considered this finite thickness; they found that:

$$R_o = R_{o1} + R_{o2} \qquad (39)$$

Where R_{o1} is given by equation (38) with "a" replaced by (a-δ), and :

$$R_{o2} = \frac{2}{q\mu_o N_D W}\left[\frac{\pi L_2}{2(a-\delta)}\cosh\left\{\frac{\pi L_2}{2(a-\delta)}\right\} - \sinh\left\{\frac{\pi L_2}{2(a-\delta)}\right\}\right] \qquad (40)$$

They reported, however, that almost all of the drain resistance correction comes from the substitution of (a-δ) for "a" in equation (38). When there is no region II, R_{o2} disappears, L_2 is zero, L_1 is L, "d" replaces "p", and :

$$R_o = \frac{L}{q\mu_o N_D a W(1-d)} \qquad (41)$$

The second resistance is a shunting one, which is introduced to account for the surface leakage, and the substrate leakage due to overall higher conductivjty and to the doping tail as described earlier. This is given as a fixed constant called, RSHUNT, in the program.

The third resistance is the one which is associated with the substrate injection current around the Gunn domain. If the Gunn domain can not form for any reason, this resistance is set to infinity. By assuming that most of the drain voltage is dropped across the Gunn domain, the substrate resistance can be obtained from the substrate current as follows :

$$R_{sub} = \frac{1}{g_{sub}} = \left(\frac{\partial I_{sub}}{\partial V_{DS}}\right)^{-1} = \frac{2V_{DS}}{I_{sub}} \qquad (42)$$

Finally, the output resistance is a nonlinear element as shown by the measured data provided in [16].

3.4.4 : Gunn Domain; Resistance and Capacitance :

In addition to the effect of the Gunn domain on the input capacitance and resistance, and the feedback capacitance, the Gunn domain also has its own resistance and capacitance. Although these terms are not by themselves dominant, the domain's effect on the three terms, mentioned above, are much more significant.

The criteria for the existence of the Gunn domain are described by Yamaguchi et al.[90] as :

if: $a \leq W_{th}$: No Gunn domain;

$W_{th} \leq a \leq 2W_{th}$: Stationary Gunn domain; (43)

$a \geq 2W_{th}$: Propagating Gunn domain.

Where "a" is the total active layer thickness, and "W_{th}" is the threshold width given by :

$$W_{th} = \left[\frac{2\epsilon}{qN_D}\left(V_{Bi} - V_{GS} + E_{th}L \right)\right]^{\frac{1}{2}} \qquad (44)$$

E_{th} is the field at which velocity saturation begins.

In microwave MESFETs, the active layer thickness is normally not sufficient for the domain propagation.

Besides Butcher[93,94], Shur and his co-worker have investigated this area [15,84,92,95-100]. The details of their approach are not repeated here.

The Gunn domain resistance is given by [84] :

$$R_{dom} = \left.\frac{\partial V_{Dom}}{\partial I_{sat}}\right|_{V_{GS}= \text{ constant}} = \frac{1.46}{D_S W(a-a_o)}\left[\frac{\epsilon V_{dom}^3}{q^3(N_D n_{cr})^{3/2}}\right]^{\frac{1}{2}} \qquad (45)$$

Where,

D_S : Diffusion coefficient at saturation.

a_o : Depletion layer (under the gate) thickness.

n_{cr}: Characteristic doping density. It is given by :

$n_{cr} = \epsilon\mu_o E_c^2 /(qD_S)$; [For GaAs, $n_{cr} \simeq 3.10^{15}$ cm^{-3}]. (46)

E_c : Characteristic value of the electric field. It depends on the shape of v(E) curve. It is given by:

$$E_c = \left[\frac{1}{\mu_o}\int_{E_S}^{E_V}\{v(E)-v_S\}dE\right]^{\frac{1}{2}} \simeq \left[(E_p-E_S)E_V/2\right]^{\frac{1}{2}} \qquad (47)$$

v_S : Saturation drift velocity.

E_V : Electric field of electron velocity saturation.

E_p : Electric field at which the drift velocity reaches its maximum value.

E_s : Sustaining domain field = v_{sat}/μ_o. (48)

V_{dom}: Domain voltage = $4\sqrt{2}\, D_X E_C^3/\{3(E_{out}-E_s)^2\}$ (49)

$V_{dom} \simeq V_{DS}$ (50)

D_X : $\sqrt{\epsilon_o KT/qN_D}$: Debye length.

K : Boltzmann constant, and T is the temperature (K°).

E_{out}: The longitudinal field at drain end of the gate and the junction between the channel and the substrate.

The measured data provided by Willing et al.[16] show the nonlinearity of the Gunn domain resistance.

The domain capacitance is given as [84]:

$$C_{dom} = \left.\frac{\partial Q_{dom}}{\partial V_{dom}}\right|_{V_{GS}=constant} = 0.364\, W\,(a-a_o)(N_D n_{cr})^{\frac{1}{4}}\left(\frac{q\epsilon}{V_{dom}}\right)^{\frac{1}{2}} \quad (51)$$

Again, $V_{dom} \simeq V_{DS}$

$$Q_{dom} = 0.728\,(a-a_o)(N_D n_{cr})^{\frac{1}{4}}\,(q\epsilon V_{dom})^{\frac{1}{2}} \quad (52)$$

3.4.5 : The Input Capacitance :

The input capacitance, C_{in}, or the gate-to-channel capacitance is a depletion region capacitance; it can be obtained as :

$$C_{in} = \left.\frac{\partial Q_{total}}{\partial V_{GS}}\right|_{V_{DS}=costant} \quad (53)$$

As mentioned before, C_{in} is not only a strong function of bias conditions, but also its value is affected by the presence or absence of the Gunn domain.

OSUFET calculates C_{in}, when the Gunn domain effect is neglected,

by utilizing Pucel's equation [14]:

$$C_{in} = \in W f_c(s,p,\xi) \tag{54}$$

Where,

$$f_c = f_{c1} + f_{c2} + CF \tag{55}$$

$$\xi = LE_s/V_{po} \tag{56}$$

$$f_{c1} = \frac{2L_1}{f_1(a-\delta)}\left[f_g\left\{\frac{2p^2(1-p)^2 + f_2}{1-p}\right\} - s(1-s)\right] \tag{57}$$

: represents the contribution of region I.

$$f_{c2} = \frac{2L_2}{(a-\delta)} f_g + (1-2pf_g)\left[\frac{2pV_{po}}{(a-\delta)E_s\cosh[\pi L_2/2(a-\delta)]} + \tanh\frac{\pi L_2}{2(a-\delta)}\right] \tag{58}$$

: represents the contribution of region II.

CF: Constant represents the fringing capacitance. Since the fringing capacitances between the electrodes are calculated separately in our analysis, this term may be cancelled by setting CF equal to zero in the program input.

f_1 and f_g are as given in equations (8) and (34) respectively.

$$f_2 = (2/3)(p^3 - s^3) - (1/2)(p^4 - s^4) \tag{59}$$

When region II does not exist, equation(55) reduces to :

$$f_c = f_{c1} + CF \tag{60}$$

With,

$$f_{c1} = \frac{2L}{af_1}\left[f_g\left\{\frac{2d^2(1-d)^2 + f_2}{1-d}\right\} - s(1-s)\right] \tag{61}$$

$$f_g = \frac{V_{po}(d-s)}{LE_s} \tag{62}$$

and "d" replaces "p" in f_1 and f_2 equations.

The calculation for C_{in}, when the Gunn domain is taken in account, follows the analysis of Shur[84]. In this case, the total

positive charge under the gate is represented as :

$$Q_{total} = Q_g + Q_e + Q_{dom} \qquad (63)$$

Where Q_g is the charge in the depletion area under the gate, Q_e is the charge of the extended depletion area beyond the gate toward the drain, and Q_{dom} is the charge of the high-field domain. See Fig. 3-5.

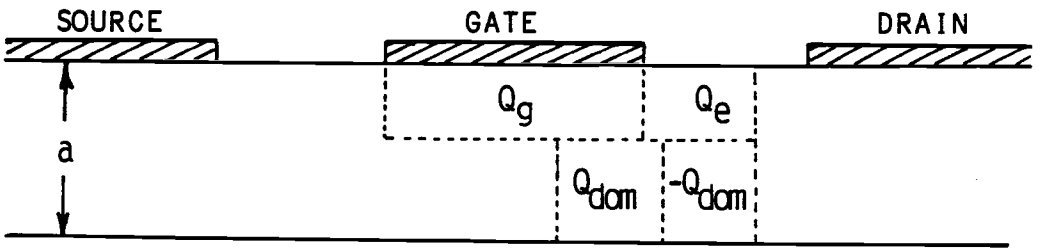

Fig. 3-5 : Conceptual charge arrangement for capacitance calculation. (After Shur[84])

For small drain-to-source voltage :

$$C_{in-o} = \frac{LW}{2\sqrt{2}} \left[\frac{\epsilon q N_D}{V_{Bi} - V_{GS}}\right]^{\frac{1}{2}} \qquad (64)$$

This is half of the well-known depletion layer capacitance.

For large drain voltage :

$$C_{in} = C_{fit}\left[2C_{in-o} + 1.46(PCDG)\epsilon W\left(\frac{N_D}{n_{cr}}\right)^{\frac{1}{4}}\left(\frac{V_{Bi}-V_{GS}}{V_{DS}}\right)^{\frac{1}{2}}\left(1 - \frac{V_{Bi}-V_{GS}}{V_{DS}}\right)\right] \qquad (65)$$

Where C_{fit} is a constant used in OSUFET to fit the measured data, and PCDG is another numerical constant.

An interpolation routine has been provided in OSUFET to calculate C_{in} when the drain voltage is between zero and half the pinch-off voltage because the experimental data indicate that in this range neither equation (64) nor (65) predicts the capacitance value accurately.

3.4.6 : Feedback Capacitance :

Pucel et al.[14] suggested that the gate-to-drain capacitance is a parasitic one; it is a fringing capacitance and does not depend on the bias conditions. But the measured data[16] shows that this capacitance is indeed a function of the bias voltages. For a common-source MESFET model used in this study, the capacitance between the gate and the drain consists of two parallel capacitances. The mutual (inter-electrode) capacitance which depends on the geometry and the dielectric constant of the substrate. It is a fringing capacitance and does not depend on the potentials of the corresponding electrodes. The second one is the feedback capacitance (C_{fb}). It represents the depletion region capacitance part which is associated with the drain. This capacitance is, of course, a bias condition function.

The model developed by Shur[84] to calculate C_{fb} is used here. When drain-to-source voltage approaches zero, the depletion region under the gate is symmetric, as shown in Fig. 3-6-a, and therefore;

$$C_{fb} = C_{in-o} \qquad (66)$$

Note that C_{fb}+C_{in-o} is equal to the total capacitance of the depletion layer. For large drain voltage, depleted region is shifted towards the drain as shown in Fig. 3-6-b, and the capacitance is given as :

$$C_{fb} = 1.46(PCDG)\in W\left[\left(\frac{V_{Bi} - V_{GS}}{V_{DS}}\right)\left(\frac{N_D}{n_{cr}}\right)\right]^{\frac{1}{2}} \qquad (67)$$

Again, PCDG is the same fitting constant used in equation (65).

To get good agreement between the calculated and measured data, the measured data have been used to interpolate between equations(66) and (67) for V_{DS} between zero and half the pinch-off voltage.

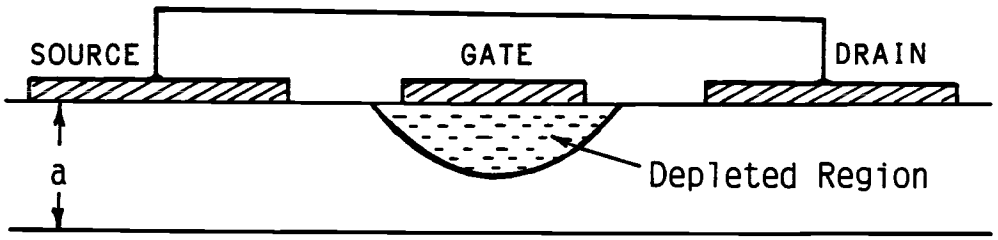

Fig. 3-6-a: Symmetric depletion region under the gate when the source and drain potentials are equal.

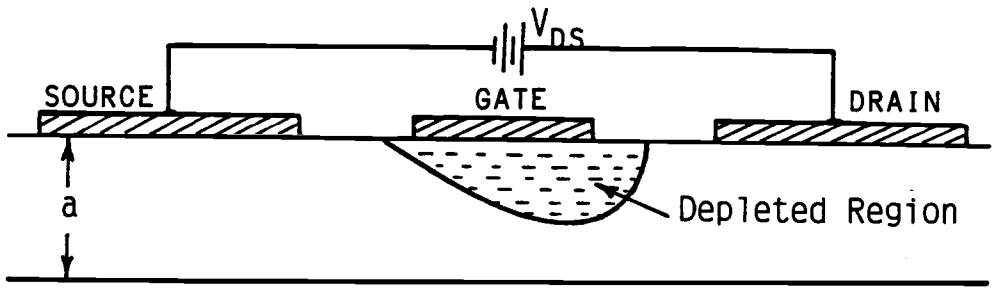

Fig. 3-6-b: Asymmetric depletion layer because of the difference in the drain and source potentials.

3.4.7 : Sidewall Capacitance :

The sidewall capacitance, C_{SW}, is the capacitance between the gate and the source due to the extension of the depletion region from under the gate in the direction of the source as shown in Fig. 3-7.

Measurements made by Willing et al.[16], using C-V profiles and the S-parameters indicate the existence of this capacitance. The analytical equations to calculate C_{SW} have been reported in [18]. For a depletion depth less than the full active layer thickness, the charge depleted from the quarter circle adjacent to the gate is:

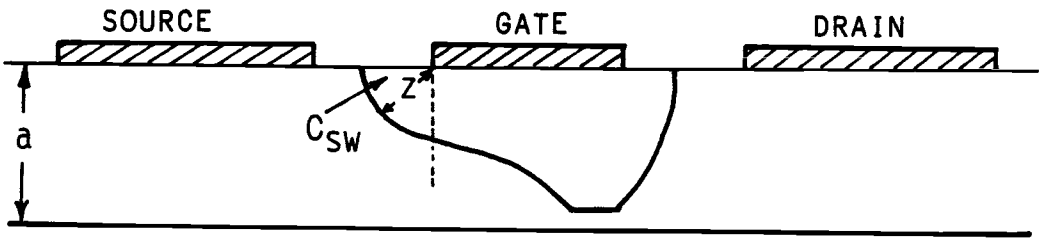

Fig. 3-7 : The physical origin of side-wall capacitance.

$$Q_{SW} = (\pi z^2/4) q N_D W \tag{68}$$

Where "z" is the radius of the sidewall depletion area.

Applying Poisson's equation for an abrupt junction gives the voltage as :

$$V = \frac{z^2 q N_D}{2\epsilon} \tag{69}$$

Therefore, the capacitance is :

$$C_{SW}\Big|_{V \le V_{po}} = \frac{dQ_{SW}}{dV_{GS}} = \frac{\pi \epsilon W}{2} \tag{70}$$

When the gate-to-source voltage is larger than the pinch-off voltage, an approximation value is given by :

$$C_{SW}\Big|_{V \ge V_{po}} = \epsilon W \sin^{-1}[\sqrt{(V_{po}/V_{GS})}] \tag{71}$$

3.5 : *PARASITIC PARAMETERS* :

The parasitic circuit elements are those external to the region under the gate as shown in Fig. 3-8. These include the series source and drain resistances, the fringing capacitances between the electrodes, the self and mutual inductances, the electrode resistances and self and pad capacitances.

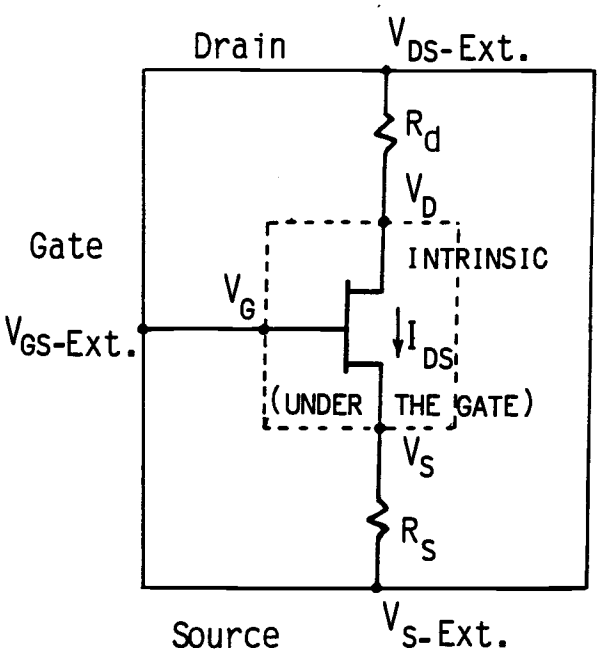

Fig. 3-8 : The parasitic circuit elements.

3.5.1 : *Drain and Source Resistances* :

The drain (source) resistance, R_d(R_s), is the resistance between the drain (source) and the channel under the gate. It consists of contact (or ohmic) resistance, R_{co}, and the active layer resistance, R_{ch}:

$$R_{d,s} = R_{co} + R_{ch} \qquad (72)$$

The ohmic metal-semiconductor resistance expression derived by

Berger[101], Murrmann and Widmann[102] and further simplified by Fukui[17] is given by:

$$R_{co} = R_1 \simeq \frac{2.1}{Wa_1^{0.5}N_1^{0.66}} \qquad (73)$$

The series active layer resistance is given as:

$$R_{ch} = \frac{1.1\ L_s}{Wa_2N_2^{0.82}} \qquad (74)$$

Here W(in mm units) is the gate width, N_1 is the doping concentration under the electrode, which is usually n^+, N_2 is the doping density of the active layer between the electrode and the gate. N_1 and N_2 are both in 10^{16} cm^{-3} units. a_1(a_2) is the active layer thickness under the electrode (between the gate and the electrode under consideration); both a_1 and a_2 are in μm units. L_s is the separation between the electrode and the gate in μm units.

If the active layer between a given electrode and the gate consists of more than one region due to change in either the doping level or the active layer thickness or both, then:

$$R_{ch} = R_2 + R_3 + R_4 + \ldots\ldots \qquad (75)$$

Where,

$$R_i = \frac{1.1\ L_i}{Wa_iN_1^{0.82}}\ , \qquad i = 2,3,4,\ldots \qquad (76)$$

3.5.2 : Interelectrode (Fringing) Capacitances :

These are fixed capacitances. They are independent of bias voltages, but depend on the device geometry, namely on electrode widths, spacings between them, and the dielectric constant of the substrate. These mutual capacitances are the fringing field capacitances.

Pucel et al.[14] suggested the use of Smythe theory[21] to calculate the fringing capacitances, C_{gs}, C_{gd} and C_{ds}. Both Pucel et al. and Neidert and Scott[18] ignored the effect of the gate-line presence in the drain-to-source capacitance, C_{ds}, calculation and the effect of the drain- (source-) line existance in the calculation of the gate-to-source capacitance, C_{gs} (or gate-to-drain capacitance, C_{gd}). A method of calculating the exact values of these capacitances using conformal mapping technique has been developed and is discussed in detail in chapter 4. OSUFET has the routines to calculate the exact values of these capacitances.

3.5.3 : Electrode Inductances :

The self and mutual inductances per unit length of the transistor's electrodes are obtained from

$$[L] = [C_{air}]^{-1}/v_1^2 \qquad (77)$$

Where v_1 is the light velocity in the free space, and $[C_{air}]$ is the matrix consisting of self and mutual electrode capacitances per unit length evaluated in a free space (or air).

3.5.4 : Electrode Resistances :

Over the band of frequencies, when the skin depth is larger than one-half of the line's shorter dimension transverse to the wave propagation direction (line length or thickness), the resistance is given by the dc value and the current is almost uniform. At higher frequencies, the resistance increases due to the skin depth and the

corresponding corrections can be made as in [103]. Because the gate-line is so narrow and long in the direction of the wave propagation, the resistance of this electrode is very large. The width of the other two electrodes i.e., drain and source is much larger than that of the of the gate; therefore, their resistances are smaller.

3.5.5 : Pad Capacitance :

The pad capacitance can be modeled as a parallel-plate capacitance with a fringing term. It is approximated as[104]:

$$C_{pad} = \pi \in W/[2\ln(H/B)] \qquad (78)$$

Where "B" is the electrode length and "H" is the semi-insulating substrate thickness. However, in OSUFET, the empirical expression by Higashisaka and Hasegawa[105] was implemented. The expression is:

$$C_{pad} = 1.3 \in \frac{WB}{H} + \frac{0.92\in[2(W+B)]}{\log_{10}(10000.H)} \qquad (79)$$

Where W, B, and H are in cm units.

If the substrate is not very thin, this capacitance is very small. The effect of the pad capacitance is more significant for gate-line than for drain-line because the gate-pad is much wider than the gate-line itself.

3.5.6 : Electrode-to-Ground Plane Capacitance :

This is a fringing field capacitance and it is considered in the same manner as a pad. That is, the calculation of such a capacitance is made by using equation (79).

3.6 : THE RESULTS AND DISCUSSION :

The elements of the equivalent small-signal model of a GaAs MESFET were calculated for different bias conditions. The program inputs are the process controlled (geometrical and material) parameters. Example of the device physical parameters and the results of the calculated electrical parameters are shown in tables 3-1 and 3-2 respectively.

Finally, OSUFET seems to be a good design tool. The results calculated by this program for nonlinear elements, which are sensitive to bias conditions, are in good agreement with the measured data obtained by Willing et al.[16].

D E V I C E P A R A M E T E R S

Gate Length [WG]= .400 um;		Gate-to-Drain Saparation [DGL] = 4.000 um	
Gate Width:[See Results Section];		Gate-to-Source Saparation [SGL] = 4.000 um	
Source Width [SL]= 150.00 um;		Matalization Thickness [HGM] = 2.500 um	
Drain Width [DL]= 150.00 um;		Substrate Thickness [H] = 300.00 um	
Gate Pad Width [GPW]= 50.00 um;		Active Layer(under gate) Thickness [A]= .125 um	
Gate Pad Length [GPL]= 50.00 um;		Active Layer(under Sourse & Dr)Thick[A1]= .600 um	
Temprature [TNOM]= 300.00 K;		Layer between Gate & Source(Drain) [A2]= .600 um	

Doping Level [CND] = .2600E+18	Characteristic Doping Level For Gunn Domain[CNCR]=.2000E+16
Saturation 'Field [ES] = 3900.0000	Gate-to-Samiconductor Built in Voltage [VBI]= .800
Saturation Velocity [AVELSAT] = .2100E+08	Relative Dielectric Constant of GaAS [EPS]= 12.900
Low Field Mobility [F0] = 4500.0000	Multiplying Constant of CIN (with Gunn Dom) [CFIT]= 2.2200
Thermal resistance [RTH] = 60000.000	Fringing Term in CIN (with no Gunn Domain) [CF]= 1.560
Diffusion Coefficient [DIF] = 45.0000	High Field Diffusion Coefficient [BDIF]= 35.0000
Test Fixture Resistance [RTFXR]= 0.0000	Feedback Cap. Multiplying Constant [PCDG]= .3200
Dividing Constant of RIN [RINFIT]= 1.1300	Drain-to-Source Shunt Resistance [RSHUNT: Ohm/um]=.9000E+26
Substrate Current Mult. Cons.[AK]= .0000	Parasitic Resistance Multiplying Cons. [PARF]= 1.0000
Area per um of Device width [DP] = 25.0000	Modifies Voltage drope in region II [CDR2]= 3.0000

Dopping Concentration under Source & Drain [CND1] = .2000E+19;

Doping Conc. of Layer between Gate & Source(Drain) [CND2]= .2000E+19;

Resistivity of Gate & Drain lines material = .2214E-04 Ohm .mm

Table 3-1: The physical (geometrical and material) parameters of the GaAs MESFET.

O S U F E T R E S U L T S

The followings are per 1000.0 microns [Gate Width i.e., Device Length]. Obtained on : Thursday; Oct. 29,1987; 12:35 pm

Rg =1.06250 Ohms; Rs = .17719 Ohms; Rd = .17719 Ohms; Cg-pad = .00972 pF; Cgd = .060590 pF;

Cgs = .06059 pF; Cds = .16521 pF; Cs-g.p= .17181 pF; Cd-g.p = .17181 pF; rg =22.1400 rd =.05904

Cgs=Cgd[Air]=.00872pF; Cds[Air]=.02377pF; Lgg = .73600 nH; Ldd = .39500 nH; Lgd = Ldg = .19750 nH

VG	VD	Cur(mA)	Gm(mmho)	Rin(GD;NGD)		Rout	Cin(GD;NGD) pF		Cfb(pF)	Cout	Cdom:pF	Rdom	Csw(pF)	Tau Pse	Cgso	Gunn Dom.
0.0	1.0	368.659	264.602	0.000	2.6834	34.90	1.4013	.906480	.204379	1.62311	.016089	154.35	.007177	2.43246	.344892	Can Form
0.0	2.0	358.594	256.305	1.340	2.7674	86.96	1.6701	.913737	.129686	1.14771	.010232	601.51	.007177	2.52869	.344892	Can Form
0.0	3.0	348.091	248.239	1.378	2.8564	141.8	1.6852	.918901	.102509	.937101	.008107	1212.4	.007177	2.62475	.344892	Can Form
0.0	4.0	338.429	240.974	1.431	2.9424	199.3	1.6797	.922976	.087365	.811553	.006925	1950.3	.007177	2.71576	.344892	Can Form
0.0	5.0	329.658	234.452	1.483	3.0244	259.4	1.6714	.926382	.077386	.725875	.006146	2795.6	.007177	2.80180	.344892	Can Form
-1.0	1.0	166.527	192.799	0.000	3.5787	51.48	.12357	.659702	.281287	1.62311	.006740	411.22	.007177	2.36087	.229928	Can Form
-1.0	2.0	165.004	188.688	2.124	3.6337	115.9	1.0014	.661483	.184429	1.14771	.004421	1458.2	.007177	2.40363	.229928	Can Form
-1.0	3.0	163.868	185.460	1.916	3.6888	181.8	1.1297	.663146	.147156	.937101	.003529	2869.4	.007177	2.44623	.229928	Can Form
-1.0	4.0	162.216	182.250	1.894	3.7500	249.3	1.1638	.664387	.126018	.811553	.003023	4566.5	.007177	2.49142	.229928	Can Form
-1.0	5.0	160.410	179.186	1.913	3.8122	318.5	1.1735	.665399	.111964	.725875	.002687	6507.1	.007177	2.53663	.229928	Can Form
-2.0	1.0	2.774	99.108	0.000	6.4012	292.2	.99947	.487470	.334572	1.62311	.000281	10690.	.007177	3.12041	.184352	Cant Form
-2.0	2.0	3.703	123.944	4.214	5.1331	356.0	.54710	.507532	.224026	1.14771	.000187	35731.	.007177	2.60520	.184352	Cant Form
-2.0	3.0	4.568	140.178	2.615	4.6000	386.2	.82002	.526781	.179850	.937101	.000150	69282.	.007177	2.42320	.184352	Cant Form
-2.0	4.0	5.377	150.505	2.282	4.3342	409.3	.90941	.540979	.154479	.811553	.000128	109666	.007177	2.34471	.184352	Cant Form
-2.0	5.0	6.141	156.585	2.161	4.1987	431.6	.94603	.550185	.137500	.725875	.000114	155964	.007177	2.31007	.184352	Cant Form

For VG = -3.0 v; VBI = .8000 v, and VPO = 2.8493 v, The Device is Beyond Pinchoff !!!

Table 3-2: The electrical parameters of the GaAs MESFET used. [calculated by OSUFET]

CHAPTER 4

ANALYSIS OF COPLANAR STRIPS

4.1 : INTRODUCTION :

Calculations of characteristic impedance and effective dielectric constant of coplanar lines by conformal mapping techniques were presented by Wen[22]. Conformal mapping had also been used by Lin to calculate the resistance between two symmetric shallow collinear contacts[23]. Wen also used this quasi-static analysis to analyze coplanar waveguides[22] and directional couplers[106]. In all these cases, the substrate thickness is assumed to be very large compared to the spacing between strips (slot widths), and the strip thicknesses are assumed to be negligibly small.

Although Wen reported that the substrate thickness becomes less critical with higher relative dielectric constant, Davis et al.[24] found that Wen's analysis is valid only when the substrate thickness is at least twice the slot width. Davis extended Wen's analysis by considering the finite thickness of the substrate. However, the mapping of the free space on the other side of the substrate as an ellipse inside the dielectric space results in an expression which is not simple to solve analytically. In addition, attempts have been made to include the effect of finite thickness of the substrate by using relaxation[107] and Green function[108] methods. Veyres and Hanna[109] and Hanna and Thebault[110] used an analytic function to transform the finite thickness to an infinite one; but this function maps the finite widths of the strips and slots into very wide ones,

especially when the substrate is thin, and as a result, the capacitance values become insensitive to any variation in the strip width.

The effect of the strip metalization thickness has also been reported in a number of papers[25,26,111-116], where numerical methods and empirical results obtained by curve fitting of these results have been used.

With the growth in microwave integrated circuits in recent years, the analysis of such circuits has become important. As a result, many approximate expressions for capacitances between strips have been presented in literature[25,111,117]. For symmetric and asymmetric two strips, analytic expressions were obtained, and the required elliptic integral of the first kind was given in an approximate form[118,119].

In order to estimate the interelectrode capacitances associated with a GaAs MESFET structure, Neidert and Scott[18] adopted Pucel's modification[14] of Smythe's method[21]. The modulus of the elliptic function presented by Neidert is similar to that given by Kneppo[120]. Although the value of the capacitance of any adjacent two asymmetric strips based on Kneppo's formula is exact in the absence of any other strip, existence of a third strip disturbs the electric field distribution and significantly modifies the results. The equation used to evaluate the capacitance of adjacent asymmetric coplanar strips was used to evaluate the drain-to-source capacitance. This equation ignores the presence of the gate line between the other two electrodes and the results become inaccurate.

In this analysis, we have studied the case of asymmetric two strips, three strips, and the capacitive shielding effect by the

central strip as well as the outer strip on the adjacent strips. Closed form expressions which are compatible with the computer aided design of such circuits have also been formulated by using basic curve fitting techniques.

4.2 : CONFORMAL MAPPING METHOD :

4.2.1: Asymmetrical Two-Coplanar Strips :

This analysis is based on the idealized assumption that the metallic strip conductors have zero thickness, the dielectric substrate extends to infinity (very large thickness compared to slot widths), and no other strips are present close to these two lines. The structure of symmetric and asymmetric coplanar strips are shown in Fig. 4-1.

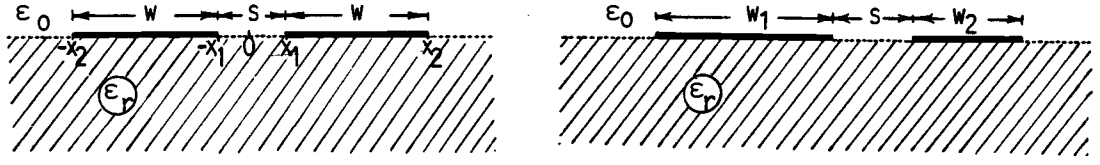

Fig. 4-1 : Two Coplanar Strips,
a : Symmetrical *b : Asymmetrical*

The simplest case of this structure is the symmetric one shown in Fig. 4-1-a, which is solved with the help of Schwartz-Christoffel transformation[23]; the capacitance per unit length of the coplanar symmetric strips is given by :

$$C = \epsilon_{eff} \frac{K'(k)}{K(k)} = (1+\epsilon_r)\epsilon_o \frac{K'(k)}{2K(k)} \qquad (1)$$

Where ϵ_{eff} is the effective dielectric constant of the structure.

$K(k)$ is the complete elliptic integral of the first kind.

$k = X_1/X_2$ is the modulus of the complete elliptic integral. (2)

$K'(k)=K(k')$ and $k'=\sqrt{1-k^2}$; the co-modulus. (3)

The more general case is the case of asymmetric coplanar strips. This structure can be transformed into a symmetric one by using the transformation presented by Hanna[121] as shown in Fig. 4-2, where :

$$t_i = \frac{(S/2)(1+\alpha X_i)}{X_i+\alpha(S/2)^2} \tag{4}$$

$$\alpha = \frac{W_1W_2+(S/2)(W_1+W_2)\pm[W_1W_2(S+W_1)(S+W_2)]^{\frac{1}{2}}}{(S/2)^2(W_2-W_1)} \tag{5}$$

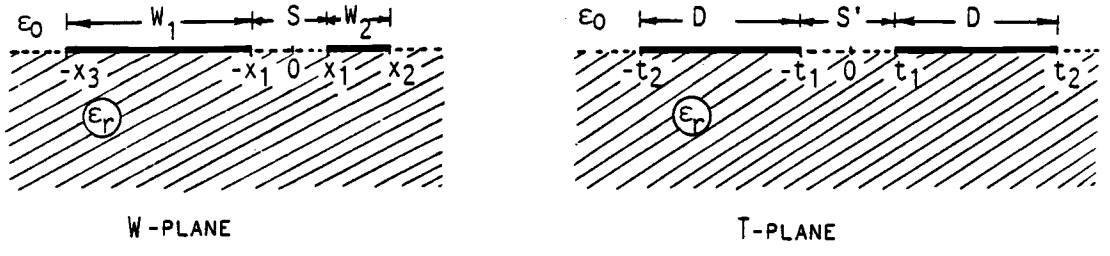

Fig. 4-2 : Transformation of an asymmetrical coplanar strips structure into a symmetrical one.

It is clear that this transformation is not applicable when $W_1=W_2$. The capacitance can be obtained by applying equation (1) with the new dimensions in t-plane, i.e.,

$$k = \frac{t_1}{t_2} = \frac{1}{t_2} = \frac{\alpha(S/2)^2+(S/2)+W_2}{(S/2)[1+\alpha(S/2+W_2)]} = \frac{W_1+(S/2)-\alpha(S/2)^2}{(S/2)[1-\alpha(S/2+W_1)]} \tag{6}$$

Notice that all values of t are normalized by t_1.

The capacitance per unit length of the two asymmetric strips can also be evaluated by applying Kneppo's equation directly[120] :

$$C = (1+\epsilon_r)\epsilon_o \frac{K'(k)}{K(k)} \qquad (7)$$

with, $$k = \left[\frac{S(W_1+S+W_2)}{(S+W_1)(S+W_2)}\right]^{\frac{1}{2}} \qquad (8)$$

We have used an exact method to evaluate the complete and incomplete elliptic integrals of the first kind as introduced by Pearson[122]. The listings of FORTRAN routines are:

```
      FUNCTION  COMELPT(XIN)
C-----------------------------------------------------------------------*
C                                                                       *
C     COMELPT calculates the complete elliptic integral of the first    *
C                                                                       *
C  kind;  K(k).            k = XIN : is the Modulus.                    *
C                                                                       *
C-----------------------------------------------------------------------*
      PI = ACOS(-1.0)
      X  = XIN
      SU = 1.0
      X1 = SQRT( 1.0 - X*X )
1     X  = (1.0 - X1) / (1.0 + X1)
      X1 = 2.0*SQRT(X1)/ (1.0 + X1)
      SU = SU * ( 1.0 + X )
      IF( X .GT. 0.0 )   GO TO   1
      COMELPT = SU * PI /2.0
      RETURN
      END
```

```
      FUNCTION  ELPTINC(PHI,ALPHA)
C-------------------------------------------------------------------*
C                                                                   *
C     ELPTINC  calculates  the  incomplete elliptic integral of the *
C                                                                   *
C   first kind;   F( Phi, Alpha ).   PHI and ALPHA are the angles in *
C                                                                   *
C   radians    ..................................................*
C-------------------------------------------------------------------*
      PI = ACOS(-1.0)
      F  = PHI
      A  = ALPHA
      Xo = SIN(A)
      X  = Xo
      Fa = 1.0
1     F  = (F + ASIN( X*SIN(F) ) )/2.0
      X  = 2.0* SQRT(X) / (1.0 + X)
      Fa = Fa * X
      IF( X .LT. 1.0)  GO TO    1
      ELPTINC = ALOG( TAN(( PI/2.0 + F)/2.0) )* SQRT(Fa/Xo)
      RETURN
      END
```

A very good numerical approximation of a complete elliptic integral was obtained by Smith[118]. It is given by:

$$K(k) = A_0 + A_1k_x + A_2k_x^2 - \ln(k_x)(B_0+ B_1k_x + B_2k_x^2) \qquad (9)$$

Where, $k_x = 1-k^2$ (10)

and

$$\left.\begin{array}{ll} A_0= 1.3862944 & B_0= 0.5 \\ A_1= 0.1119723 & B_1= 0.1213478 \\ A_2= 0.0725296 & B_2= 0.0288729 \end{array}\right\} \qquad (11)$$

Shwartz-Christoffel Transformation of (Two) Asymmetrical-Strips :

Shwartz-Christoffel transformation is one of the most powerful techniques which transform a certain geometry, whose characteristics (impedance, capacitance, etc.) are incalculable, into another one where the characteristics can be calculated easily. "This transformation takes an arbitrary polygon in a W-plane into a series of segments along the real axis in a Z-plane"[123]. The transformation can be found by integrating the following equation[124]:

$$\frac{dw}{dz} = A \prod_{i=1}^{N} (z-x_i)^{-\alpha_i/\pi} \qquad (12)$$

Where, A is an arbitrary constant.

α_i *is an outer angle in radians, as in Fig. 4-3.*

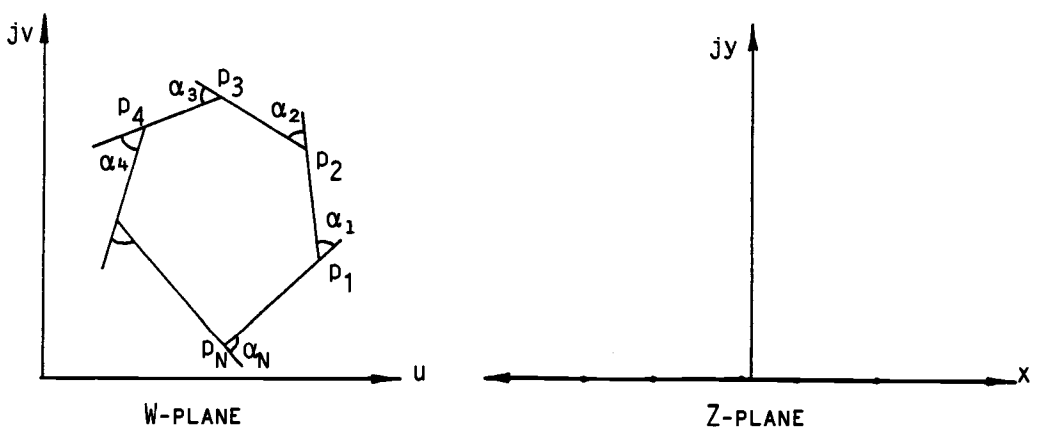

Fig. 4-3: Shwartz-Christoffel Transformation.

If this transformation is applied to the asymmetrical coplanar strips shown in Fig. 4-3-a, it will be transformed into a rectangular form as in Fig. 4-3-b, where :

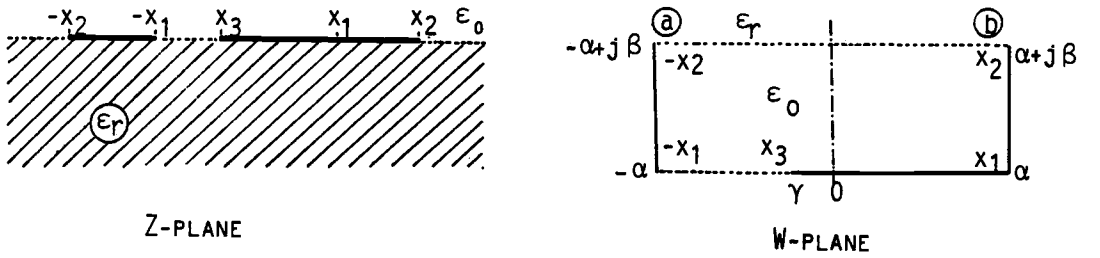

Fig. 4-4 : Asymmetrical Coplanar Strips,
a: Z-Plane. b: W-Plane.

$$\alpha = K(k_o)/X_2 \qquad (13\text{-a})$$

$$\beta = K'(k_o)/X_2 \qquad (13\text{-b})$$

$$\gamma = F(\varphi_o,\theta_o)/X_2 \qquad (13\text{-c})$$

$K(k_o)$ *is the complete elliptic integral of the first kind.*

$$K'(k_o) = K(k_o') \quad \text{and} \quad k_o' = \sqrt{1-k_o^2} \qquad (14)$$

$F(\varphi_o,\theta_o)$ *is the incomplete elliptic integral of the first kind as in reference [125].*

$$k_o = X_1/X_2 \qquad (15\text{-a})$$

$$\varphi_o = Sin^{-1}(X_3/X_1) \qquad (15\text{-b})$$

$$\theta_o = Sin^{-1}(k_o) = Sin^{-1}(X_1/X_2) \qquad (15\text{-c})$$

By mirroring the structure in Fig. 4-4-b about a-b line, the capacitance of Fig. 4-5 becomes twice bigger than that of the original structure.

The final structure shown in Fig.4-6-b represents a coplanar waveguide with :

$$\alpha = K'(k_1)/2t_2 \qquad (16\text{-a})$$

$$\beta = K(k_1)/t_2 \qquad (16\text{-b})$$

$$\gamma = \frac{1}{t_2}\left[\frac{K'(k_1)}{2} - F(\varphi_1,\theta_1)\right] \qquad (16\text{-}c)$$

Where,

$$k_1 = t_1/t_2 \qquad (17\text{-}a)$$

$$k_2 = t_3/t_2 \qquad (17\text{-}b)$$

$$\theta_1 = \cos^{-1}(k_1) = \cos^{-1}(t_1/t_2) \qquad (17\text{-}c)$$

$$\varphi_1 = \sin^{-1}\left[\frac{1}{k_2}\left\{\frac{k_2^2 - k_1^2}{1-k_1^2}\right\}^{\frac{1}{2}}\right] \qquad (17\text{-}d)$$

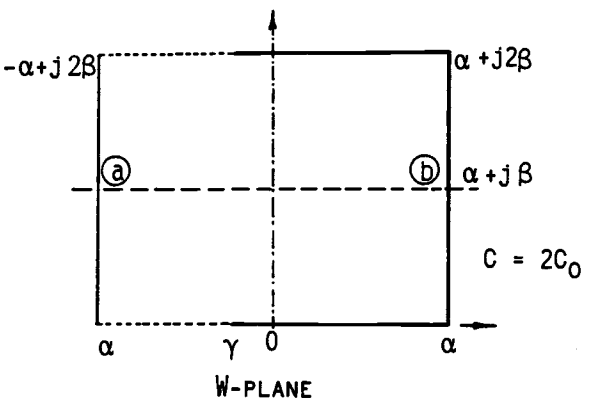

Fig. 4-5: Mirroring Fig.4-4-b about a-b line.

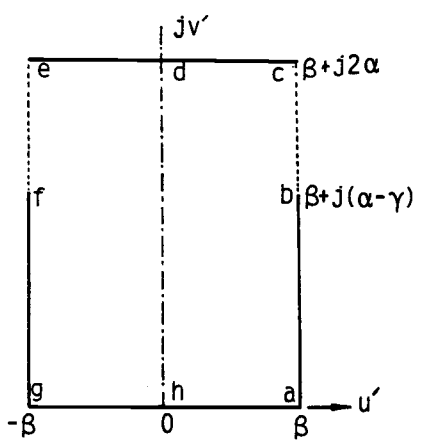

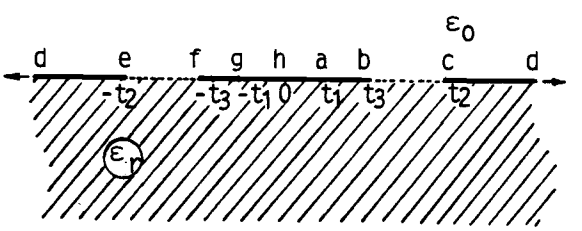

Fig.4-6-a: Rotating Fig.4-5. *Fig.4-6-b: Coplanar waveguide structure.*

Eliminating α, β and γ gives :

$$\frac{K(k_1)}{K'(k_1)} = \frac{K'(k_o)}{2K(k_o)} \tag{18}$$

$$F(\varphi_1,\theta_1) = \frac{K'(k_1)}{2}\left[1 - \frac{F(\varphi_o,\theta_o)}{K(k_o)}\right] \tag{19}$$

Having k_1 and $K(k_1)$ from equation (18), and hence, $F(\varphi_1,\theta_1)$ and θ_1 from equation (19), φ_1 can be deduced. Therefore, k_2 can be obtained from equation (17-d) :

$$k_2 = \frac{t_3}{t_2} = \frac{k_1}{\sqrt{1-(1-k_1^2)\,Sin^2(\varphi_1)}} \tag{20}$$

The capacitance of a coplanar waveguide is introduced in reference[22] as :

$$C = (1+\epsilon_r)\,\epsilon_o\,\frac{2K(k_2)}{K'(k_2)} \tag{21}$$

Since the capacitance of the coplanar waveguide shown in Fig. 4-6-b is twice the capacitance of the original structure, the capacitance per unit length of two asymmetric coplanar strips is :

$$C = (1+\epsilon_r)\,\epsilon_o\,\frac{K(k_2)}{K'(k_2)} \tag{22}$$

4.2.2: Three Coplanar Strips :

The three-line structure to be analyzed is shown in Fig. 4-7. Besides assuming a thick dielectric substrate and infinitesimally thin metallic strips, the structure is assumed to be symmetric about the midpoint of the central line. Because of this symmetry, the capacitances [C_{gs} and C_{gd}] between the central strip and the outer ones are

equal.

Even and odd modes of excitation can be used to analyze this problem. In the even mode, the potentials of the outer strips are equal in magnitude and are in phase (say, +1 volt) and the central strip is grounded. The field lines from both sides are terminated on the central strip and none of these lines cross over to the second outer strip. The wall perpendicular to the central strip at the mid-point is a magnetic wall and therefore, it is possible to break the structure into two parts as shown in Fig. 4-8.

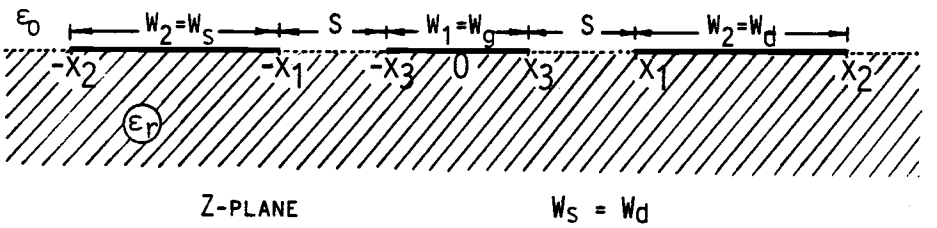

Fig. 4-7 : Three Coplanar Strips Structure.

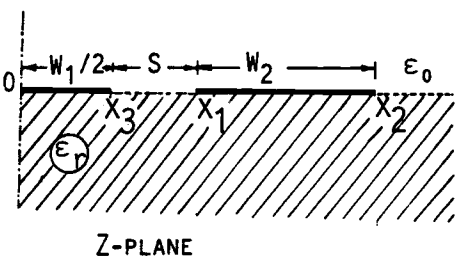

Fig. 4-8: Asymmetrical coplanar strips associated with even mode capacitance.

As it is seen in this figure, only one-half of the central line is considered in calculating C_{gd}; this explains the effect of a presence of the third line or what we call a shielding effect. Therefore, the value of C_{gd} is smaller than the one evaluated by applying Neidert's or Pucel's formula, where the third line effect is ignored.

Fig. 4-8 represents an asymmetric coupled two coplanar strip problem similar to the one discussed in the previous section. The even mode capacitance C_{gd} (C_{gs}) can be obtained by applying the same techniques.

In the odd mode excitation, the potentials of the outer strips are equal in magnitude but 180° out of phase (say, +1 and -1 volt); the central line is assumed to be grounded. The electric field lines are terminated on two strips, the central one as well as the second outer strip, whose potential is negative.

By using Shwartz-Christoffel transformation, Fig. 4-7 is mapped into Fig. 4-9, where α, β, γ, φ_o, θ_o and k_o are as given in equations (13-15). Since in the odd mode excitation, the wall a-b shown in Fig. 4-9-a is an electrical wall, either half of the figure can be used as shown in Fig. 4-9-b to study the problem.

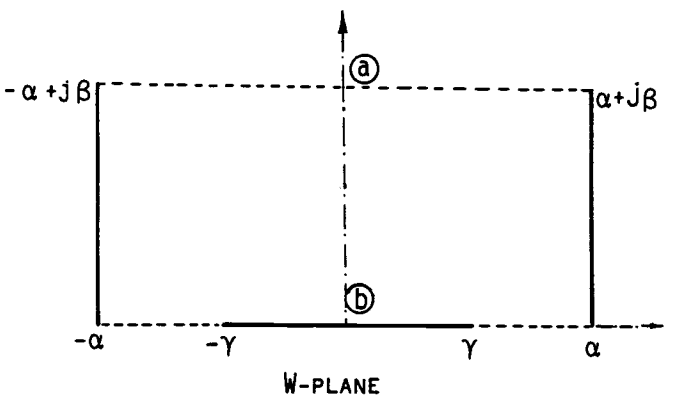

Fig. 4-9-a: W-plane

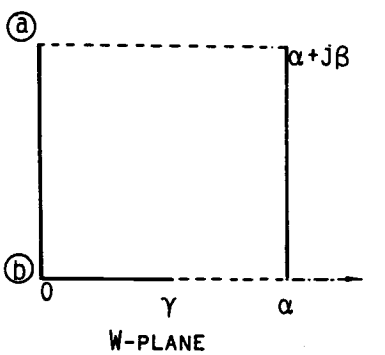

Fig. 4-9-b: The electric wall representation.

Applying the same technique used in the two asymmetric coplanar strips case, mirroring, rotating, and transforming, a coplanar waveguide structure is obtained with :

k_1, β, φ_1 and θ_1 are as given in equations (16-17);

$$\alpha = K'(k_1)/t_2 \qquad (23\text{-a})$$

$$\gamma = F(\varphi_1,\theta_1)/t_2 \qquad (23\text{-b})$$

Therefore,

$$\frac{K(k_1)}{K'(k_1)} = \frac{K'(k_o)}{K(k_o)} \qquad (24)$$

$$\frac{F(\varphi_1,\theta_1)}{K'(k_1)} = \frac{F(\varphi_1,\theta_1)}{K(k_o)} \qquad (25)$$

Equation (24) leads to :

$$k_1 = k_o' \quad \text{and} \quad k_1' = k_o \qquad (26)$$

$$K(k_1) = K'(k_o) \quad \text{and} \quad K'(k_1) = K(k_o) \qquad (27)$$

$$\theta_1 = \theta_o \qquad (28)$$

and therefore,

$$F(\varphi_1,\theta_1) = F(\varphi_o,\theta_o) \qquad (29)$$

which gives: $\varphi_1 = \varphi_o$ (30)

Finally,

$$k_2 = \frac{t_3}{t_2} = \frac{\cos[\sin^{-1}(X_1/X_2)]}{\sqrt{1-(X_3/X_2)^2}} \qquad (31)$$

and the odd-mode capacitance is found to be:

$$C_{odd} = (1+\epsilon_r)\,\epsilon_o \frac{K(k_2)}{K'(k_2)} \qquad (32)$$

The capacitance between the outer strips is obtained from the two capacitances associated with the even and odd modes of excitation and is given by :

$$C_{ds} = \frac{C_{odd} - C_{even}}{2} \qquad (33)$$

4.3 : CURVE FITTING METHODS :

4.3.1: Asymmetrical Coplanar Strips :

A closed form expression for the capacitance of asymmetrical coplanar strips was derived based on curve fitting and is given by :

$$C = \frac{(1+\epsilon_r)}{2} \{ k_0[\frac{C_1+C_2}{2}] - k_1[\frac{C_1+C_2}{2}]^2 + k_2\sqrt{C_1C_2} + k_3C_1C_2 \} \qquad (34)$$

Where, C_1 is the capacitance of two symmetrical coplanar strips, of width W_1 and separated by S, evaluated in the free space.

C_2 is the capacitance of two symmetrical coplanar strips, of width W_2 and separated by S, evaluated in the free space.

$$\left.\begin{array}{ll} k_0 = 0.9695 & k_1 = 0.08 \\ k_2 = 0.02868 & k_3 = 0.08 + Wr \times 7.6474 \times 10^{-5} \end{array}\right\} \qquad (35)$$

$$Wr = Max\{W_1,W_2\} \,/\, Min\{W_1,W_2\}$$

The above expression can be used to calculate the capacitance between asymmetrical two-coplanar strips and is accurate to within 1.6% for the practical range of dimensions for strip and slot widths. More details about the accuracy of this expression are presented in the results section at the end of this chapter.

4.3.2: Three Coplanar Strips :

The presence of a central strip between two symmetrical coplanar lines reduces the capacitance between these strips. As the width of the central strip increases, the effect becomes more significant and the capacitance becomes smaller. By using curve fitting, it is found

that a closed form expression for the capacitance between the outer strips C_{ds} is given by :

$$C_{ds} = \frac{C_o}{2} \left[e^{-k_1 W_{gn}^{.25}} + e^{-k_2 W_{gn}} \right] \qquad (36)$$

Where, C_o is the capacitance between two symmetric strips of width W_{dn} and slot width $2S+W_g$.

$$W_{gn} = \frac{W_g}{2S + W_g} \; ; \qquad W_{dn} = \frac{W_d}{2S + W_g} \qquad (37)$$

$$k_1 = \frac{2.11751}{W_{dn}^{.39457}} \qquad (38)$$

$$k_2 = A_1 e^{-B_1 W_{dn}} + A_2 e^{-B_2 W_{dn}} + A_3 e^{-B_3 W_{dn}} \qquad (39)$$

$$\left.\begin{array}{ll} A_1 = 0.20542 & B_1 = 0.01098 \\ A_2 = 0.58190 & B_2 = 0.72609 \\ A_3 = 1.25746 & B_3 = 5.19427 \end{array}\right\} \qquad (40)$$

The accuracy of this expression is within 3.8% as compared with the exact results when W_{gn} is varied from 0.2 to 0.98 and W_{dn} varied from 0.2 to 20.

Not only does the presence of a central strip affects the capacitance between the outer strips, but also the existence of an adjacent strip has some shielding effect on the capacitance between the neighboring strips. For example, in the case of three-strip structure with equal widths, it is found that :

$$C_3 = C_2(1-\Delta) \qquad (41)$$

Where C_3 is the capacitance between two adjacent strips in the presence of a third one of the same width, located on either side and separated from the nearest strip by the same spacing

between these two adjacent strips.

C_2 is the capacitance between two adjacent strips in the absence of any other strips.

$$\Delta = A_1(W/S)^{k_1} - A_2(W/S)^{k_2} \qquad (42)$$

Where,

$$k_1 = 0.232573 \qquad k_2 = 0.293035 \qquad (43\text{-a})$$

and for W/S between 3. and 37.0 :

$$A_1 = 0.33642 \quad \text{and} \quad A_2 = 0.248667 \; ; \qquad (43\text{-b})$$

Otherwise,

$$A_1 = 0.390526 \quad \text{and} \quad A_2 = 0.288660 \qquad (43\text{-c})$$

The percentage error in this numerical expression is less than 1.0% for W/S less than 57.5 and within 3.55% if W/S is less than 100. However, applying equation (43-b) alone for the entire range of W/S results in a maximum error of 1.66% for W/S less than 1.0 and 0.87% for W/S greater than 1.0 and up to 50. If equation (43-c) is applied for the whole range, the maximum percentage error is 1.66% when W/S is less than 2.0, less than 1.% if W/S is between 2.0 and 41.5, and within 1.42% if W/S=50. The above results can be used to design inter-digital structures used in photoconductive detectors[126].

Similarly, the capacitance C_{gs} (or C_{gd}) value is less than the capacitance value of a similar structure without a third strip. Therefore, a numerical correction can be made to obtain the correct value of C_{gs} (C_{gd}) from the capacitance of asymmetric lines if a third strip is present as shown in Fig. 4-7. The corrected value is found to be :

$$C_{gs} = C_{gd} = C_{gso}(1-\vartheta) \qquad (44)$$

Where C_{gso} is the capacitance between two asymmetric coplanar strips

of widths W_g and W_s and slot width S.

$$\vartheta = A_1(W_a/S)^{-k_1} - [A_2(W_b/S)^{k_2} \ln(W_b/S)]/(W_a/S), \qquad (45)$$

$$\left.\begin{array}{ll} W_a = Max\{W_g, W_s\} & W_b = Min\{W_g, W_s\} \\ A_1 = 0.101866 & k_1 = 0.003704 \\ A_2 = 0.008019 & k_2 = 0.556532 \end{array}\right\} \qquad (46)$$

Comparing the calculated values of C_{gs} (C_{gd}) obtained by this closed form expression with the exact results obtained by conformal mapping method, the accuracy is within 5% when $W_g/(2S+W_g)$ is varied from 0.05 to 0.98 and $W_d/(2S+W_g)$ varied from 0.2 to 20.

4.4 : EFFECT OF STRIP THICKNESS :

When the strip conductors are of finite thickness t, this thickness modifies the effective dielectric constants, the characteristic impedance and the capacitance. Although Kaupp[127], Schwarzmann[128], and Ross and Howes[129] show that the effective dielectric constant increases with the strip thickness and become even greater than ϵ_r [129], the theoretical analysis and experimental measurements[130] confirm that the effective dielectric constant and the characteristic impedance decrease with increasing the strip thickness. This is what is expected because the fraction of the total energy propagating in air increases with strip thickness, and as a result of that, the effective dielectric constant should decrease with increasing thickness.

The empirical correction terms to account for strip thickness are presented by Bahl[26] and Gupta[25] in the following closed form

approximation:

$$W_e = W + \kappa \tag{47}$$

$$S_e = S - \kappa \tag{48}$$

$$\kappa = \begin{cases} \dfrac{1.25t}{\pi}\left[1 + \ln\dfrac{4\pi W}{t}\right] & \text{for } W/h \le \dfrac{1}{2\pi} \quad (49) \\ \dfrac{1.25t}{\pi}\left[1 + \ln\dfrac{2h}{t}\right] & \text{for } W/h \ge \dfrac{1}{2\pi} \quad (50) \end{cases}$$

Where,

W *and* S *are the actual strip and slot width respectively.*

W_e *and* S_e *are the effective width of the strip and the slot respectively.*

h *is the substrate thickness.*

4.5 : THE RESULTS AND CONCLUSIONS :

Calculation of the characteristics of coplanar strips requires a good estimation of the capacitances associated with these strips. The conformal mapping technique presented in this chapter is a very powerful method, which can be applied to calculate the exact values of these capacitances, and the resulting effective dielectric constant and the characteristic impedances. However, the accuracy of this method depends on the accuracy of calculating the complete and incomplete elliptic integrals. As mentioned in the introduction, these integrals can be evaluated by using an approximate expression. However, we have used analytical function to evaluate these integrals. The results obtained by using these functions are in excellent

agreement with those tabulated by Legendre in 1825[122], but they are off of those tabulated in reference [125], which are obtained by applying infinite series.

The analysis of three coplanar strips of finite dimensions which is presented here for the first time, is important in numerous applications in microwave circuits. This analysis shows that the presence of a third strip between two coplanar strips or adjacent to them decreases the capacitance between these two strips, and this degradation in the capacitance depends on the width of the strip and how far it is from the other two strips if not centered between them. In other word, unless the potential of the two strips is the same and the capacitance between them is zero, some of the electric field lines end on the third strip. This is the shielding effect which is demonstrated analytically and in numerical expressions.

Closed form expressions for these capacitances were also obtained by using curve fitting procedures. Such expressions are useful in the computer aided design of coplanar lines.

For the case of asymmetrical two-coplanar strips, the accuracy of the closed form expression obtained is as follows :

The error is less than 0.92% for $W_1/S = 1$ *and* $0.3<(W_2/S)<49$.

For $W_1/S = 5$, *the error is :*

less than 1.% for $0.8<(W_2/S)<35$ *(i.e.,* $0.16<(W_2/W_1)<7$ *), and*

less than 1.6% for $36<(W_2/S)<100$ *(i.e.,* $7<(W_2/W_1)<20$ *).*

For $W_1/S = 10$, *the error is :*

less than 1.% for $0.4<(W_2/S)<58$ *(i.e.,* $0.04<(W_2/W_1)<5.8$ *), and*

less than 1.46% for $59<(W_2/S)<100$ *(i.e.,* $5.9<(W_2/W_1)<10$ *).*

The results of the exact calculation and those obtained by applying the closed form expression are plotted in Fig. 4-10 over the practical range of applications.

For the three coplanar strips, Fig. 4-11 shows the capacitance between the adjacent strips. The effect of the third neighboring strip is clear. The percentage error associated with the CAD expression (equations 44-46) is less than 5% in the worst case for the ranges of dimensions shown in Fig. 4-11. The shielding effect becomes even stronger when the third strip is centered between another two symmetrical coplanar strips. Ignoring the effect of this strip as approximated by the others[14,18], gives a constant capacitance whatever the width of the third strip as shown in Fig. 4-12. The error in such approximation is very high. The closed-form expression obtained (equations 36-40) is accurate to within 3.8% for the dimensions shown in the figure.

Fig. 4-13 represents a special case, where all three strips are equal in width. In this figure the capacitance per unit length between adjacent symmetrical strips is plotted as a function of strip to slot widths ratio. The closed form expression used (equations 41-43) gives a percentage error of 1.% or less if W/S is less than 57.5, but the error may increase to 3.55% if W/S increases to 100.0 as shown in Fig. 4-13-a. In Fig. 4-13-b, equation (43-b) was used for the entire range of W/S shown in that figure. Comparing the calculated results with those obtained by conformal mapping shows that the percentage error is within 1.66% for W/S less than 1 and less than 0.87% for W/S greater than 1 and up to 50. In Fig. 4-13-c, the numerical expression

used is equation 41-43, excluding 42-b, i.e., equation 43-c was used for the entire range of W/S. The percentage error of the calculated capacitances as compared with the exact results is as follow :

a. *Error is less than 1.66% for W/S less than 2.*
b. *Error is less than 1% for W/S greater than 2.0 but less than 41.5.*
c. *Error is less than 1.42% for W/S greater than 41.5 and up to 50.*

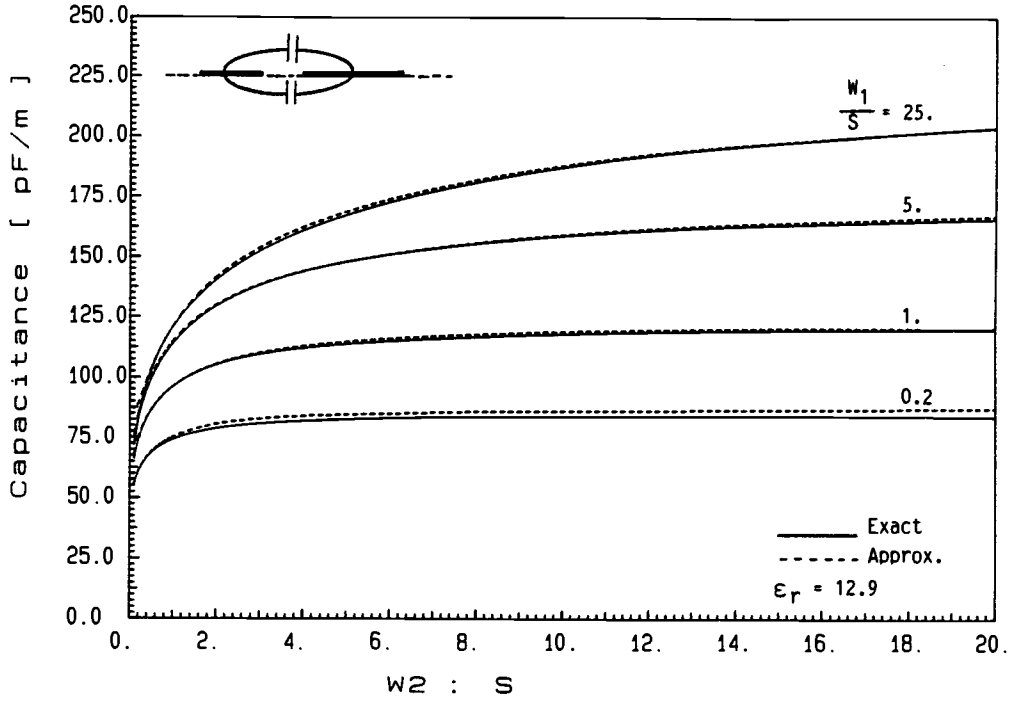

Fig. 4-10: The capacitance of asymmetric coplanar strips.

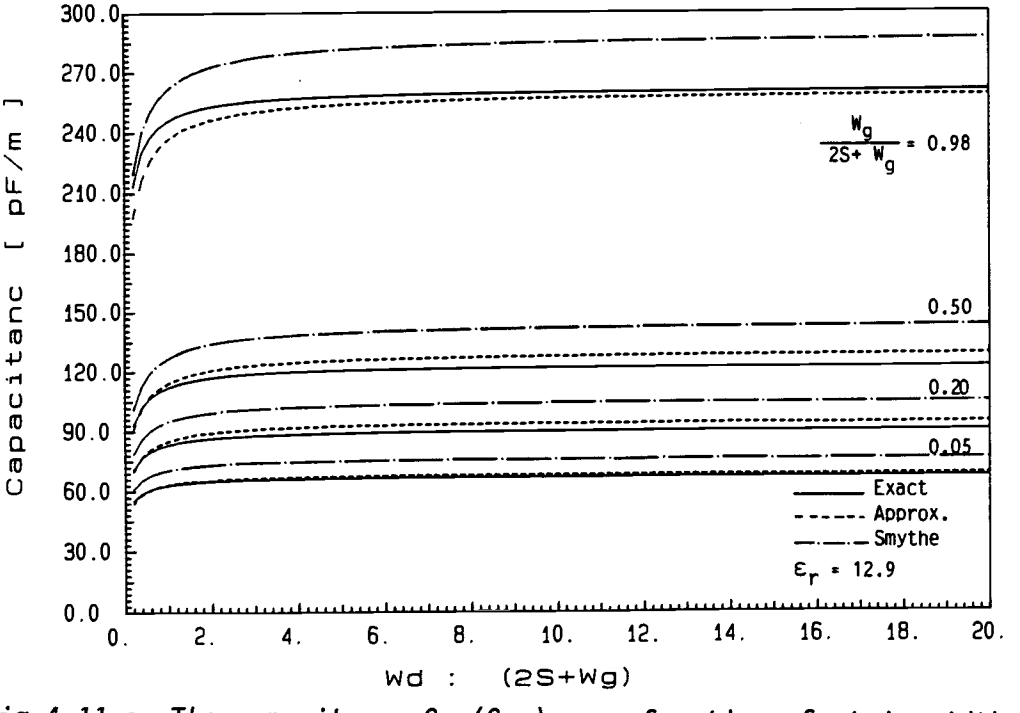

Fig.4-11-a: The capacitance $C_{gs}(C_{gd})$ as a function of strip widths.

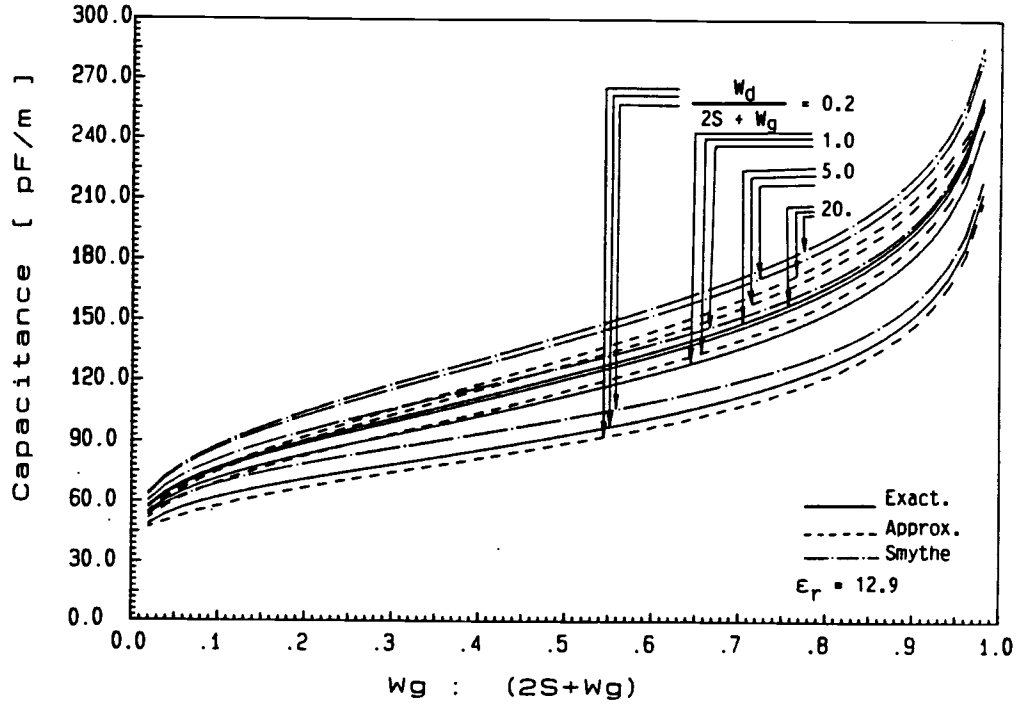

Fig.4-11-b: The capacitance $C_{gs}(C_{gd})$ as a function of strip widths.

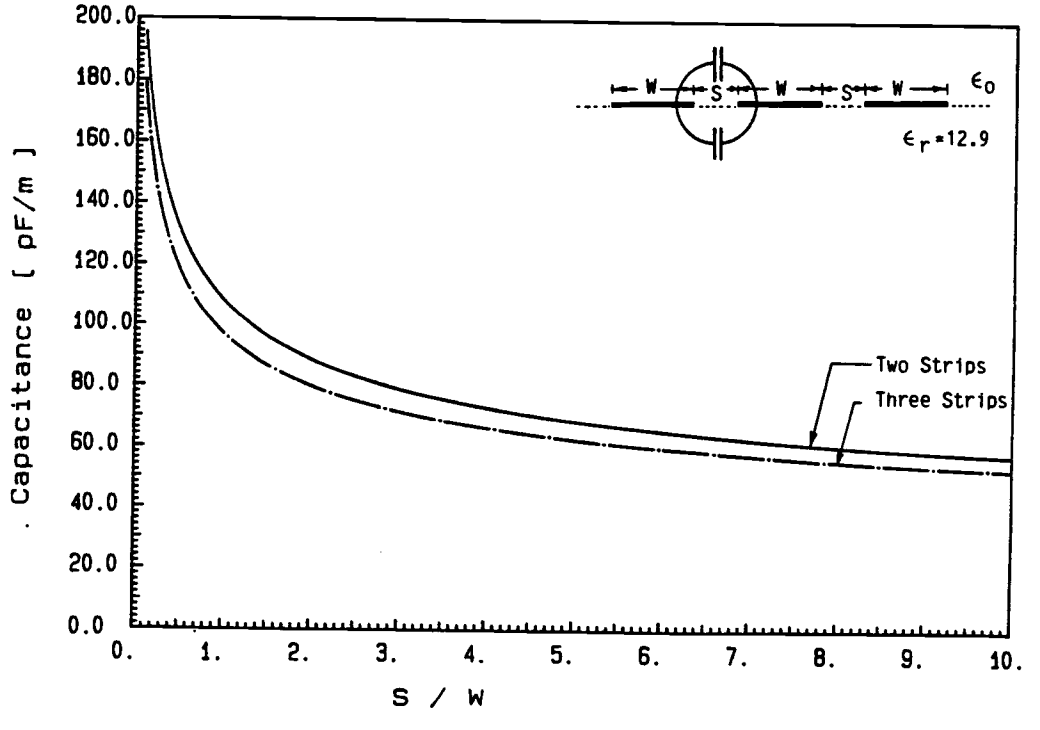

Fig. 4-11-c: The effect of an adjacent strip on $C_{gs}(C_{gd})$.

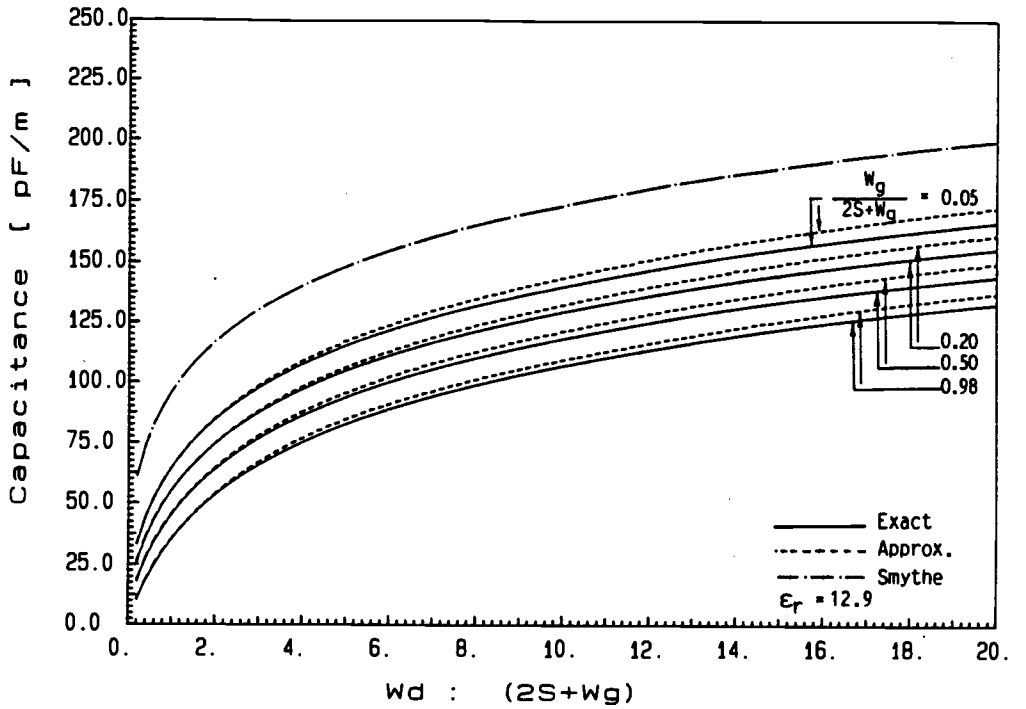

Fig. 4-12-a: The capacitance C_{ds} dependence on the strip widths.

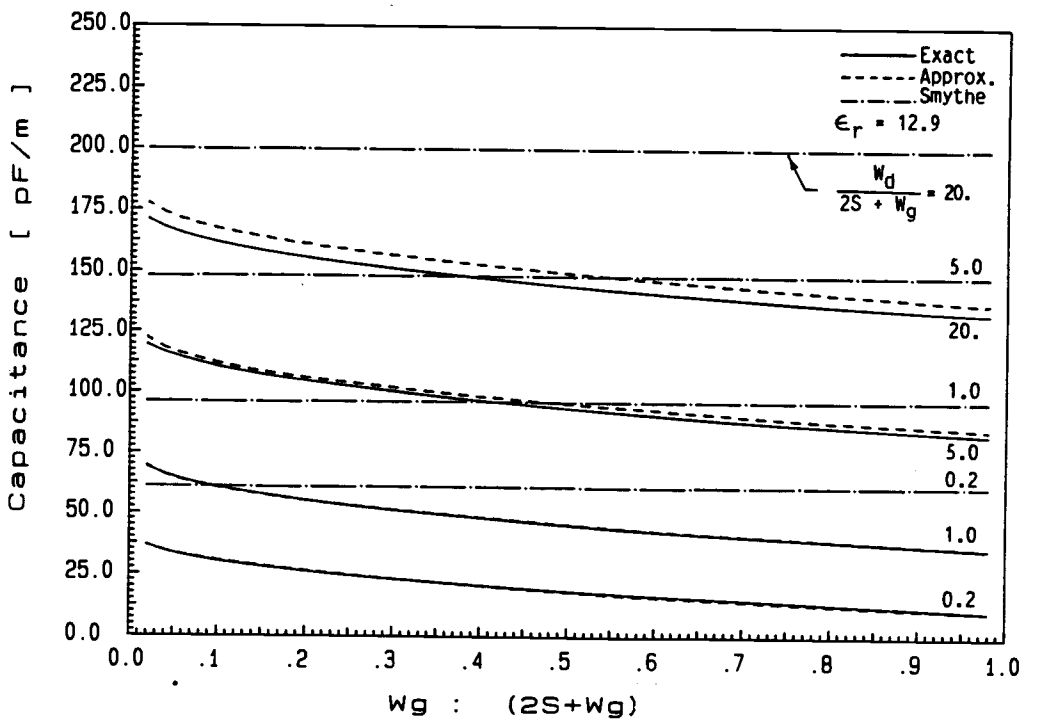

Fig.4-12-b: The capacitance C_{ds} dependence on the central strip.

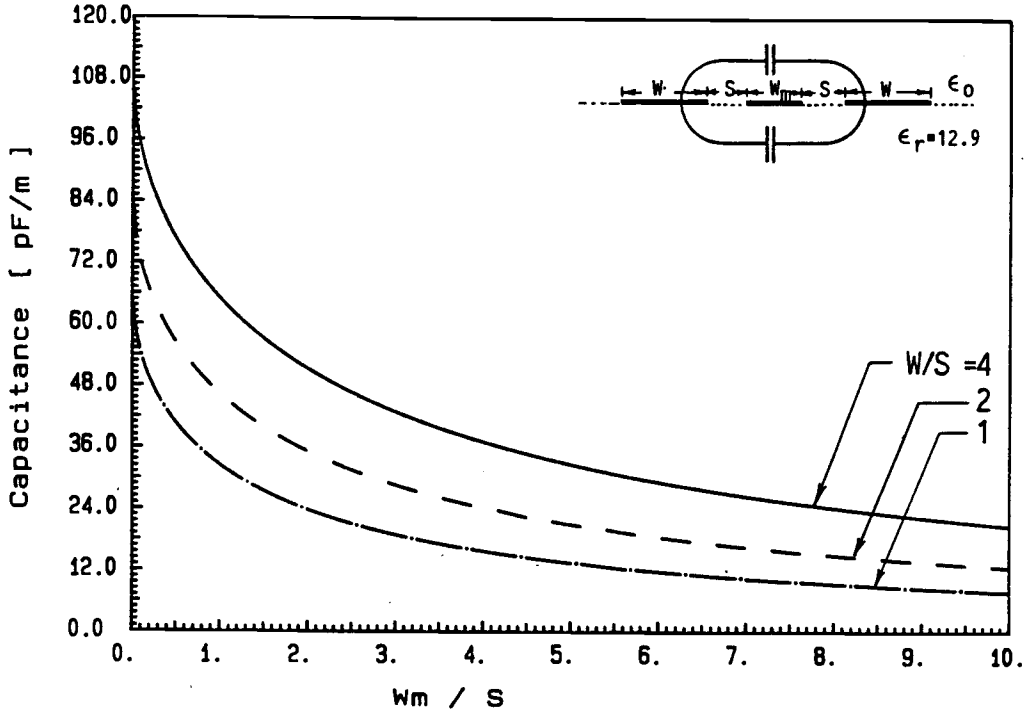

Fig.4-12-c: The effect of a central strip on the capacitance C_{ds}.

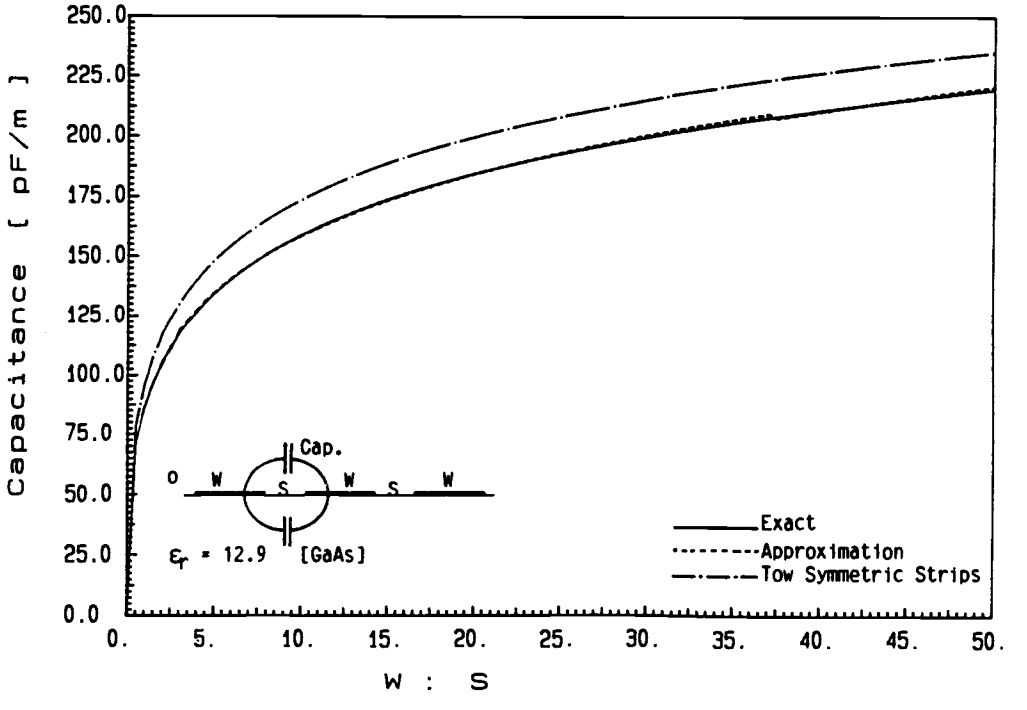

Fig. 4-13-a: The adjacent strips' capacitance in a structure of three coplanar strips of equal widths.

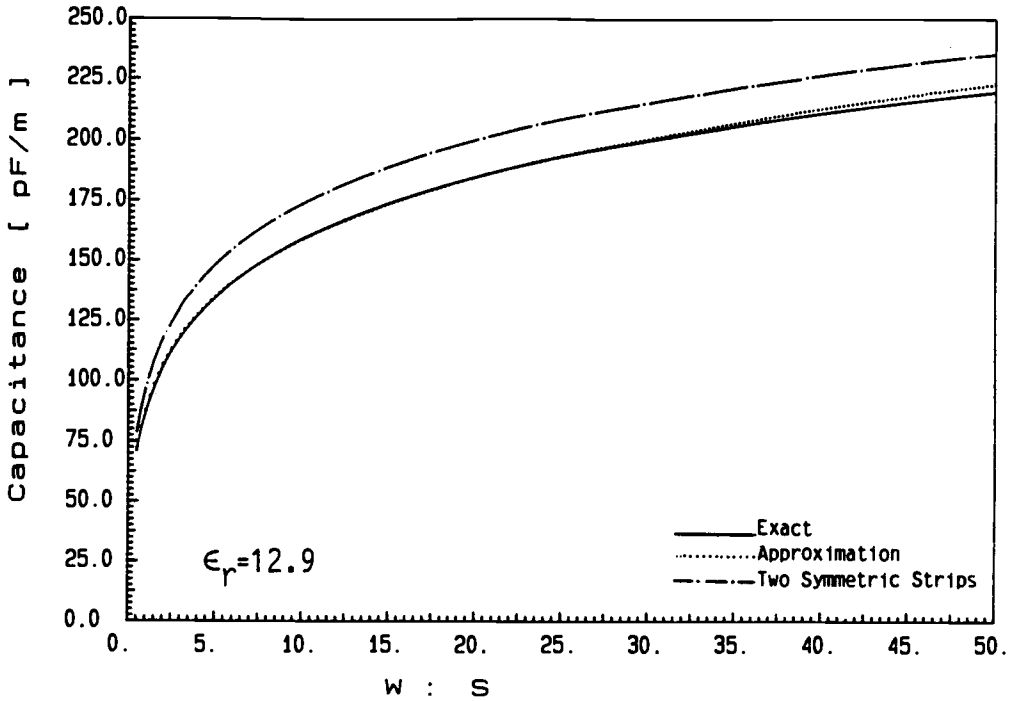

Fig.4-13-b: C_{gs} with the closed-form expression given in eqn. 43-b.

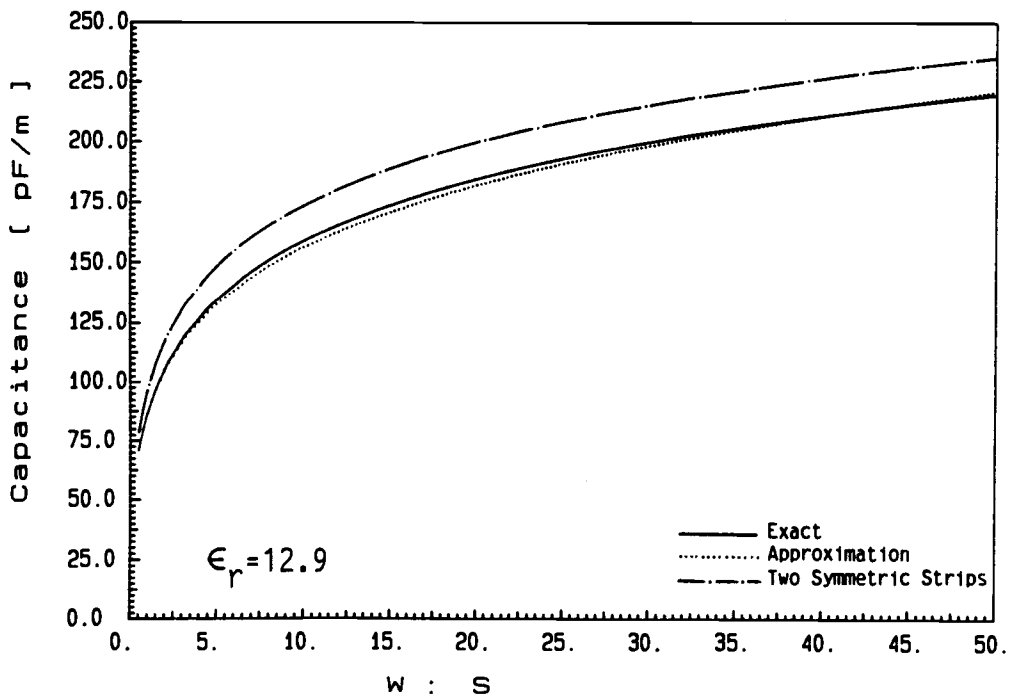

Fig.4-13-c: C_{gs} with the closed-form expression given in eqn. 43-c.

CHAPTER 5

TRAVELING-WAVE FIELD EFFECT TRANSISTOR

5.1: INTRODUCTION :

The principle of the distributed amplifier is not a new idea. It was first proposed by Percival in 1936[1]. However, the concept did not go into widespread active use until 1948 when Ginzton et al.[2] published their analysis of cascaded amplifier. The first experimental results were reported shortly thereafter by Rudenberg and Kennedy in 1949[3] and Horton et al. in 1950[131]. More detailed mathematical theory was reported in 1953 by Payne[132]. At that time, thermionic devices were used for active elements in realizing the distributed amplifiers.

The three terminal solid-state devices now play a dominant role in the design of cascaded traveling-wave amplifiers. Wahl[5] presented the distributed theory for microwave bipolar traveling-wave transistors. Shackle[133], Meyer[134] and Roeshot[135] performed the experimental study of the distributed effect in microwave Si-bipolar transistors. Si-MOSFETs[6,136] and Si-MESFETs[7,137-139] were also used to realize distributed amplifiers.

In 1967, Robson et al.[140] reported the possibility of using space charge waves (Gunn effect) to obtain amplification in an n-type electrically long slab of GaAs. In recent years, GaAs MESFET amplifiers have achieved a high level of maturity and their superlative performance makes them suitable for high frequency broad-band applications including satellite communications. The obvious advantages of

MESFET amplifiers are their light weight, small volume, low distortion and low operating voltage which can be directly obtained from the main power supply of the satellite. The increased demand for greater communication bandwidth and radar applications, and the success in applying the concept of distributed amplifiers to monolithic GaAs MESFET[82,141-144], has inspired other work in the field.

The recent availability of high-quality semi-insulating GaAs and sufficient GaAs processing maturity make distributed amplifiers using GaAs MESFET's integrated with all the required passive components an attractive circuit approach for ultra broad-band amplification.

The concept of distributed amplifiers is based on the idea of separating the parasitic input and output capacitances of the active devices by means of an artificial transmission line while adding their transconductances. The parasitic capacitances of the distributed transistors are combined with lumped inductors to form artificial transmission lines, whose characteristic impedances are frequency independent. This design appears to offer potential improved impedance and gain characteristics over a broad frequency band when compared to conventional cascade amplifiers, where the increase in the conductance is compensated for by the corresponding increase in input and output capacitances.

Before proceeding further, it is important to distinguish between two categories of distributed amplifiers. The traveling-wave amplifiers (TWA), where a number of discrete active devices are cascaded, and the traveling-wave transistor (TWT), where only one long device is used and the waves travel along the active lines. In the former case,

the drain current associated with each transistor adds if they are in phase. The phase velocity on both gate and drain lines in such cascaded amplifiers have to be synchronized for the current and the signal to add along the lines.

In order to synchronize the velocities, various techniques have been reported. Archer et al.[145] connected MOS chip capacitance to the drain of each FET. Kim[146] used a series capacitor loading shunted by a resistor in the gate electrode. Aysali et al.[147] used discrete series capacitors to couple the active devices to the input gate line with the dc-bias of the gate supplied by a separate line via extra resistors. Other techniques include connecting the active devices by transmission lines having suitable characteristic impedances and lengths between transistors on the gate and drain sides [9, 52,148-150]. These lines are designed to provide the necessary inductance required to equalize the phase shift as they are combined with the input or output capacitance of each single device. In addition, Aysali et al.[8,151] and Christ et al.[152] have reported the use of parallel-gate transmission lines with a single drain line, which has been reported to yield better flatness of the gain curve.

Cascaded traveling-wave amplifiers discussed above are particularly suited to MMIC's (Monolithic Microwave Integrated Circuits) because the passive circuits predominantly consist of inductors or transmission lines, which can be realized in microstrip form.

Discrete FET distributed amplifiers (TWA) can be designed to give flat response up to nearly the cutoff frequency of the lines[147], and they give higher gain[153]. Although the amplifiers of this set have

been called distributed amplifiers for historical reasons, they are, in fact, cascaded amplifiers since they are realized by cascading discrete devices.

The second group of devices is the traveling-wave field-effect transistors or simply, traveling-wave transistors (TWT). This device is an electrically long structure and its operation depends on the distributed interaction. However, unlike the conventional two-port FET amplifier, this is a four-port device. The device length in the direction of wave propagation is usually much longer than the length of a single device in TWA. The compensation required to equalize the phase velocities of the input and output waves can be accomplished by adding a capacitance onto the drain line either by direct overlays [10,11] or by a novel image gate arrangement[12].

In both TWA and TWT the gain does not increase indefinitely either with an increase in the gate width[6,139,154] or the number of MESFETs in TWA case[57,145,155]. There is an optimum number of active devices to be used in TWA depending on the gate width of each individual transistor and optimum length (gate width) for TWT. These limitations are not only due to signal attenuation along the gate electrode, but also due to the difference in the propagation constants of the waves on the gate and drain lines, unwanted reflections of the waves due to imperfect impedance matching at both ends of each electrode, and the possible drain-to-gate breakdown voltage. Fricke[156] shows that this is not only relevant for long FET structures as used for power amplification or for traveling-wave MESEFTs, but also for electrically short transistors as long as the gate width is about an

eighth of the wavelength.

It is well known that various mechanisms limit the power in microwave distributed amplifiers[8,151]. These include :

a. *A finite RF voltage swing that can be allowed on the input gate line which is limited on the positive RF cycle by the forward condition of the gate, and the negative cycle by the pinch-off voltage of the device as shown in Fig. 5-1.*

b. *The maximum total gate periphery for a specific maximum frequency of operation and given FET.*

c. *Drain-to-gate breakdown voltage. The drain electrode must be able to sustain the amplitude of RF voltage swings.*

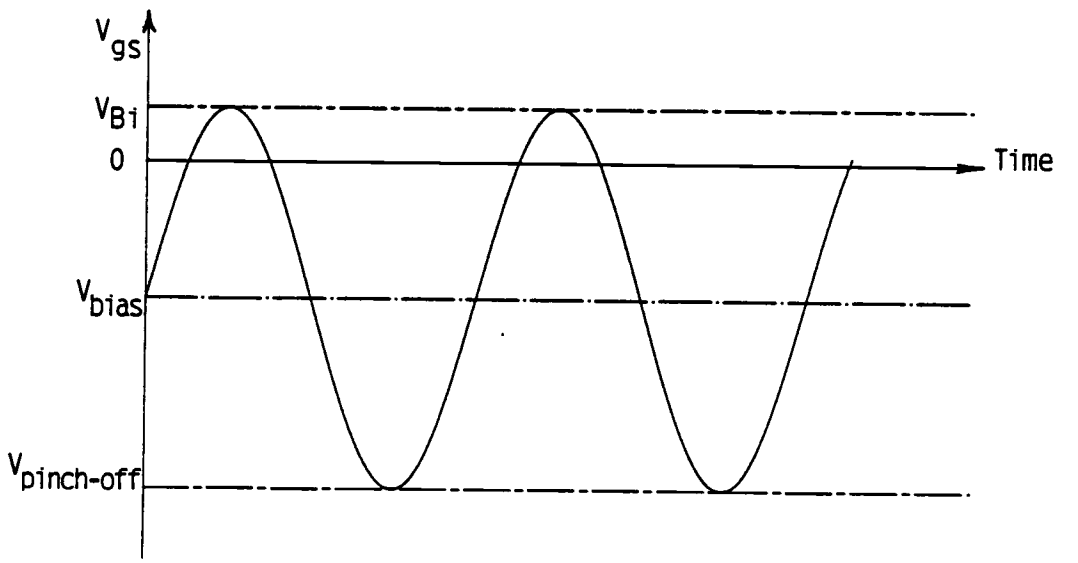

Fig. 5-1 : Maximum RF voltage swing allowed on the gate line. (After Ayasli et al.[8])

Our objective is to conduct a comprehensive study of a traveling-wave transistor (TWT), which have been a topic of continued interest in recent years[10,11,29,31,40,157-161], by applying rigorous coupled distributed parameters theory. The first reports of wave propagation

on FET structures were reported by McIver(1965)[6], Kopp(1966)[139], and Kohn and Landauer(1968)[138]. However, they all considered the active coupling only which is due to the transistor's transconductance. Since the passive coupling can not be neglected, Jutzi(1969)[7] took the capacitive coupling between the electrodes into consideration, but in order to simplify the analysis, no inductive coupling was included. Fukuta[162] and Higashisaka[155] considered the wave attenuatin of the signal along the gate line and assumed that the drain is lossless. Recently, Podgorsky and Wei[40] published their study which took into account the inductive and capacitive coupling as well as the wave attenuation due to losses on both gate and drain lines.

In this chapter, the linear active coupled line analysis is applied to an electrically long GaAs MESFET structure. Such structures have many potential applications including harmonic generator and traveling-wave amplifier devices [29,30,54,163,164]

Since the lossy elements (gate- and drain-line resistances and the channel resistance) and the parasitic capacitances or inductances are not the only factors that limit the gain in TWT, all of the different types of coupling between electrodes (transconductive, capacitive and inductive), all of the other parasitic elements, and the attenuation of both the input and output waves must be considered. The properties of the TWT are derived based on the general theory of active coupled transmission lines presented in chapter 2. All the propagation constants, mode voltage and current ratios, and the overall amplifier gain as a function of frequency are evaluated. To achieve optimal gain-bandwidth product, TOUCHSTONE[27] was also used

to simulate the circuit for optimizing the termination impedances and determining the nature and values of the compensation element(s) which need to be added to the input and/or output electrodes. More importantly, TOUCHSTONE is used as a tool to validate the results obtained by using the S-parameters matrix of the distributed parameter TWT four-port.

5.2: THEORETICAL ANALYSIS :

The properties of the active coupled-line circuit representing long GaAs MESFET structures can be obtained in terms of quasi-TEM waves traveling along the electrodes transverse to the electron-drift direction. The quasi-TEM assumption is valid since all transverse dimensions are much smaller than the wavelength of the maximum frequency of operation. This model of traveling-wave transistors is best treated by the coupled-line analysis which considers all the properties of wave propagation, such as passive coupling (inductive and capacitive) between all three electrodes (source, gate and drain), active coupling by the charge-carrier drift in the channel, attenuation of the waves along the input (gate) and output (drain) lines, and reflection due to the mismatched impedances at both ends of each electrode.

The general method of calculating the terminal characteristics of uniform, asymmetric, active or passive coupled transmission lines in an inhomogeneous medium is presented in detail in chapter 2.

For small sinusoidal signal, the voltages and currents on the gate and drain lines of common source MESFET are given by the

transmission line equations :

$$-\frac{dv_g}{dx} = z_{gg}i_g + z_{gd}i_d \qquad (1\text{-a})$$

$$-\frac{dv_d}{dx} = z_{dg}i_g + z_{dd}i_d \qquad (1\text{-b})$$

$$-\frac{di_g}{dx} = y_{gg}v_g + y_{gd}v_d \qquad (1\text{-c})$$

$$-\frac{di_d}{dx} = y_{dg}v_g + y_{dd}v_d \qquad (1\text{-d})$$

Where z_{jj} and y_{jj} $(j=g,d)$ are the self series impedance and shunt admittance of line g (:gate) or d (:drain) in the presence of line k ($k=g,d;\ k\neq j$) per unit length of the line. z_{jk} and y_{jk} are the mutual impedance and admittance per unit length, respectively.

If the source is not grounded, the MESFET structure can be treated as an active symmetrical three coupled lines structure. For which the series impedance matrix per unit length is given by :

$$[z] = \begin{bmatrix} z_{gg} & z_{gd} & z_{gs} \\ z_{dg} & z_{dd} & z_{ds} \\ z_{sg} & z_{sd} & z_{ss} \end{bmatrix} = \begin{bmatrix} Sl_{gg}+r_g & Sl_{gd} & Sl_{gs} \\ Sl_{dg} & Sl_{dd}+r_d & Sl_{ds} \\ Sl_{sg} & Sl_{sd} & Sl_{ss}+r_s \end{bmatrix} \qquad (2)$$

Where $l_{mn}=l_{nm}$ and $S=j\omega$. (3)

The shunt admittance is also 3×3 matrix.

$$[y] = \begin{bmatrix} y_{gg} & y_{gd} & y_{gs} \\ y_{dg} & y_{dd} & y_{ds} \\ y_{sg} & y_{sd} & y_{ss} \end{bmatrix} \qquad (4)$$

Note that, in general, $y_{mn} \neq y_{nm}$.

The above system can be analyzed in the same manner as the passive system[165].

The elements of this matrix, [y] are obtained from the admittance matrix of the equivalent circuit of the GaAs MESFET shown in Fig.3-4-b by terminal (node) suppression :

$$[Y] = \begin{bmatrix} S(C_{gd}+C_{gs}+C_{in}+C_{fb}+C_{sw}) & -SC_{gd} & -SC_{gs} & -SC_{sw} & -SC_{in} & -SC_{fb} \\ -SC_{gd} & S(C_{gd}+C_{ds}+C_d)+\frac{1}{R_d} & -SC_{ds} & 0 & 0 & -\frac{1}{R_d} \\ -SC_{gs} & -SC_{ds} & S(C_{ds}+C_{gs}+C_s)+\frac{1}{R_s} & -\frac{1}{R_s} & 0 & 0 \\ -SC_{sw}-g_m & 0 & -\frac{1}{R_s} & SC_{sw}+\frac{1}{R_{in}}+\frac{1}{R_s}+\frac{1}{R_o} & g_m-\frac{1}{R_{in}} & -\frac{1}{R_o} \\ -SC_{in} & 0 & 0 & -\frac{1}{R_{in}} & S(C_{in}+C_{dom})+\frac{1}{R_{dom}}+\frac{1}{R_{in}} & -(SC_{dom}+\frac{1}{R_{dom}}) \\ g_m-SC_{fb} & -\frac{1}{R_d} & 0 & -\frac{1}{R_o} & -(g_m+SC_{dom}+\frac{1}{R_{dom}}) & S(C_{fb}+C_{dom})+\frac{1}{R_o}+\frac{1}{R_d}+\frac{1}{R_{dom}} \end{bmatrix}$$

These elements are found to be :

$$y_{gg} = S(C_{gs} + C_{sw} + C_{in} + C_{fb} + C_{gd}) - \delta/\sigma \qquad (6\text{-a})$$

$$y_{gd} = -SC_{gd} - \mu/\sigma \qquad (6\text{-b})$$

$$y_{gs} = -SC_{gs} - \tau/\sigma \qquad (6\text{-c})$$

$$y_{dg} = -SC_{dg} - \lambda/\sigma \qquad (6\text{-d})$$

$$y_{dd} = S(C_d + C_{ds} + C_{gd}) + (1/R_d) - \upsilon/(R_d^2\sigma) \qquad (6\text{-e})$$

$$y_{ds} = -SC_{ds} - \zeta/(R_dR_s\sigma) \qquad (6\text{-f})$$

$$y_{sg} = -SC_{gs} - \Psi/\sigma \qquad (6\text{-g})$$

$$y_{sd} = -SC_{ds} - \Omega/(R_dR_s\sigma) \qquad (6\text{-h})$$

$$y_{ss} = S(C_{gs} + C_{ds} + C_s) + (1/R_s) - \alpha/(R_s^2\sigma) \qquad (6\text{-i})$$

Where,

$$\delta = (SC_{sw}+ g_m)(\alpha SC_{sw}+ \theta SC_{in}+ \zeta SC_{fb}) + SC_{in}(\beta SC_{sw}+ \varnothing SC_{in}+\kappa SC_{fb}) + (SC_{fb}- g_m)(\Omega SC_{sw}+ \eta SC_{in}+ \upsilon SC_{fb}) \qquad (7\text{-a})$$

$$\mu = S(\Omega C_{sw} + \eta C_{in} + \upsilon C_{fb}) / R_d \qquad (7\text{-b})$$

$$\sigma = [SC_{sw} + \frac{1}{R_o} + \frac{1}{R_s} + \frac{1}{R_{in}}][(SC_{in} + \frac{1}{R_{in}} + y_{dom})(SC_{fb} + \frac{1}{R_o} + \frac{1}{R_d} + y_{dom}) - y_{dom}(y_{dom} + g_m)] + [g_m - \frac{1}{R_{in}}][\frac{y_{dom}}{R_o} + \frac{1}{R_{in}}(SC_{fb} + \frac{1}{R_o} + \frac{1}{R_d} + y_{dom})] - \frac{1}{R_o}[\frac{1}{R_{in}}(y_{dom} + g_m) + \frac{1}{R_o}(SC_{in} + \frac{1}{R_i^n} + y_{dom}) \quad (7\text{-}c)$$

$$\tau = S(\alpha C_{sw} + \theta C_{in} + \zeta C_{fb}) / R_s \quad (7\text{-}d)$$

$$\lambda = [\zeta(SC_{sw} + g_m) + \kappa SC_{in} + \upsilon(SC_{fb} - g_m)] / R_d \quad (7\text{-}e)$$

$$\Psi = [\alpha(SC_{sw} + g_m) + \beta SC_{in} + \Omega(SC_{fb} - g_m)] / R_s \quad (7\text{-}f)$$

$$\alpha = (SC_{in} + y_{dom} + \frac{1}{R_{in}})(SC_{fb} + y_{dom} + \frac{1}{R_o} + \frac{1}{R_d}) - y_{dom}(y_{dom} + g_m) \quad (7\text{-}g)$$

$$\beta = \frac{1}{R_o}(y_{dom} + g_m) + (\frac{1}{R_{in}} - g_m)(SC_{fb} + y_{dom} + \frac{1}{R_o} + \frac{1}{R_d}) \quad (7\text{-}h)$$

$$\Omega = y_{dom}(\frac{1}{R_{in}} - g_m) + \frac{1}{R_o}(SC_{in} + y_{dom} + \frac{1}{R_{in}}) \quad (7\text{-}i)$$

$$\theta = \frac{y_{dom}}{R_o} + \frac{1}{R_{in}}(SC_{fb} + y_{dom} + \frac{1}{R_o} + \frac{1}{R_d}) \quad (7\text{-}j)$$

$$\varnothing = (SC_{sw} + \frac{1}{R_o} + \frac{1}{R_s} + \frac{1}{R_{in}})(SC_{fb} + y_{dom} + \frac{1}{R_o} + \frac{1}{R_d}) - \frac{1}{R_o^2} \quad (7\text{-}k)$$

$$\eta = \frac{1}{R_{in}R_o} + y_{dom}(SC_{sw} + \frac{1}{R_o} + \frac{1}{R_s} + \frac{1}{R_{in}}) \quad (7\text{-}l)$$

$$\zeta = \frac{1}{R_{in}}(y_{dom} + g_m) + \frac{1}{R_o}(SC_{in} + y_{dom} + \frac{1}{R_{in}}) \quad (7\text{-}m)$$

$$\kappa = \frac{1}{R_o}(\frac{1}{R_{in}} - g_m) + (y_{dom} + g_m)(SC_{sw} + \frac{1}{R_{in}} + \frac{1}{R_o} + \frac{1}{R_s}) \quad (7\text{-}n)$$

$$v = (SC_{sw} + \frac{1}{R_{in}} + \frac{1}{R_o} + \frac{1}{R_s})(SC_{in} + y_{dom} + \frac{1}{R_{in}}) - \frac{1}{R_{in}}(\frac{1}{R_{in}} - g_m) \quad (7\text{-}o)$$

and

$$y_{dom} = SC_{dom} + (1/R_{dom}) \quad (7\text{-}p)$$

The series impedance matrix per unit length of a common source MESFET as derived from the equivalent model of Fig. 3-4-b is given by:

$$[z] = \begin{bmatrix} Sl_{gg} + r_g & Sl_{gd} \\ Sl_{dg} & Sl_{dd} + r_d \end{bmatrix} \quad (8)$$

and the admittance matrix is :

$$[y] = \begin{bmatrix} y_{gg} & y_{gd} \\ y_{dg} & y_{dd} \end{bmatrix} \quad (9)$$

The accuracy of the above equations for the admittance parameters was checked by simulating the equivalent circuit shown in Fig. 3-4-b (page 37) on SPICE for a wide range of frequencies from dc to 100 GHz and comparing the admittances obtained by using SPICE with those obtained directly by using the above equations over the entire frequency band.

The solution of the above equations (1:a-d) is of the form :

$$v_{g,d}(x) = v_{go,do}e^{\gamma x} \quad (10)$$

and

$$i_{g,d}(x) = i_{go,do}e^{\gamma x} \quad (11)$$

Where $v_{go}(v_{do})$ and $i_{go}(i_{do})$ are the amplitudes of the voltage and the current on the gate (drain) line respectively and γ is the propagation constant whose values can be found by solving the eigenvalue problem. The source is taken to be the reference electrode and the two voltages

(gate voltage and drain voltage) are with respect to the source voltage. The two eigenvalues represent the two orthogonal modes of the system are defined as c- and π- for the co- and anti-mode.

The 4×4 impedance and admittance matrices of the four-port circuit are obtained in terms of these normal mode parameters as demonstrated in detail in chapter 2. The scattering parameters can be calculated in terms of these admittance or impedance functions by applying the well-known expressions :

$$S = [Z_n-U][Z_n+U]^{-1} = [Z_n+U]^{-1}[Z_n-U]$$
$$\text{and} \qquad S = [U-Y_n][U+Y_n]^{-1} = [U+Y_n]^{-1}[U-Y_n] \qquad (12)$$

Where U is the identity matrix and Z_n (Y_n) is the impedance (admittance) matrix of the four-port network normalized by the termination impedances (admittances) :

$$(Z_n)_{kl} = Z_{kl} / \sqrt{Z_{Tk}Z_{Tl}} \quad ; \quad (Y_n)_{kl} = Y_{kl} / \sqrt{Y_{Tk}Y_{Tl}} \qquad (13)$$

Where Z_{Tm} is the termination impedance of line m.

5.3: THE PROGRAM "FETGAIN" :

A FORTRAN program called FETGAIN was written to calculate the gain of the distributed transistor or amplifier. The program uses the element values per millimeter of the equivalent circuit of the GaAs MESFET model and the termination impedances (admittances) to calculate the gain of a specific device of a specific length. FETGAIN allows the connection of series impedances and/or shunt admittances to any or all four ports of the circuit. It also handles the traveling-wave amplifier by allowing the cascading of as many MESFETs as wanted through series impedances or parallel admittances for both gate and drain

lines. In case of a traveling-wave transistor, the compensation elements are distributed along the corresponding electrode. The transconductance of an active MESFET is made frequency dependent and the frequency at which its magnitude is down by 3 dB can be chosen. The expression used is [27] :

$$g_m = g_{mo}\, e^{-j\omega t} /[1+ (jf/f_{3dB})] \qquad (14)$$

Where g_{mo} is the dc value of the MESFET transconductance.

5.4: EFFECTS OF THE TRANSISTOR'S ELECTRICAL PARAMETERS :

The performance of the distributed field-effect transistor is mostly determined by the characteristics of the device which, in turn, depend on the process controlled parameters (i.e., geometrical and material parameters). Although some authors have reported that the amplifier's performance is relatively insensitive to the circuit parameters[8,152], the measured data and our study show that the performance is, indeed, quite sensitive to variations in these parameters.

The influence of the gate length and the channel thickness on some of the circuit elements were investigated by Curtice[71], who showed that as the gate (or the active channel) length decreases, the current, pinch-off voltage and transconductance increase while the input capacitance and output resistance decrease. The increase in the pinch-off voltage due to the decrease in the active channel length is attributed to the two-dimensional effects. Increasing the active channel thickness increases the pinch-off voltage of the device which increases the current monotonically but the transconductance increases

slightly to a maximum value before falling down. The current gain cut-cutoff frequency behaves in a similar manner as the transconductance. Dean and Matarese[157] proposed a very thin layer to maximize the frequency at which the maximum gain occurs. This, of course, is limited by the technology available and even if the gain is increased, the pinch-off voltage decreases and, hence, the maximum voltage swing allowed on the gate line decreases.

Law and Aithchison[150] suggested that the requirements for broad bandwidth and gain flatness include low value of input resistance and capacitance and high value of output resistance and transcondutance. We have noticed that the output resistance and the device transconductance have a significant impact on the amplifier gain, and higher values for both of them is desired. However, there is a trade off between the device transconductance and the output resistance; any attempt to increase one of them yields a reduction in the other.

The channel doping and the doping profile are also important factors. Increasing the carrier concentration up to about $10^{16}cm^{-3}$ gives higher current and, therefore, higher transconductance. The mobility of the electrons in this range is decreasing slightly with an increase in the doping level. However, as the doping is increased further, the impurity scattering reduces the mobility substantially and the expected increase in the drain current due to the increase in carrier concentration is compensated for by the reduction in the drift mobility of these carriers.

As the spacing between the gate and the drain (source) increases, the fringing coupling capacitance between these two electrodes becomes

smaller, but the active layer resistance R_d (R_g) becomes larger and the voltage drop across these parasitic resistances becomes larger and decreases the intrinsic drain-to-source voltage. As a result, the current and the transistor's transconductance are reduced. Making the drain and the source electrodes wider leads to a decrease in their inductance and resistances, and to an increase in their self and mutual capacitances.

From the above discussion, one can conclude that the improvement of one or more of the circuit elements which might result in a higher gain-bandwidth product, has a negative effect on other elements. This means that there is an optimum value for each process controlled parameter. Since these parameters have a direct effect on all the circuit elements, it is not possible to optimize one parameter for two or three elements and ignore its effect on the other elements. Due to the interaction between the circuit elements, an optimizer which is able to calculate the optimum values of the process controlled parameters for maximum gain-bandwidth product is needed. Unfortunately, such a program has yet to be developed.

After many runs of FETGAIN, we came up with a device whose physical (geometrical and material) parameters are listed in table 3-1. The values of these parameters do not, by any means, represent the optimum values, but they do represent the best choice of parameter values we have tried.

There is another factor which affects the gain drastically; it is the resistance of the gate line along the direction of the wave propagation. Since the gate dimension in the carriers flow direction is

much smaller than that of the other two electrodes, the input signal suffer a considerable attenuation as it propagates along the gate line. It is desirable to reduce the gate electrode resistance to a lowest possible value. However, since it is impossible to reduce the gate line resistance to a negligible value, suggestions have been made to reduce it. These suggestions include thicker metalization of the gate line, and lines having T-shape or mushroom-type cross section. The effect of the gate resistance on the gain of the field-effect transistor is shown in Fig. 5-2.

The resistance of the output drain line is also important , but because the drain has a larger cross section than the gate strip, its resistance is smaller and has little effect on the gain.

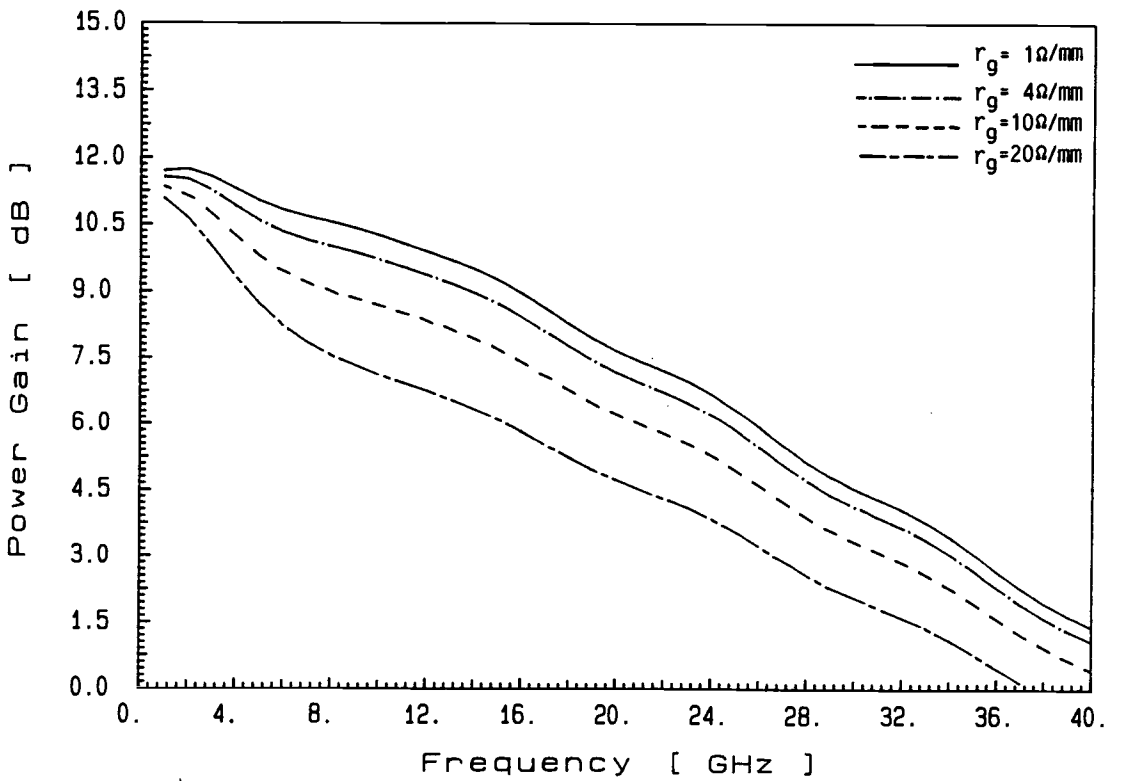

Fig. 5-2 : The effect of the gate-line metalization resistance the power gain.

5.5: TOUCHSTONE OPTIMIZATION :

The termination impedances in the microwave circuits play a significant role in the performance of the multiport circuits. The backward signal due to the reflection at the far end of both the input and output lines and the reflected forward signal at the sending terminals reduce the efficiency of the amplifier by distorting the propagating input and output waves. To avoid such reflections, a perfect match for the entire frequency range of operation between the termination and the line is required. Amemiya[28] suggested the use of T or π sections to terminate both the coupled lines simultaneously. But Amemiya's equations are limited to the lossless transmission lines and are not applicable to the general case where the losses and active couplings are involved. For the case of lossy lines such that T or π networks consist of frequency dependent coupled impedances and hence, the perfect match over the entire frequency band is not possible.

The impedance matching is the first difficulty one faces in designing such circuits. The other difficulty is the synchronization of the wave velocities on the input and output lines so that the interaction between the propagating waves is maximum. Since it is difficult to calculate analytically the value of the compensation element(s) required to equalize the phase velocities due to the complexity of the model used, we have used computer simulation by using TOUCHSTONE to obtain the optimum values of the required compensation element(s) as well as estimating values of the termination impedances. The other objective of using TOUCHSTONE is to validate the results obtained by using the scattering parameters

matrix of the distributed parameters structure.

The GaAs MESFET is simulated by cascading lumped element sections. In doing so, an artificial active coupled line is formed in a manner similar to simulating transmission lines by artificial LC lines. It is found that as the number of the sections increases, the simulation results become closer to those obtained by applying the rigorous distributed parameters method which utilizes the S-parameters matrix. However, as the number of lumped element sections increases, the optimization time increases drastically. For optimization purposes, a limited number of sections were used.

The device is simulated by using five sections of 300μm long devices with the circuit elements shown in table 5-1. The values of these elements were obtained by OSUFET program when the gate width is 300μm, V_{gs} = 0 and V_{ds} = 5 volts. The GaAs MESFET model used is the

Circuit Elements	Value	Circuit Elements	Value	Circuit Elements	Value
R_{in}	4.9450	C_{in}	0.50143	g_m	70.336
R_{out}	864.80	C_{out}	0.187556	L_{gg}	0.22080
R_{dom}	9318.7	C_{dom}	0.001844	L_{dd}	0.11850
R_s	0.59063	C_{gs}	0.018180	L_{gd}= L_{dg}	0.05925
R_d	0.59063	C_{gd}	0.018180	$C_{g\text{-}g.p.}$	0.00972
r_g	1.2	C_{sw}	0.002153	C_{fb}	0.023216
r_d	0.01771	C_{ds}	0.049560	$C_{d\text{-}g.p.}$	0.06045

Table 5-1 : The circuit elements used in TOUCHSTONE simulation. Gate width (device length) = 300. μm; capacitances in pF; resistances in Ohms; inductances in nH; conductance in mS.

model used in TOUCHSTONE. Since the TOUCHSTONE model does not contain all the circuit elements contained in our complete model, they were augmented by adding the missing elements.

Simulating the distributed MESFET by lumped element sections using TOUCHSTONE helps the design process by trying different possibilities for compensation elements. The five sections were connected via series inductors, transmission lines, L-C T-sections, parallel capacitors, and M-derived sections[59]. After optimizing the circuit in each case, it is found that the connection of the successive sections by series inductors gives higher gain as shown by the results plotted in Fig. 5-3. For this case, the termination impedances were found to be :

$Z_{g\text{-}in}$ = 21.80 Ohms; $Z_{d\text{-}in}$ = 36.33 Ohms;

$Z_{g\text{-}out}$= 21.80 Ohms; $Z_{d\text{-}out}$= 72.657 Ohms.

Except the termination impedance of the input end of the drain line ($Z_{d\text{-}in}$), these impedances are equal to the characteristic impedances of the two lines at the higher end of the considered frequency band. The line characteristic impedance is defined for this purpose as :

$$Z_{char\text{-}k} = \sqrt{Z_{kk}\, Y_{kk}} \quad ; \quad (k = g,d : \text{gate, drain}) \qquad (15)$$

It is found also that only one inductor having an inductance of 2.14 nH/mm has to be added to the drain line to synchronize the velocities. The velocity of the propagating wave can be modified either by varying the inductance or the capacitance of the line. The drain capacitance was modified such that the velocity is the same as the previous case with inductance compensation and the lines were terminated by their new characteristic impedances. The results are shown in Fig. 5-4. It is clear from this figure that the power gain

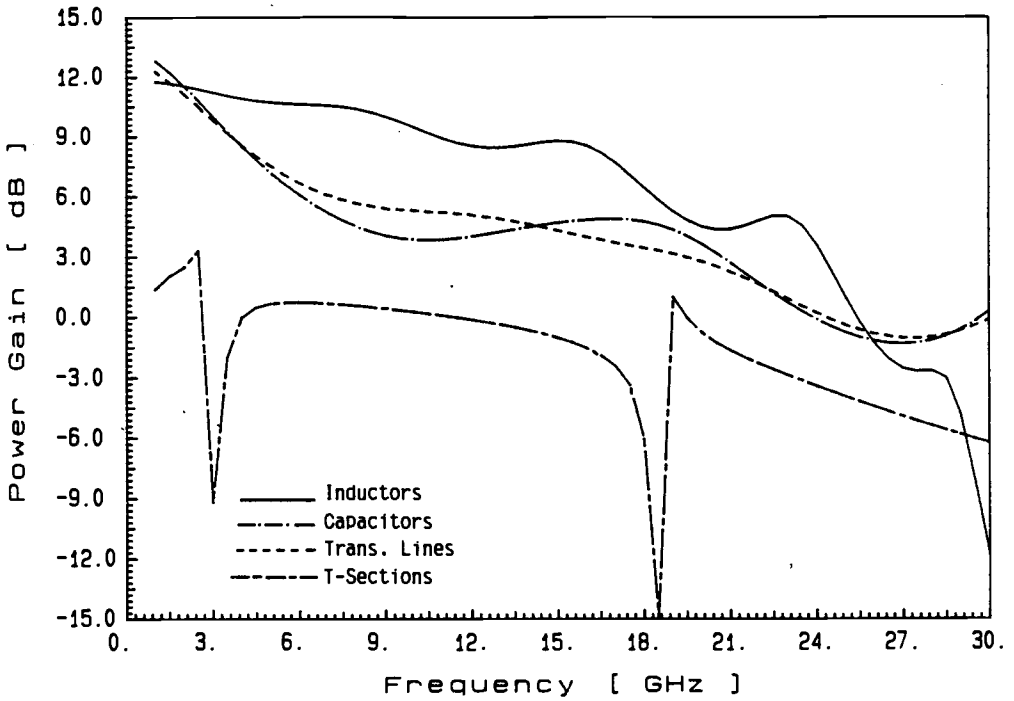

Fig. 5-3: The power gain of the 5-section MESFET of 300μm long each as the compensation elements optimized by TOUCHSTONE.

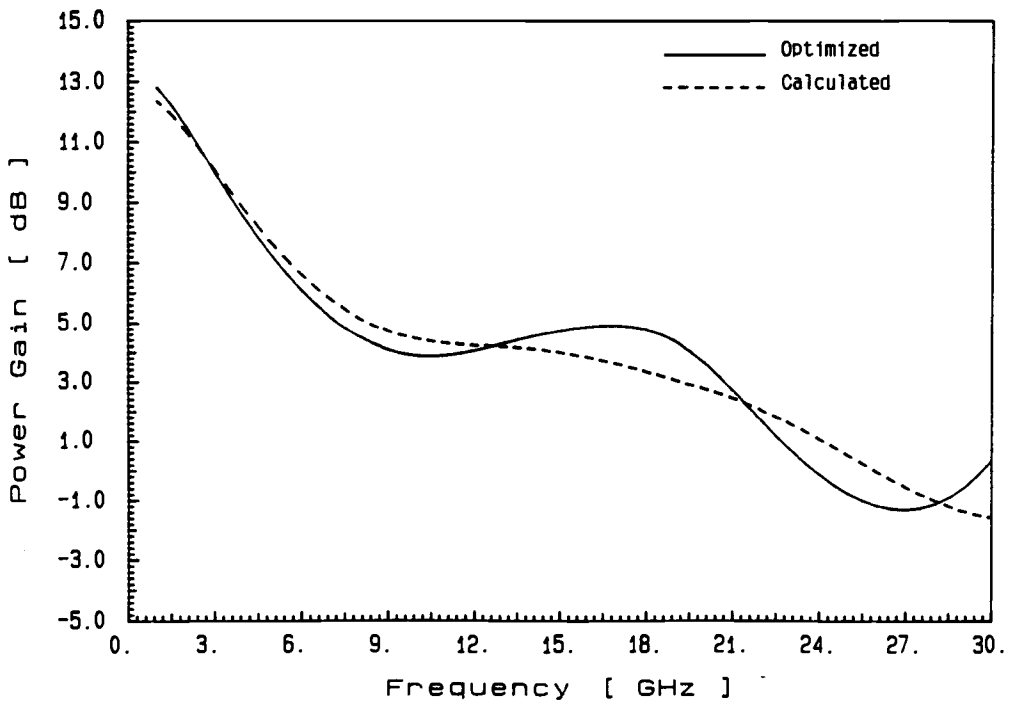

Fig. 5-4: The optimized capacitive compensation versus the calculated one.

is very close to that obtained by using the capacitance value obtained by the optimization and very much different from the results obtained by using inductive compensation as shown in Fig. 5-3. This means that not only the velocities have to be equal, but also the characteristic impedances of the two lines have their own effects on the gain. Increasing the drain inductance increases the drain characteristic impedance and reduces the phase velocity, while increasing its capacitance decreases its characteristic impedance as well as the wave velocity. In short, higher power gain requires equal velocities on gate and drain lines and higher drain characteristic impedance.

Although the gain curve obtained by TOUCHSTONE optimization is not flat because the device was simulated with relatively small number of sections, distributing the compensation element(s) i. e., the inductance and capacitance along the drain line gives better results as shown in Fig.5-5. As it can be seen in Fig.5-5-a, the phase velocities on the drain line using capacitive and inductive compensations are extremely close and both are very close to the phase velocity on the gate line. But the power gain obtained by using capacitive compensation is much smaller than obtained by utilizing inductive one as shown in Fig. 5-5-b.

5.6: <u>THE RESULTS AND CONCLUSIONS</u> :

Using the circuit elements (per millimeter along the electrodes transverse to the electron-drift direction) as given in table 3-2, and the termination impedances and the compensation drain inductance obtained by TOUCHSTONE, the distributed MESFET power gain is improved

substantially as shown in Fig. 5-6. The gain obtained by adding distributed inductance along the drain line is higher than both the gain obtained for asynchronized wave velocities and the one obtained by introducing the same inductance as lumped elements at specific points along the output electrode. The gain obtained is about 12 dB at 1 GHz and about 1.2 dB at 40 GHz.

Fig. 5-5-a shows the effect of the compensation element on the normalized wave velocities on the gate and drain lines, where the velocity on the drain line is reduced by the extra inductance such that it becomes very close to the wave velocity on the gate line. The phase or wave velocities are normalized by the velocity of light in free space and calculated from :

$$v_k = \omega/\beta_k = 2\pi f/Imag.[\sqrt{Y_{kk}Z_{kk}}]; \qquad (k = gate, drain) \qquad (16)$$

where ω is the angular frequency, β_k is the phase constant of line k, and Z_{kk} (Y_{kk}) is the self impedance (admittance) per unit length of line k.

Synchronization of the velocities has the most important effect on the power gain of the GaAs MESFET amplifier, because in this case the current adds up in phase along the output line. However, the added inductance has an opposite effect on the characteristic impedance of the drain line. As shown in Fig. 5-7, the magnitude of the drain characteristic impedance increases with compensation and the difference between the magnitudes of the gate and drain characteristic impedances becomes greater than before. This means that the higher gain is achieved with higher drain characteristic impedance. Because this difference in the line impedances, the termination impedances of

the two lines are also different. Nevertheless, no effect was noticed in the phase of the line characteristic impedance. The effect of the inductive compensation distributed along the drain electrode on the real and imaginary parts of the drain characteristic impedance is shown in Fig. 5-8. The line characteristic impedance is calculated by applying equation (15). Since the impedance is defined for a single line, i.e., in the absence of any other lines or couplings, the gate line is not affected by distributing an inductance along the drain line.

The synchronization of the phase velocities has a similar effect on the phase constant of the two lines as shown in Fig. 5-9. This is what is expected, because the phase constant and the phase velocity are related to each other. But the effect on the attenuation constant is minor as shown Fig. 5-10, where a small increase can be noticed in the drain attenuation constant due to the extra drain inductance.

Equalizing the phase velocities of the input and output waves along the gate and drain electrodes of the GaAs MESFET distributed amplifier affects the characteristics of the two modes of propagation i.e., the c-mode and the π-mode. For example, the c-mode phase constant increases and becomes close to the π-mode phase constant as seen in Fig. 5-11. The effect on the attenuation constants of the two modes is shown in Fig. 5-12. The two mode propagation constants (attenuation and phase) are calculated by applying equation 6 of chapter 2.

When the line characteristic impedances are obtained from the impedances of these lines for the two modes of propagation as :

$$Z_{char\text{-}k} = \sqrt{Z_{ck}\, Z_{\pi k}} \quad ; \quad (k = g,d), \qquad (17)$$

The impedance of both lines are affected by the compensation element due to the interaction coupling between them. Although the magnitude of the characteristic impedance of the gate line is increased sharply at low frequency, its final value at 40 GHz is about twice its original value before the velocity equalization. However, the magnitude of the characteristic impedance of the drain line is increased by a factor of four. The effect on the magnitude and phase of these impedances is shown in Fig. 5-13-a. As it can be seen in Fig.5-13-b, where the impedances are plotted as a function of the frequency, the maximum or most of the effect comes from the real part of the impedances. Finally, the synchronization effect on both voltage and current ratios of the two lines associated with the two modes of propagation is shown in Fig. 5-14 and Fig. 5-15.

In conclusion, the general normal mode analysis has proven to be very useful in the study of distributed parameter devices such as traveling-wave transistors. The higher power gain for a wide microwave frequency bands requires both the synchronization of the phase velocities on the gate and drain electrodes and higher output line characteristic impedance. A gain of more than 3 dB was achieved and maintained for frequencies up to 34 GHz. This could make the device useful for many applications through the millimeter-wave frequencies.

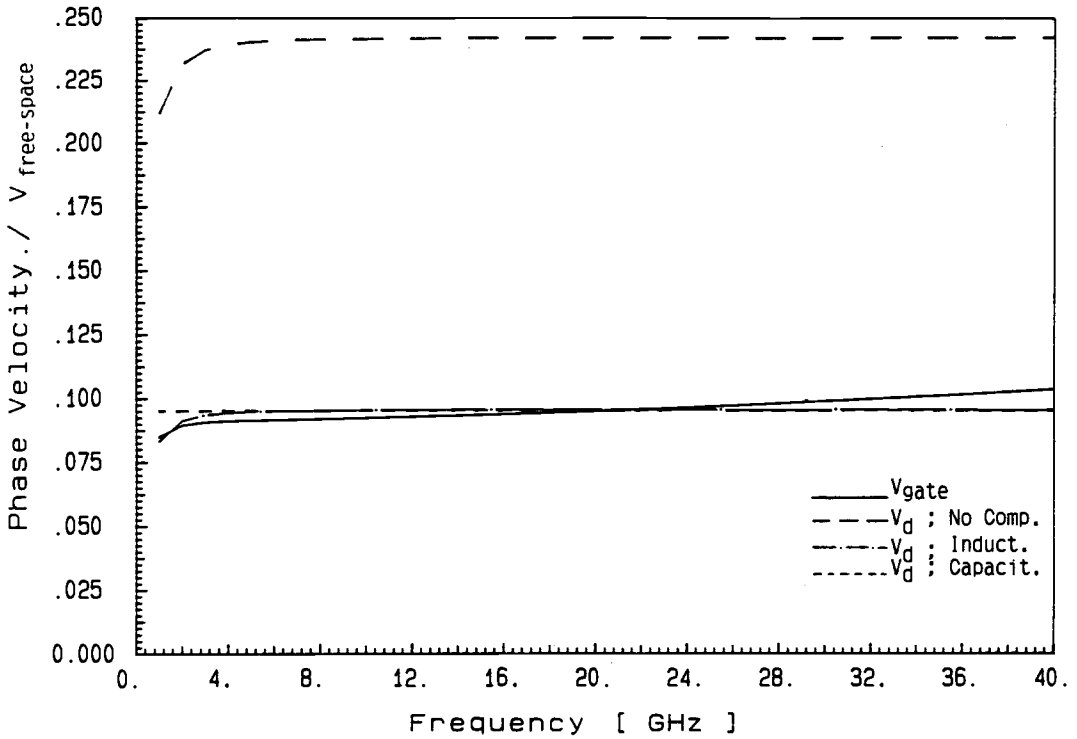

Fig. 5-5-a: The phase velocity on the gate and drain lines for different compensation elements.

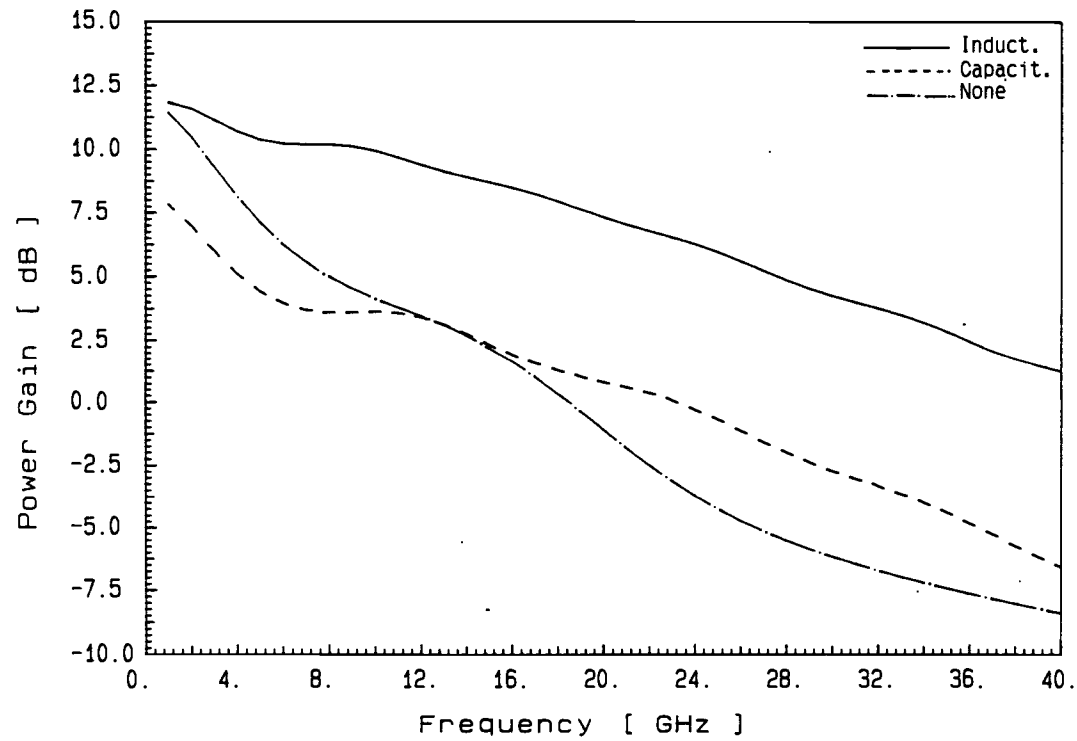

Fig.5-5-b: The power gain with distributed inductive and capacitive compensations versus non-compensated device's gain.

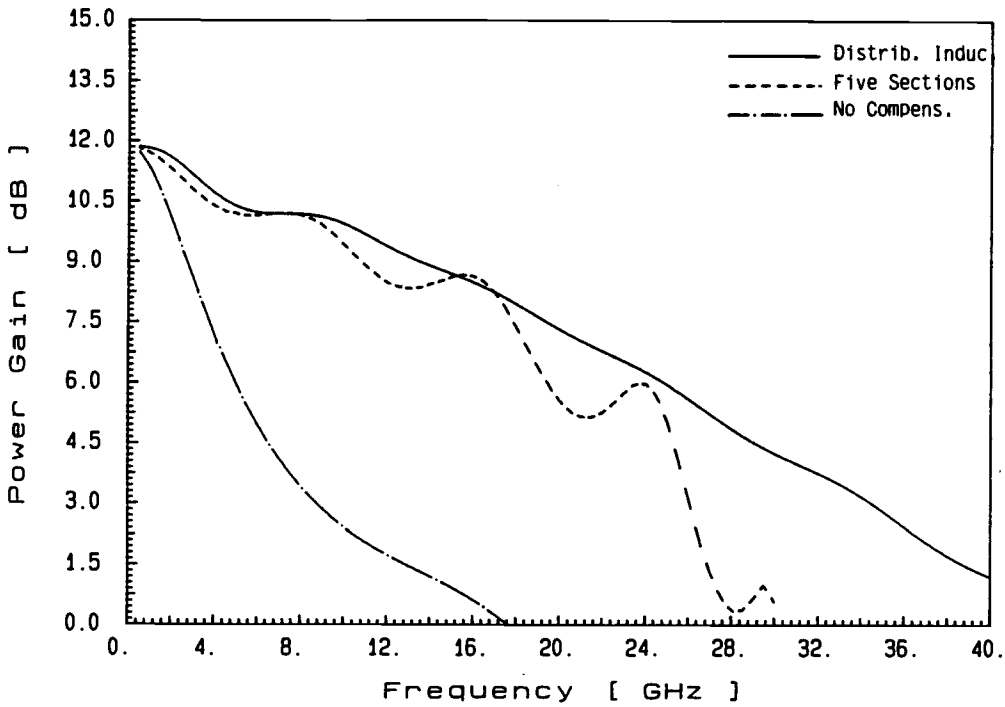

Fig. 5-6: The power gain of the distributed parameter GaAs MESFET.

Gate width = 1500 μm; V_{gs} = 0 and V_{ds}= 5 volts.

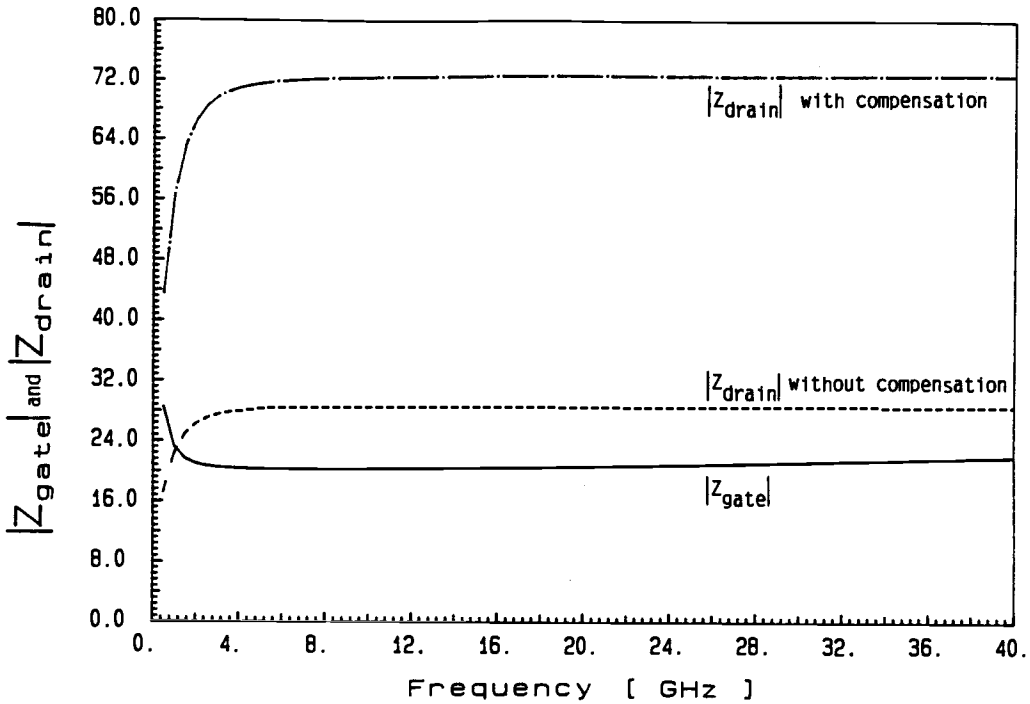

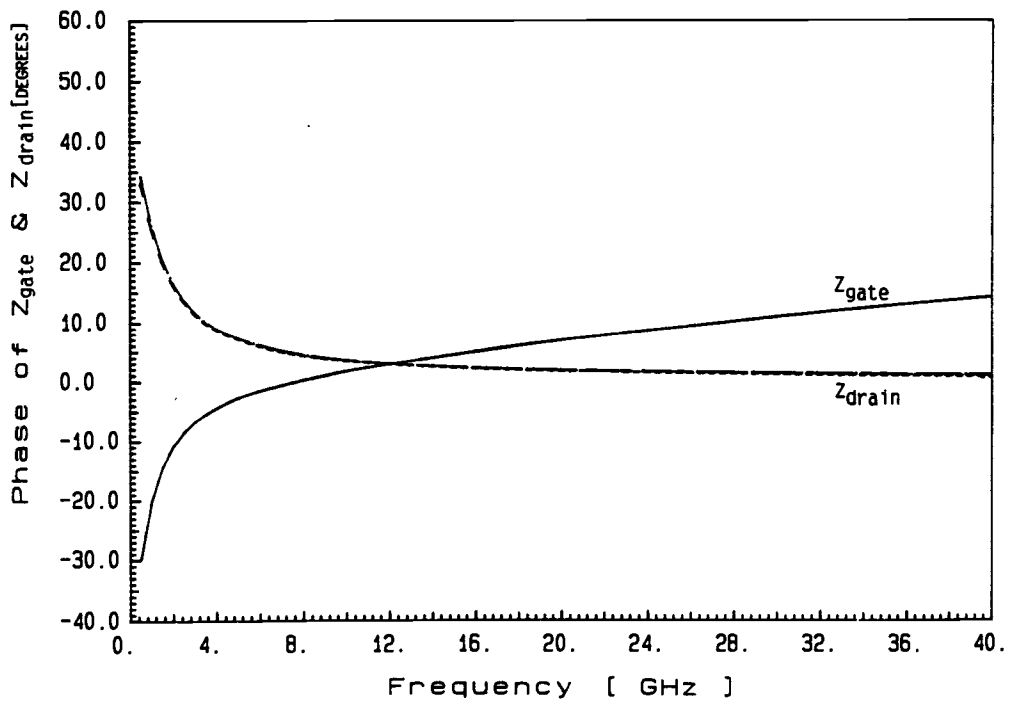

Fig. 5-7: The gate and drain characteristic impedances. [Magnitude and phase]

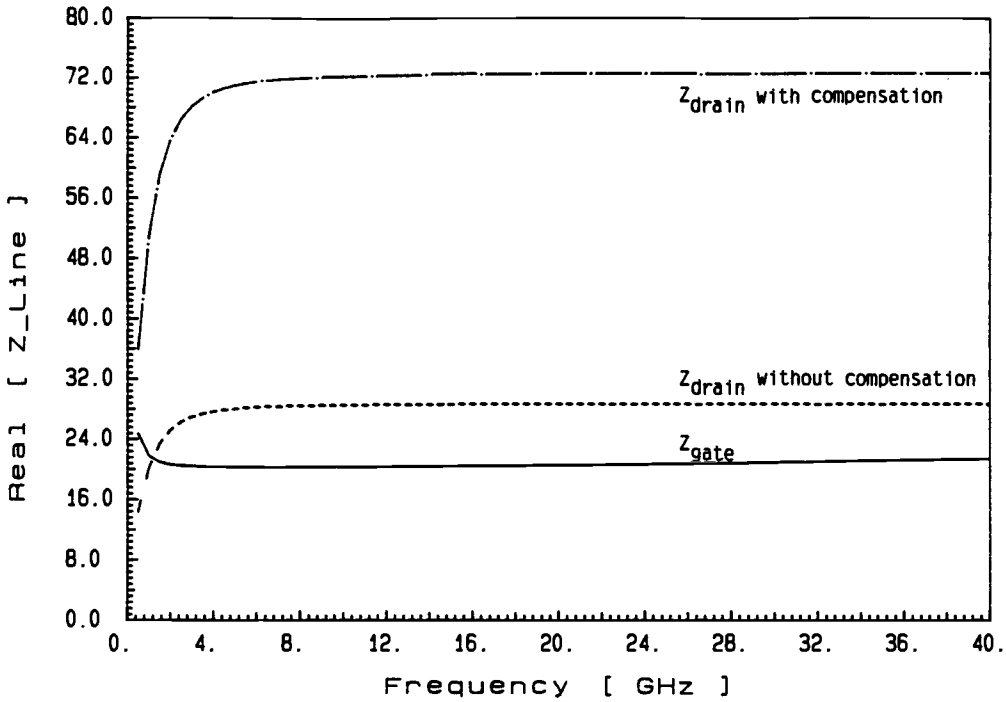

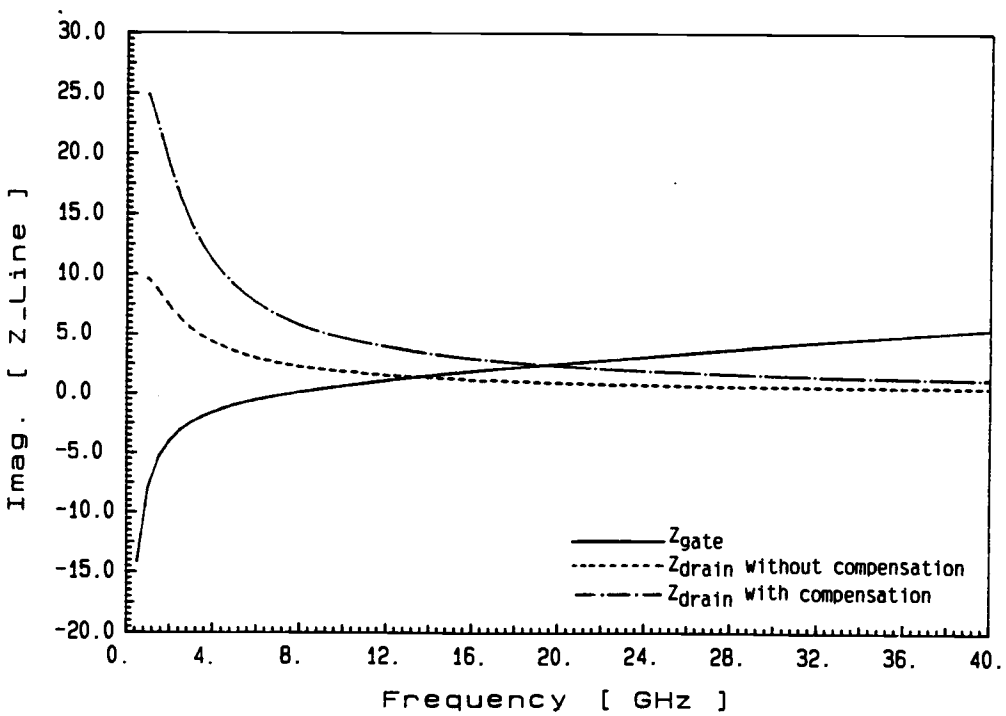

Fig. 5-8: The gate and drain characteristic impedances. [Real and imagenary parts]

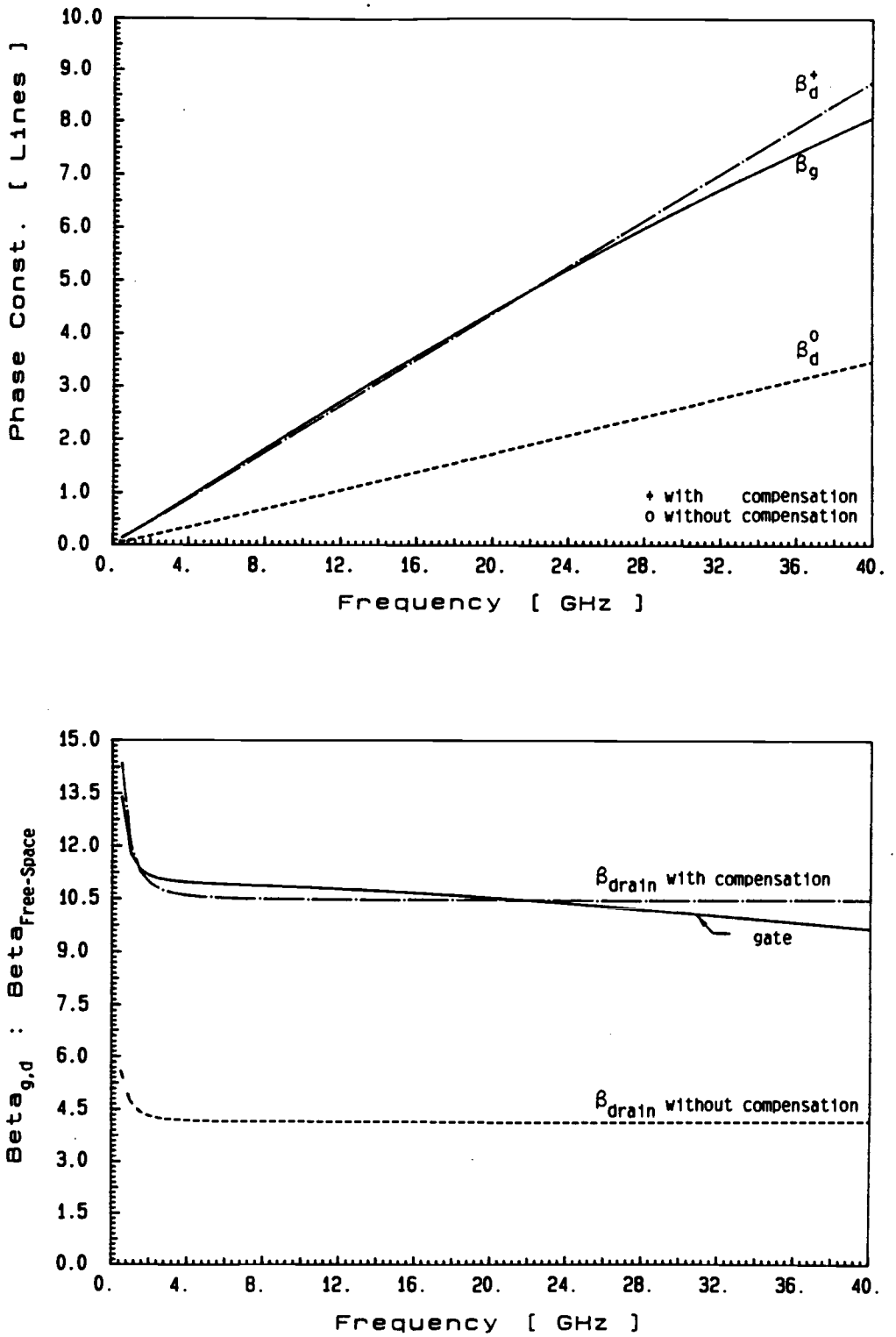

Fig. 5-9: The effect of the velocity synchronization on the phase constants of the gate and drain lines.

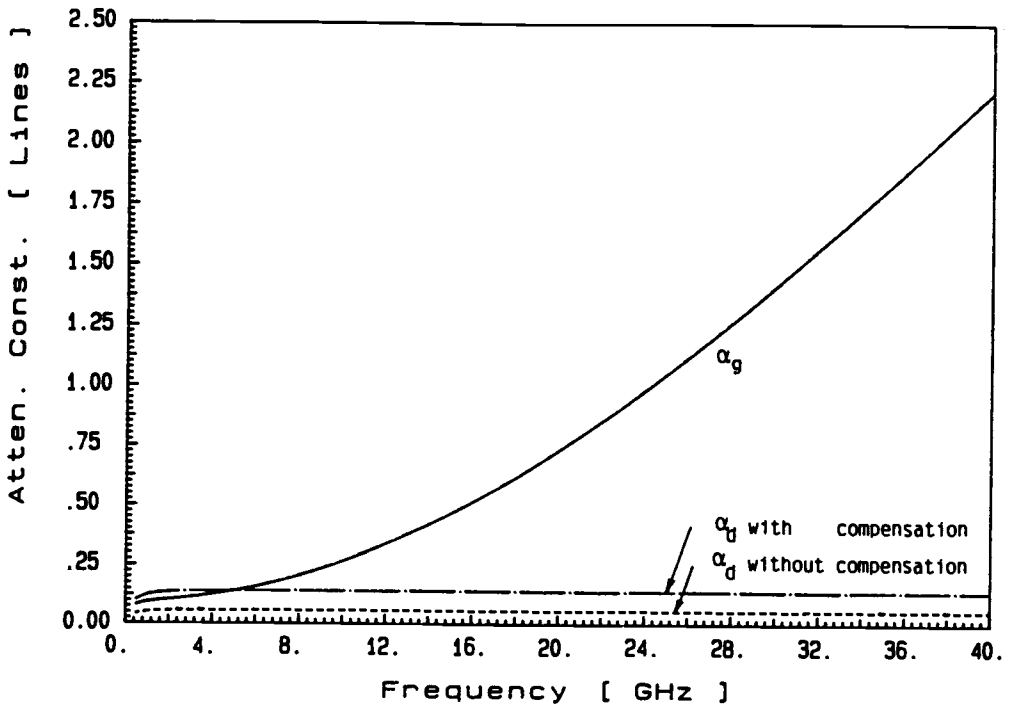

Fig. 5-10: The attenuation constants of the gate and drain electrodes.

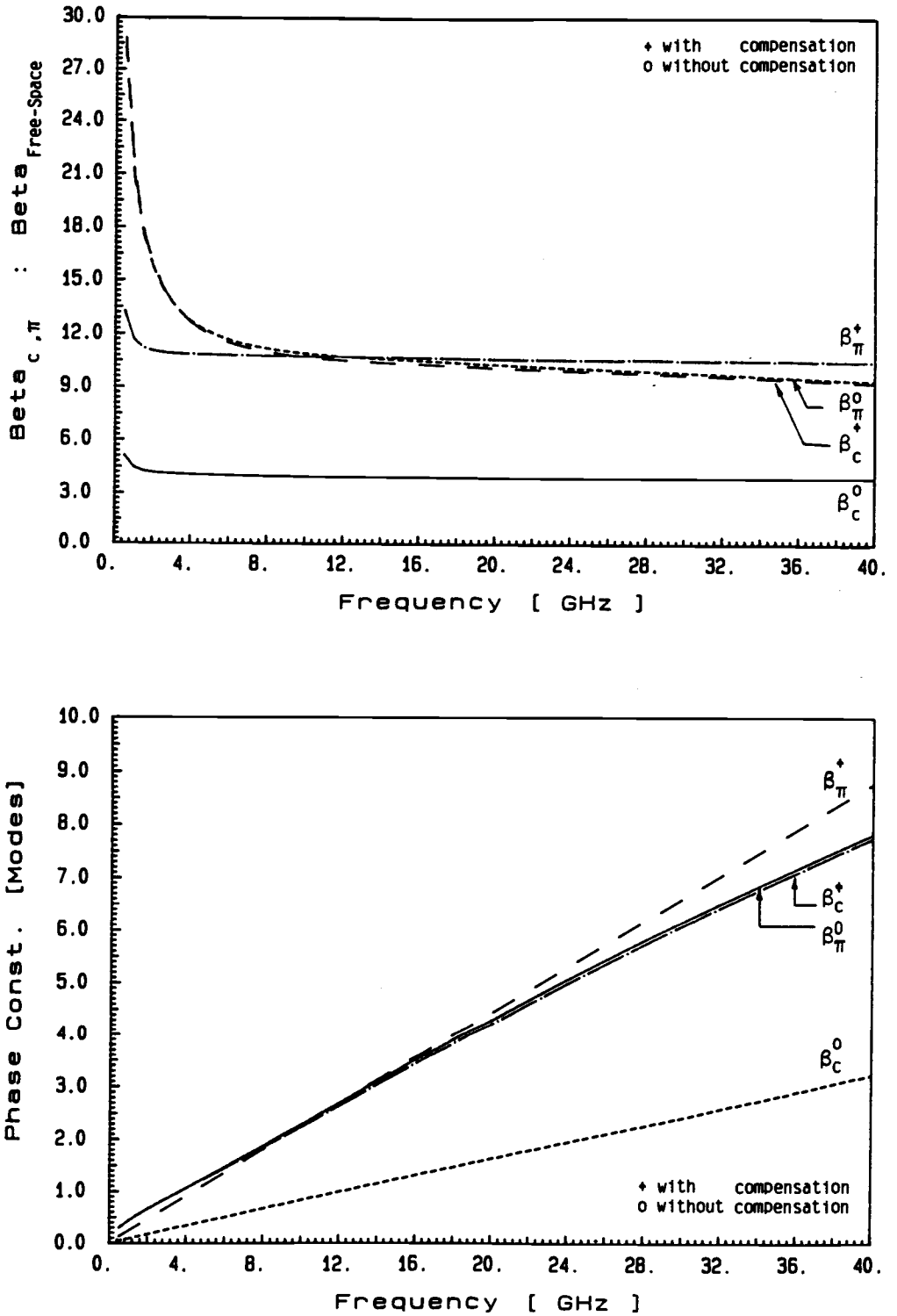

Fig. 5-11: The effect of the phase velocity equalization on the phase constants of the two normal modes of propagation.

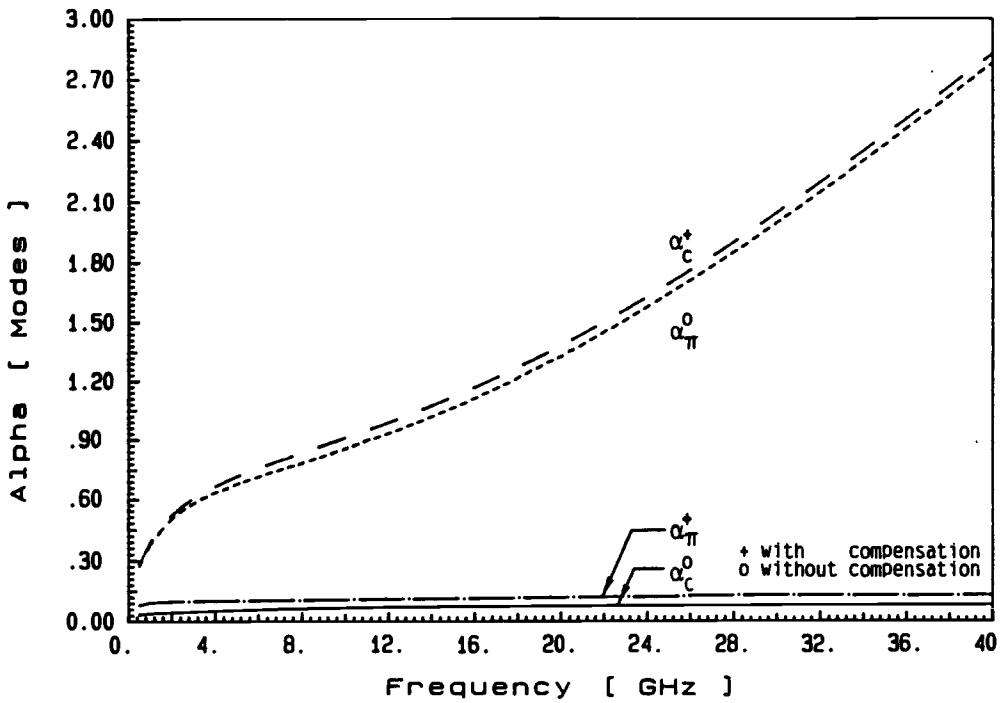

Fig. 5-12: The attenuation constants of the two normal modes; c- and π-mode [or co- and anti-mode].

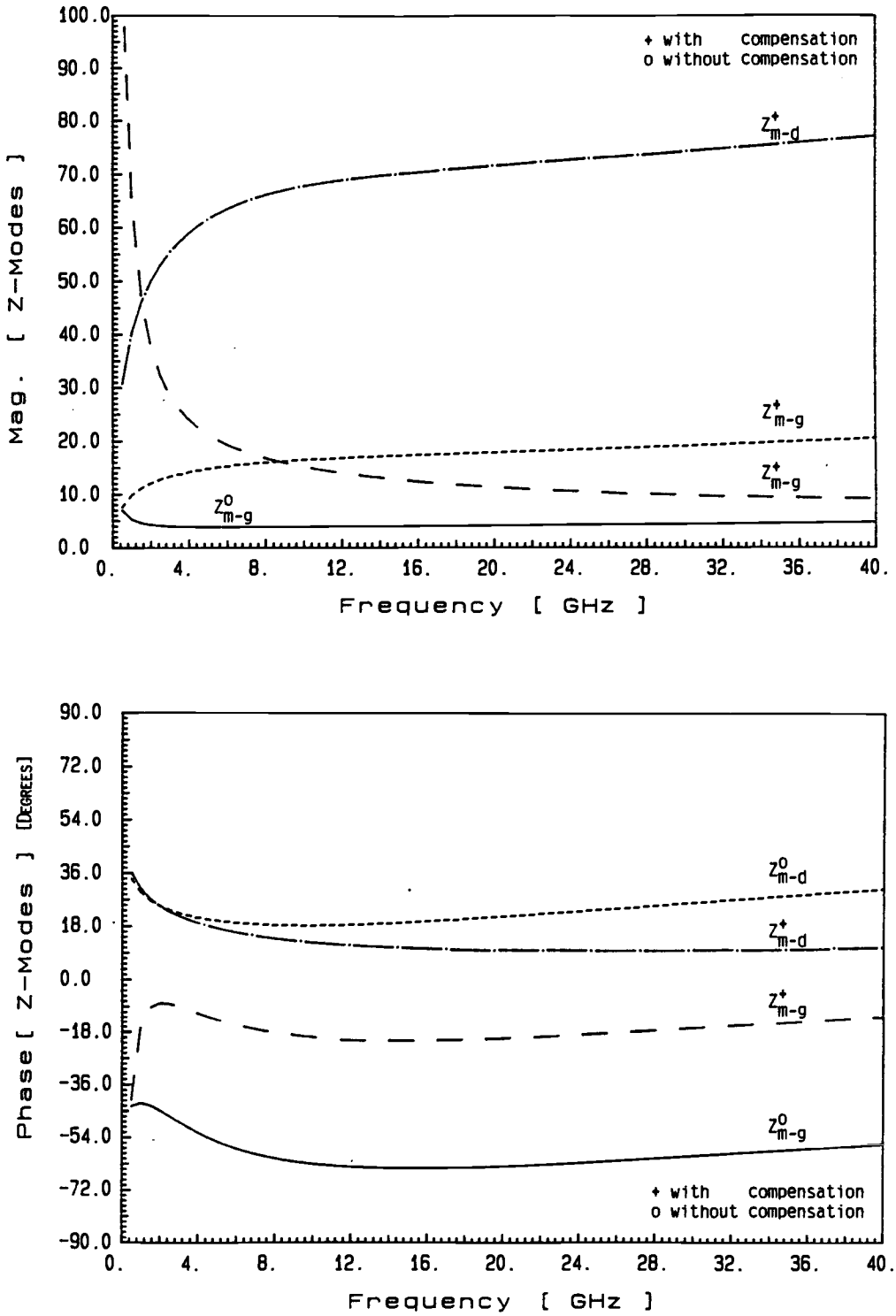

Fig. 5-13-a: The gate and drain characteristic impedances associated with the two normal modes of propagation.

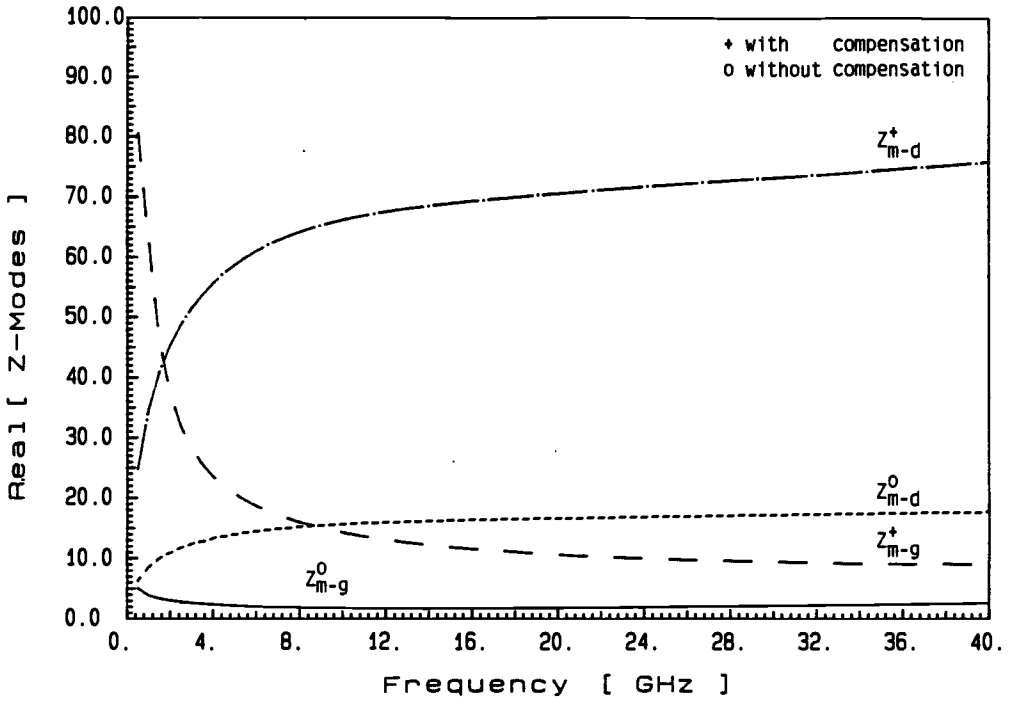

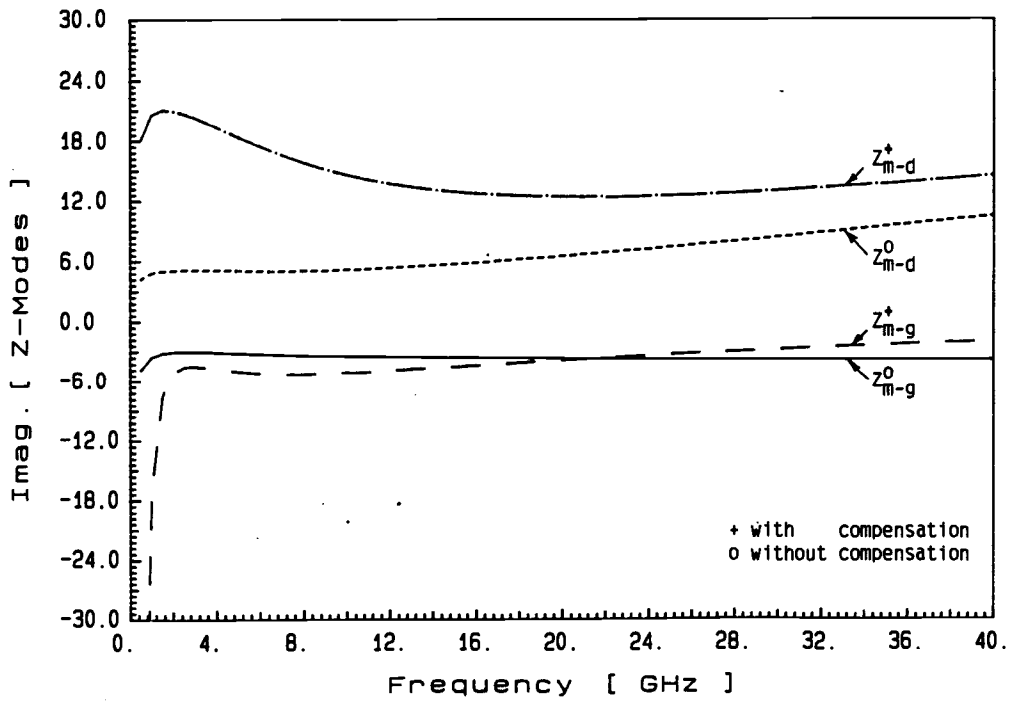

Fig. 5-13-b: The gate and drain characteristic impedances associated with the two normal modes of propagation.

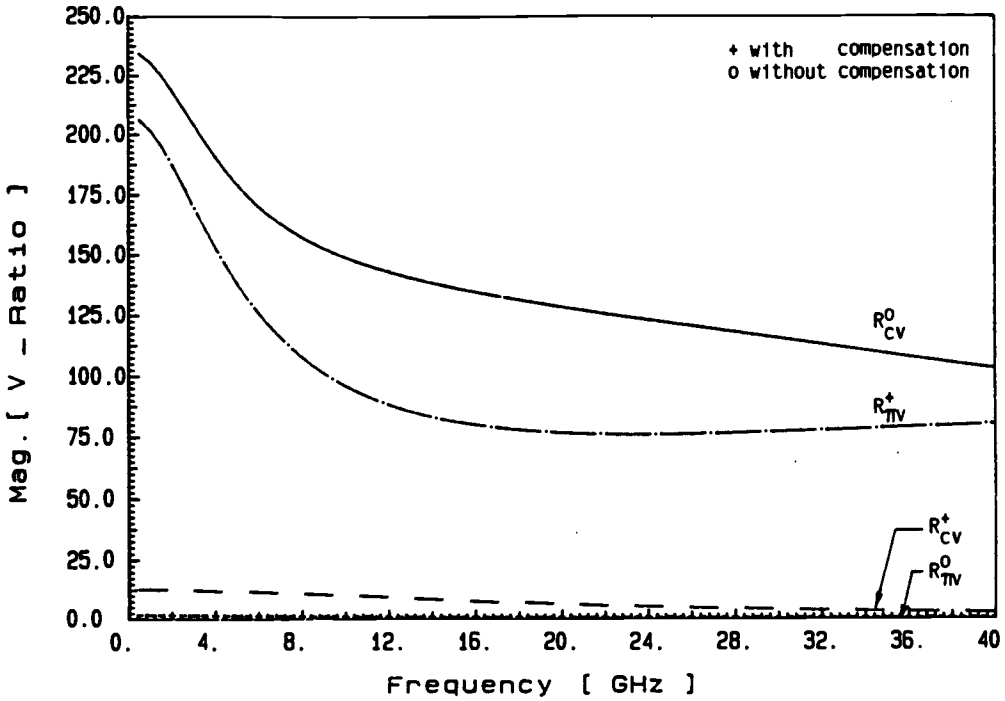

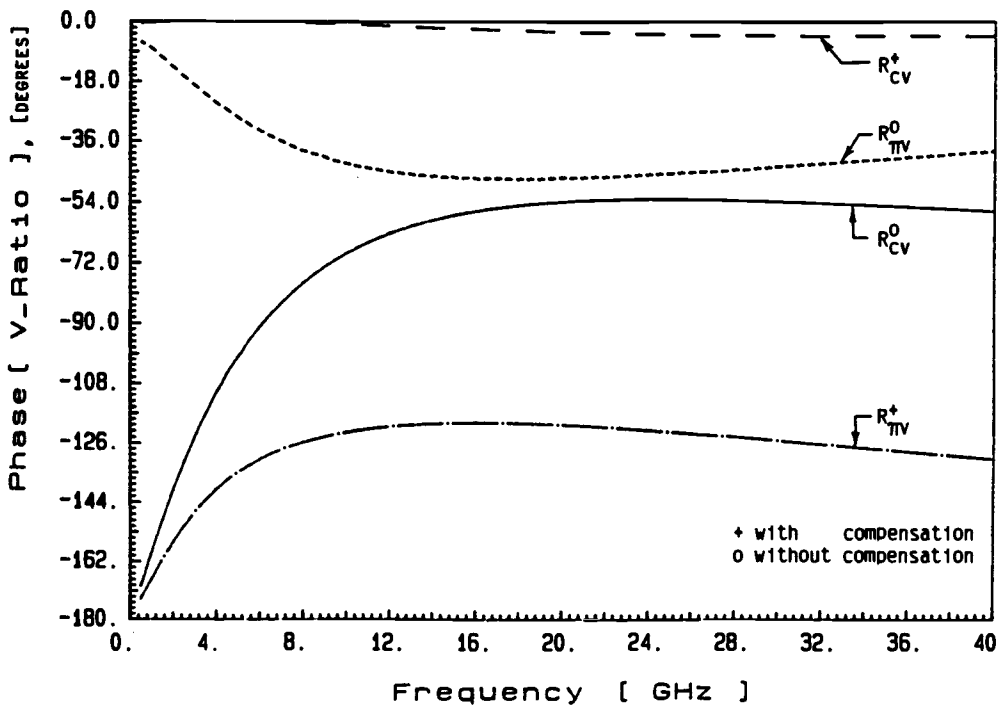

Fig. 5-14: The drain-to-gate voltage ratio associated with the two normal modes of propagation.

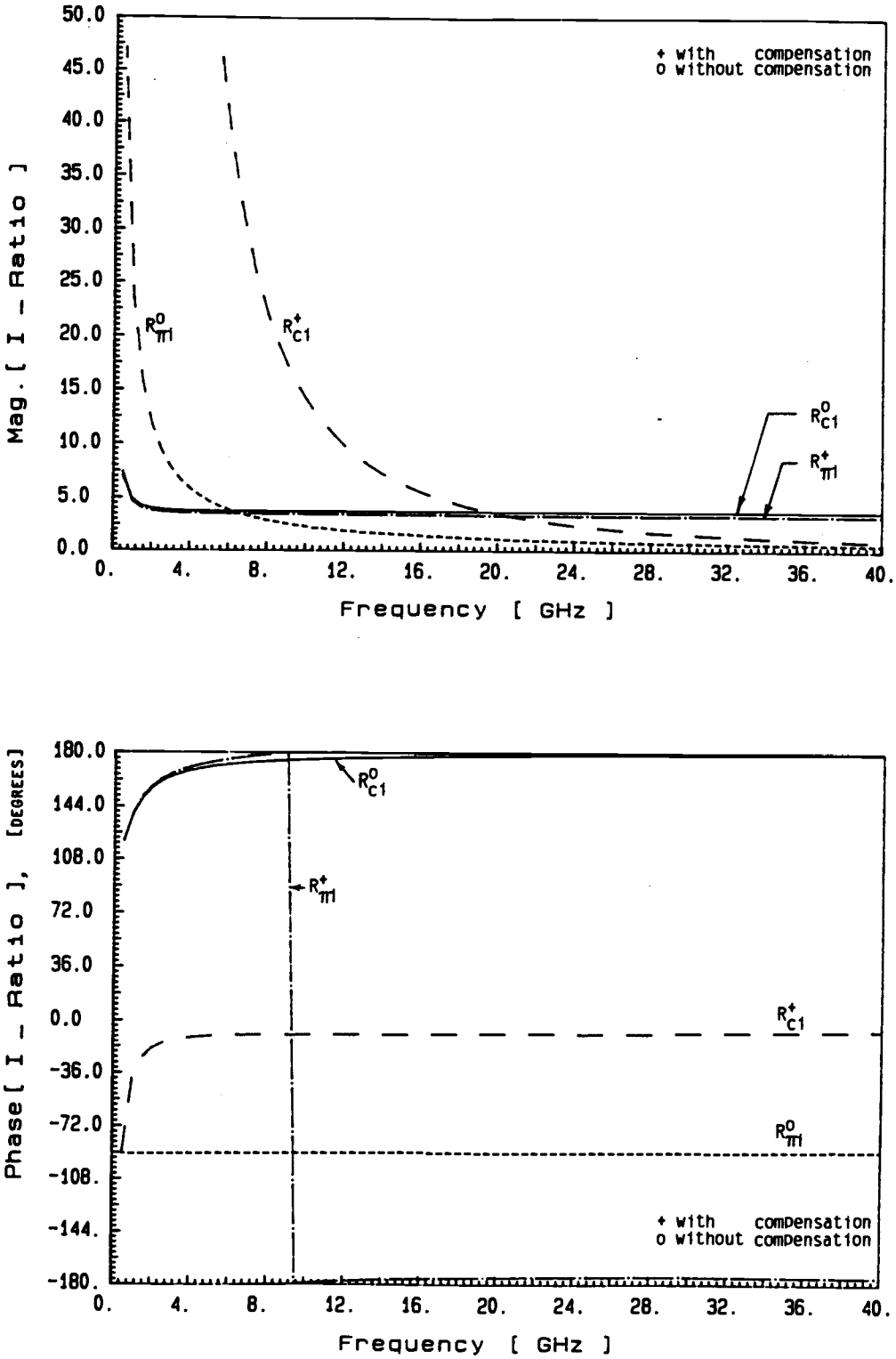

Fig. 5-15: The drain-to-gate current ratio associated with the two modes of propagation.

CHAPTER 6

SMALL-SIGNAL AND QUASI-HARMONIC ANALYSIS OF COUPLED SCHOTTKY LINES

6.1 : INTRODUCTION :

The analysis of active and passive coupled distributed parameter systems has been a topic of continued interest because of its application in a wide range of useful circuits and systems. Examples include : electromagnetic couplers such as microwave and optical directional couplers[13,117,166-170], multimode and multiconductor transmission systems including VLSI interconnects [171-174], distributed parametric amplifiers and harmonic generators [29,30,175], and Traveling-Wave Field-Effect Transistors[10,31,138,139,153].

One of the important techniques used to study these systems is the coupled mode theory. Much of the previous work on the coupled mode theory has been focused on lossless linear systems and nonlinear transmission lines have been studied for special cases such as harmonic generation and parametric mixing[176]. Our study covers the case of a coupled lossy nonlinear system.

The system to be analyzed consists of two-lossy, identical uniformly coupled transmission lines, having uniformly distributed nonlinear capacitances. The nonlinearity of these capacitances may be attributed to either the nonlinearity of the dielectric medium or to the voltage dependence of the depletion-layer capacitance of Schottky lines. The effect of the nonlinearity of Schottky junction on the properties of microstrip lines has been studied by Jager[177-180]. The nonlinearity in both cases considered here is assumed to be small enough such that the quasi-harmonic analysis can be applied. In this

analysis, a nonlinear element is substituted by a linear element the magnitude of which depends upon the amplitude of excitation. It is assumed that the excitation is sinusoidal and the approximate response is taken to be the component of the actual response which has the same frequency and phase[181]. This procedure is also called the equivalent linearization procedure of Kryloff and Bogoliuboff[182].

The two coupled nonlinear transmission lines are excited by applying the signal to the input end of one of the two lines. The voltage (power) as a function of the position along the lines is analytically determined. It is assumed that the lines are semi-infinite in the direction of the wave propagation so that backward wave propagation is not present.

The identical coupled Schottky lines are analyzed by utilizing a linearized model for possible applications as voltage tunable circuits. Although it is possible to apply any dc-bias to the system, the same voltage must be applied to both lines if we want them to have the same depletion-layer capacitance and keep them identical. For this case, the circuits considered consist of finite length and the backward waves are included in the analysis. The scattering parameters are calculated for this four-port network as a function of frequency, dc-bias voltage and the line length.

For the case of a nonlinear dielectric substrate, the linear part of the self and mutual capacitances are calculated by the technique developed by Lee and Tripathi[183-185] using CPWNG, the computer program developed at OSU to compute the quasi-TEM parameters of general single asymmetrical and multiple coupled coplanar waveguide

structures with finite dielectric thickness and without a ground plane. The same method is used to calculate the self and mutual interelectrode capacitances of the nonlinear Schottky lines. The linear part of the overall self capacitance is formed by a sum of two terms, the self interelectrode capacitance and the Schottky junction capacitance.

In general, the nonlinear capacitance can be a function of space and time as in the case of Traveling-Wave MESFETs[29,30] and distributed parametric amplifiers[175]. In these cases the effect of the higher order time-dependent terms are important. For the quasi-harmonic analysis to be applicable, the effective linearization has to be made such that the capacitance becomes time-independent and the higher harmonics become negligible. In our study, the type of the capacitance used is the same type as described by Scott[181].

6.2 : *THEORETICAL ANALYSIS* :

The system of two identical transmission lines to be analyzed is shown in Fig.(6-1)-(6-3).

The self and mutual inductance L and L_m, the metalization resistance R, and the conductance G all are linear elements. The self capacitance C_{eq} is, in general, a nonlinear element. It consists of two parts, the linear part, which is independent of the signal (ac-excitation) and a nonlinear part, which is excitation dependent. The former represents the self electrode capacitance and the depletion-layer capacitance for the case of Schottky lines. The

nonlinear part represents the variation in the depletion-layer capacitance due to the ac-excitation. If the medium is nonlinear, so is the mutual capacitance. All the circuit elements are normalized per unit length of the line.

The analysis of the identical nonlinearly coupled transmission lines presented here consists of two parts, the linearized model of Schottky lines and a quasi-harmonic analysis of the nonlinear model.

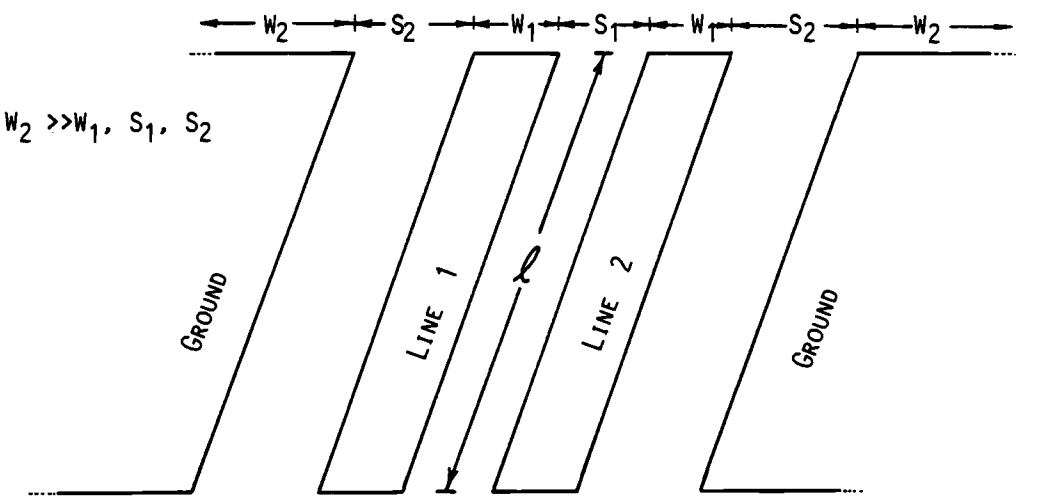

Fig.6-1: Two-identical coupled transmission lines; Overview.

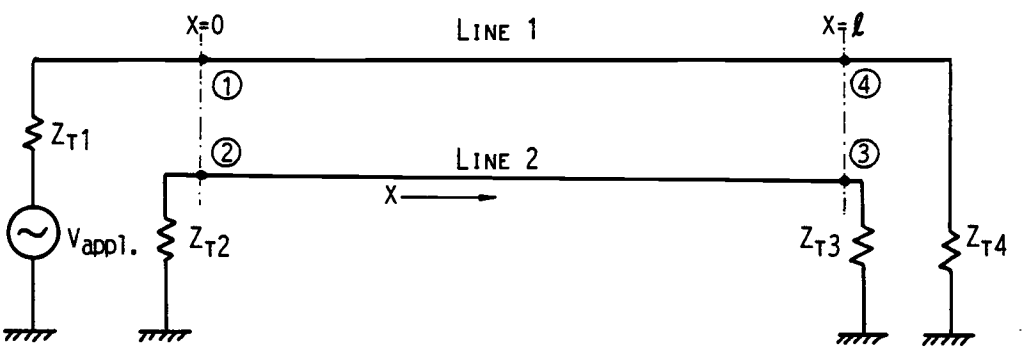

Fig. 6-2: Coupled transmission lines.

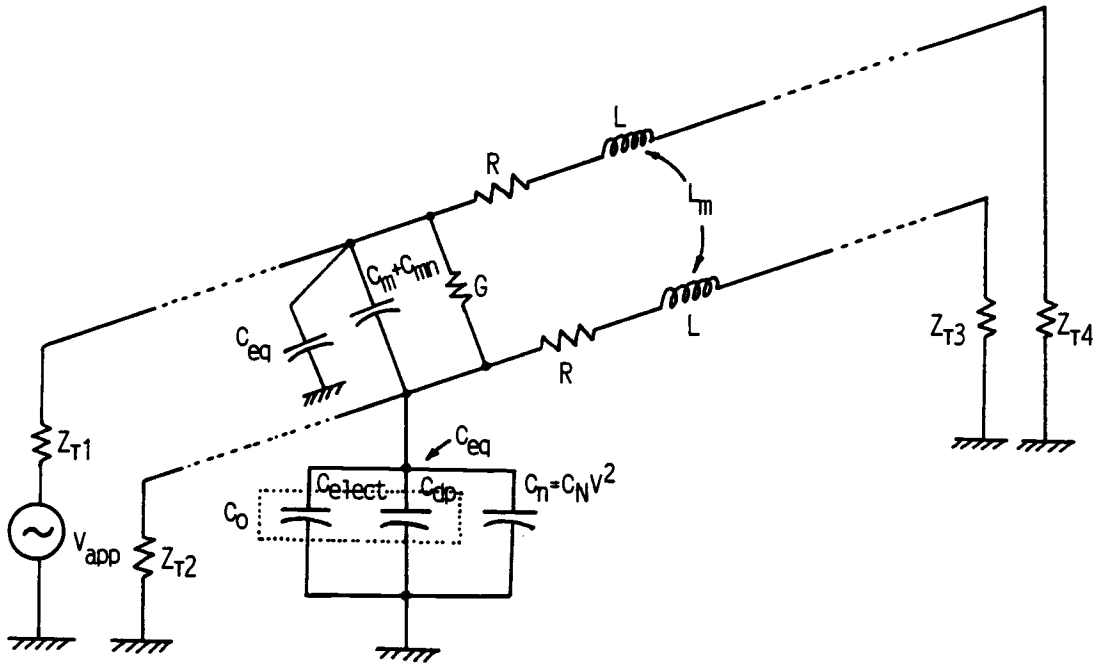

Fig. 6-3: The equivalent circuit of the identical coupled transmission lines.

6.2.1 : Linear Analysis of Coupled Schottky Lines :

In a linear analysis of Schottky lines, the signal amplitude is assumed to be much smaller than the net sum of the built-in voltage and the dc-bias such that its effect on the depletion-layer capacitance is negligible. Therefore, the self capacitance of each line is assumed to be a linear element, but the Schottky junction capacitance is still a function of the dc-bias. This dependence on dc-bias makes the structure useful for applications in voltage tunable and switching circuits. The linear active coupled line analysis developed in chapter 2 is applied to this linearized model in a similar manner as in the case of the MESFET structure described in chapter 5 but without active

coupling. The structure is assumed to be finite in length and the four ports are terminated by proper termination impedances. The power at each port is calculated from the scattering parameters at these ports.

Both co- and contra-directional couplers can be designed by using coupled Schottky lines since the even and odd mode phase velocities are not equal. For a given dc-bias and length, the system can be described as a co- or contra-directional coupler depending upon the values of the line constants. In a codirectional coupler the forward wave on one line couples with the forward waves on the other line, while the backward wave couples with the backward waves[166]. This is seen to occur when the capacitive and inductive factors of the coupling are equal (i.e., $k_c = k_l$). The coupling factors are defined as:

$$k_c = \frac{C_m}{\sqrt{C_{11}C_{22}}} \qquad \text{and} \qquad k_l = \frac{L_m}{\sqrt{L_{11}L_{22}}} \tag{1}$$

Where $C_{jj}(L_{jj})$ is the shunt self capacitance (series self inductance) per unit length of line j in the presence of line i, and $C_m(L_m)$ is the mutual capacitance (inductance) per unit length. If $k_c = -k_l$, the situation is referred to as contra-directional coupler.

Since the two lines considered here are identical,

$$k_c = C_m / C \qquad \text{and} \qquad k_l = L_m / L \tag{2}$$

Where,

$$C = C_{11} = C_{22} \qquad \text{and} \qquad L = L_{11} = L_{22} .$$

$$\text{For } k_c = |k_l|, \quad C_{dp} = (C_m/L_m)\times L - C_{electrode} \tag{3}$$

Where C_{dp} is the depletion region capacitance of Schottky junction and $C_{electrode}$ is the electrode self capacitance of the line excluding C_{dp}. Obtaining the junction capacitance from equation (3), the dc-bias required to achieve this value can be calculated from the depletion-

layer capacitance equation, i.e., $C_{dp} = W \left[\frac{q\epsilon N_D}{2(V_{Bi}+V_{dc\text{-}bias})}\right]^{\frac{1}{2}}$.

When the lines are terminated by the characteristic termination impedance, port 3 is completely isolated and the power is transferred to port 2 or port 4. Thus, the terminating impedance used for a contra-directional coupler is given by :

$$Z_{char.} = \sqrt{Z_{even}\, Z_{odd}} = \sqrt{Z_{c1} Z_{\pi 1}} \qquad (4)$$

Generally, $k_c \neq k_l$ and the system behaves as a non-ideal directional coupler. If the lines are terminated by their own characteristic impedances, the structure can be designed to act as a codirectional coupler, i.e., the power is transferred back and forth between the two lines as we change the line length. A small fraction of the reflected power on both lines appear on the sending ports due to the imperfect match at ports 3 and 4. The reflected waves are coupled and interact with the waves moving in the opposite direction as well.

For a given structure, the inductance matrix is independent of the voltage applied to the Schottky lines. However, the self capacitance of these lines depends on the applied voltage through the junction capacitance where the variation is quite large when the net sum of the bias voltage and the built-in voltage is small (as shown in Fig. 6-4). By utilizing the dependence of the self capacitance on the voltage applied to the Schottky lines, the capacitive coupling factor can be modified accordingly. This feature can be used to design electronic switches.

Using the coupled mode theory, it is found that the normal mode

propagation constant of the coupled waves is in the form [168],

$$\beta = \pm j\beta_o\sqrt{1 \pm \delta} \tag{5}$$

Where,

$$\beta_o = \left[\frac{\beta_1^2 + \beta_2^2}{2} - \beta_1\beta_2 k_1 k_c \right]^{\frac{1}{2}} \tag{6}$$

$$\delta = \left[1 - \left(\frac{\beta_1^2\beta_2^2}{\beta_o^4}\right)(1-k_1^2)(1-k_c^2)\right]^{\frac{1}{2}} \tag{7}$$

and

$$\beta_i = \omega\sqrt{L_{ii}C_{ii}} \qquad (i=1,2) \tag{8}$$

For identical lines, $\beta_1 = \beta_2 = \beta$,

$$\beta_o = \beta\sqrt{1 - k_1 k_c} \tag{9}$$

and

$$\delta = [1-(\beta/\beta_o)^4(1-k_1^2)(1-k_c^2)]^{\frac{1}{2}} \tag{10}$$

Louisell[175] defined the normal mode propagation constants of of the codirectional coupler as :

$$\gamma_{1,2} = -j(\beta_a \pm \beta_b) \tag{11}$$

Where,

$$\beta_a = (\beta_1+\beta_2)/2 \tag{12}$$

$$\beta_b = \pm [\beta_d^2 + |C_{12}|^2]^{\frac{1}{2}} \tag{13}$$

$$\beta_d = (\beta_1-\beta_2)/2 \tag{14}$$

and C_{12} is the mutual coupling coefficient.

For identical lines, $\gamma_{1,2} = -j(\beta \pm |C_{12}|)$ (15)

Furthermore, if the medium surrounding the identical conductors is homogeneous, and for the even mode of excitation, $k_1 = k_c = \delta = C_{12} = 0$ and equations(5) and (11) reduce to : $\gamma = \pm j\beta$ and $\gamma_1 = -j\beta$ respectively. Therefore, the negative root of Krage and Haddad { equation (5)} must be chosen to match the propagation constants as defined by Louisell {equation (11)} :

$$\beta_o\sqrt{1 \pm \delta} = \beta \pm |C_{12}| \tag{16}$$

The two solutions have to be satisfied simultaneously, i.e.,

$$\beta_o \sqrt{1 + \delta} = \beta + |C_{12}| \qquad (17)$$

$$\beta_o \sqrt{1 - \delta} = \beta - |C_{12}| \qquad (18)$$

Subtracting equation (17) from (18) gives :

$$|C_{12}| = (\beta_o/2)(\sqrt{1+\delta} - \sqrt{1-\delta}) \qquad (19)$$

The solution for the power on the two lines as a function of the position along the lines is given by[175] :

$$P_1(x) = P_1(0) \cos^2(|C_{12}|x) \qquad (20\text{-a})$$

$$P_2(x) = P_1(0) \sin^2(|C_{12}|x) \qquad (20\text{-b})$$

Where $P_1(0)$ is the input power in line 1 and $|C_{12}|$ is the coupling coefficient. Note that no signal power is applied at the input end of line 2.

It is seen from the above equations that a complete power transfer from the first line to the second line takes place when :

$$x = \pi/(2|C_{12}|)$$

If for $V_{dc} = V_1$, $C_{12}(V=V_1)l$ is chosen to be $n\pi/2$, where n is an odd integer number, the condition for complete power transfer is given by:

$$C_{12}(V=V_2) = C_{12}(V=V_1) \pm \pi/(2l) \qquad (21)$$

In this case, when the dc-bias switched from V_1 to V_2, the power is transferred from line 2 to line 1 at $x=l$ and vice versa. On the other hand, if $C_{12}(V=V_1)l$ is chosen to be πn, where n is an integer (even or odd) number, $C_{12}(V=V_2)$ is still given by equation(21), but switching the dc-bias from V_1 to V_2 switches the power from line 1 to line 2 at $x = l$.

6.2.2 : Nonlinear Quasi-Harmonic Analysis :

According to the equivalent linearization procedure of Kryloff and Bogoliuboff[182], the nonlinear element can be replaced by a linear element whose magnitude depends upon the excitation amplitude, where the excitation is assumed to be sinusoidal and the approximate response is taken to be the component of the actual response which has the same frequency and phase. As described by Scott[181], this method is also useful in dealing with nonlinear energy storage elements. For a nonlinear capacitance, it is usually possible to specify the charge as a single valued function of the terminal voltage: $Q = Q(v)$ (22)

Where v is the total voltage (dc-bias and ac-signal).

If the excitation voltage is sinusoidal of the form given by :

$$v(t)_{signal} = V\cos(\omega t), \tag{23}$$

the charge is expected to be an even periodic function with a frequency equal to ω. Therefore, we can express the charge as a Fourier cosine series;

$$Q(t) = Q_0 + Q_1\cos(\omega t)+Q_2\cos(2\omega t)+Q_3\cos(3\omega t)+ \ldots \tag{24}$$

To use the quasi-harmonic analysis appropriately, Q_1 *must be large with respect to the other coefficients and therefore,*

$$Q(t) \simeq Q_1\cos(\omega t) \tag{25}$$

Q_1 *can be evaluated as:*

$$Q_1 = \frac{1}{\pi}\int_0^{2\pi} Q(V.\cos\theta)\,\cos\theta d\theta \; ; \qquad \theta = \omega t \tag{26}$$

Since

$$i = \frac{dQ}{dt} = -\omega Q_1 \sin(\omega t) \tag{27}$$

and for an equivalent time-independent capacitance C_{eq}, the current would be :

$$i = C_{eq} \frac{dv}{dt} = - \omega C_{eq} V \sin(\omega t) \qquad (28)$$

Combining equations (26),(27) and (28) :

$$C_{eq} = \frac{1}{\pi V} \int_{o}^{2\pi} Q(V.\cos\theta) \cos\theta d\theta \qquad (29)$$

However, if Q(v) is described by the Taylor's series :

$$Q(v) = \sum_{n=0}^{\infty} a_n v^n = a_o + a_1 v + a_2 v^2 + a_3 v^3 + a_4 v^4 + \ldots, \qquad (30)$$

only the odd terms will contribute to the integral of equation (29), and the equivalent capacitance C_{eq} would be:

$$C_{eq} = a_1 + 3a_3 \frac{V^2}{4} + 5a_5 \frac{V^4}{8} + \ldots\ldots \qquad (31)$$

If the signal amplitude is not sufficiently large, only the first two terms will contribute to C_{eq} and equation (31) becomes :

$$C_{eq} = a_1 + 3a_3 V^2/4 \qquad (32)$$

This equation represents two parallel capacitances; the first term on the right-hand side represents a linear capacitance, while the second term represents a nonlinear capacitance which depends on the square of the excitation voltage amplitude.

The field-strength dependence of the dielectric constant of some materials, such as $BaTiO_3$ ceramic, makes these materials useful for many applications such as dielectric amplifiers, modulators, memory devices and for the tuning circuits because it permits the control of the nonlinear dielectric properties by applying auxiliary fields[186].

Since the deviations from the linearity are usually very small,

the nonlinear effect can be represented by expanding the dielectric constants in a power series in field quantities, such as the electric field[187]. For the case of coupled transmission lines on a nonlinear dielectric substrate, it is assumed that the dielectric constant of the material depends on the square of the signal amplitude. Therefore, we can write :

$$C_{eq} = C_0(1+\alpha V^2) \qquad (33)$$

Comparing equation (33) with (32) gives: $\alpha=3a_3/4$. Hence, the nonlinear part is given by :

$$C_n = \alpha C_0 V^2 = C_N V^2 \qquad (34\text{-}a)$$

and,

$$C_{eq} = C_0 + C_N V^2 \qquad (34\text{-}b)$$

Where C_0 is the linear part of the capacitance (self or mutual).

For the case of Schottky lines,

$$v(t) = V_{dc\text{-}bias} + V_{signal} = V_{dc\text{-}bias} + V.\cos(\omega t) \qquad (35)$$

From equation (30),

$$dQ(v)/dv = a_1 + 2a_2 v + 3a_3 v^2 + 4a_4 v^3 + \ldots\ldots \qquad (36)$$

a_1 represents the Schottky junction capacitance, which is a result of the dc-bias only and independent of the sinusoidal excitation.

Since equations (27)-(30) are still valid, a_0 represents the charge corresponding to the dc-conditions. To evaluate a_3, recall that the expansion of any function $f(x)$ around $x=a$, using Taylor's series, is given by :

$$f(x)=f(a) + \frac{f'(a)\times(x-a)}{1!} + \frac{f''(a)\times(x-a)^2}{2!} + \frac{f'''(a)\times(x-a)^3}{3!} + \ldots \qquad (37)$$

Comparing this equation with equation(30), where the expansion of $Q(v)$ is taken around $v = V_{dc}$, gives :

$$x-a = v-V_{dc} = V_{signal}(t) = V\cos(\omega t) \qquad (38)$$

and $a_3 = f'''(a)/6 = Q'''(V_{dc})/6$ (39)

Since the instantaneous charge per unit length of Schottky line capacitance $C_{eq\text{-}ins}(v)$ equals to $C_{eq\text{-}ins} \times v$, where v is the instantaneous voltage (ac and dc) across the capacitance,

$$Q(v) = v\,W\left[\frac{q\epsilon N_D}{2(V_{Bi}+v)}\right]^{\frac{1}{2}} \qquad (40)$$

a_3 follows from this equation as :

$$a_3 = \frac{C_{dp}}{8(V_{Bi}+V_{dc})}\left[3 - 2.5\,\frac{V_{dc}}{V_{Bi}+V_{dc}}\right] \qquad (41)$$

Where C_{dp} is the Schottky junction capacitance per unit length of the line, which depends on the dc-bias only. Hence, the nonlinear part of the capacitance can be expressed as :

$$C_n = \frac{3\,W\,V^2}{32(V_{Bi}+V_{dc})}\left[\frac{q\epsilon N_D}{2(V_{Bi}+V_{dc})}\right]^{\frac{1}{2}}\left[3 - \frac{5V_{dc}}{2(V_{Bi}+V_{dc})}\right] = C_N V^2 \qquad (42)$$

with, $C_{eq} = C_o + C_N V^2$ as stated in equation (34-b), W is the line width, q is the electronic charge, N_D is the substrate doping level, ϵ is the permittivity of the substrate material and V_{Bi} is the built-in voltage of the Schottky barrier.

After the type of a nonlinear shunt capacitance has been specified, the equations that characterize the system can be stated. Using Kirchhoff's law under steady-state condition and assuming that the quasi-harmonic analysis is applicable and the time-dependence is given by exp(jwt), the voltage and current equations for the two identical uniformly coupled transmission lines are given by :

$$\frac{dV_1}{dx} = -(R+j\omega L)I_1 - j\omega L_m(I_1+I_2) \qquad (43\text{-a})$$

$$\frac{dI_1}{dx} = -(G+j\omega C_o)V_1 - j\omega C_m(V_1-V_2) - j\omega C_n V_1 - j\omega C_{mn}(V_1-V_2) \qquad (43\text{-b})$$

$$\frac{dV_2}{dx} = -(R+j\omega L)I_2 - j\omega L_m(I_2+I_1) \qquad (43\text{-c})$$

$$\frac{dI_2}{dx} = -(G+j\omega C_o)V_2 - j\omega C_m(V_2-V_1) - j\omega C_n V_2 - j\omega C_{mn}(V_2-V_1) \qquad (43\text{-d})$$

Where C_{mn} is the nonlinear part of the mutual capacitance of the nonlinear substrate medium. For Schottky lines, $C_{mn}=0$.

To solve these coupled differential equations, we define :

$$V_o \equiv V_{odd} = V_1 - V_2 \qquad (44\text{-a})$$

$$I_o \equiv I_{odd} = I_1 - I_2 \qquad (44\text{-b})$$

$$V_e \equiv V_{even} = V_1 + V_2 \qquad (44\text{-c})$$

$$I_e \equiv I_{even} = I_1 + I_2 \qquad (44\text{-d})$$

Differentiation of equations (44) with respect to the distance 'x' gives :

$$\frac{dV_o}{dx} = -[R+j\omega L]I_o \equiv -A_1 I_o \qquad (45\text{-a})$$

$$\frac{dI_o}{dx} = -[G+j\omega(C_o+2C_m+C_n+2C_{mn})]V_o \equiv -(B_1+j\omega C_n)V_o \qquad (45\text{-b})$$

$$\frac{dV_e}{dx} = -[R+j\omega(L+2L_m)]I_e \equiv -A_2 I_e \qquad (45\text{-c})$$

$$\frac{dI_e}{dx} = -[G+j\omega(C_o+C_n)]V_e \equiv -(B_2+j\omega C_n)V_e \qquad (45\text{-d})$$

In even mode excitation, the voltages on the two lines are equal

in magnitude and phase, i.e., $V_1 = V_2$; but in odd mode, the voltages are 180° out of phase, i.e., $V_2 = -V_1$. Therefore,

$$V_e^2 = V_1^2 + V_2^2 + 2V_1V_2 = 4V_1^2 \qquad (46\text{-a})$$

$$V_o^2 = V_1^2 + V_2^2 - 2V_1V_2 = 0 \qquad (46\text{-b})$$

From equation (46), C_n for the even mode is given by:

$$C_{n\text{-even}} = C_N V_1^2 = C_N V_2^2 = C_N V_e^2/4. \qquad (47\text{-a})$$

and for the odd mode :

$$C_{n\text{-odd}} = C_{mn\text{-odd}} = 0 \qquad (47\text{-b})$$

Where C_N is independent of the excitation.

Now, it is possible to rewrite equations (24) as :

$$\frac{dV_o}{dx} = -A_1 I_o \qquad (48\text{-a})$$

$$\frac{dI_o}{dx} = -B_1 V_o \qquad (48\text{-b})$$

$$\frac{dV_e}{dx} = -A_2 I_e \qquad (48\text{-c})$$

$$\frac{dI_e}{dx} = -(B_2 + j\omega C_N V_e^2/4) V_e \qquad (48\text{-d})$$

For the odd mode, differentiating equation (48-a) with respect to the distance 'x' and substituting from equation (48-b) for I_o gives :

$$\frac{d^2V_o}{dx^2} = A_1 B_1 V_o \equiv \gamma^2 V_o \qquad (49)$$

The solution of this equation can be written as:

$$V_o(x) = k_1 e^{-\gamma x} + k_2 e^{\gamma x} \qquad (50)$$

$$\gamma = \alpha + j\beta \qquad ; \text{ the propagation constant.} \qquad (51)$$

The second term on the right-hand side of equation (50) represents a

growing wave in the direction of wave propagation. This implies that $V_o \Rightarrow \infty$ as $x \Rightarrow \infty$ when $\alpha \neq 0$, which is impossible. Therefore, k_2 must be set to zero.

Also at $x=0$, $V_o = V_{applied}$, the voltage applied to line 1. Equation (50) becomes :

$$V_o(x) = V_{applied} e^{-\gamma x} \tag{52}$$

For the even mode, dividing equation (48-c) by (48-d) gives :

$$\frac{dI_e}{dV_e} = (B_2 + j\omega C_N V_e^2/4) V_e / (A_2 I_e) \tag{53}$$

$$\equiv (A_e + B_e V_e^2) V_e / I_e \tag{54}$$

Where $A_e = B_2/A_2$ and $B_e = j\omega C_N/(4A_2)$ (55)

Integrating equation (54) leads to :

$$I_e^2 = A_e V_e^2 + B_e V_e^4 / 2 + \text{Constant} \tag{56}$$

The constant of integration is equal to zero since whenever V_e equals zero, I_e must also be zero. Therefore,

$$I_e = \pm V_e \sqrt{A_e + B_e V_e^2/2} \tag{57}$$

The negative root represents the even mode current propagating in the negative direction, which is not allowed in this analysis since a semi-infinite or matched system has been assumed. Differentiating equation (57) corresponding to the positive root with respect to x gives :

$$\frac{dI_e}{dx} = \left[(A_e + B_e V_e^2) / \sqrt{A_e + B_e V_e^2/2} \right] \frac{dV_e}{dx} \tag{58}$$

Equating equations (48-d) and (58) :

$$-A_2 dx = dV_e / \left[V_e \sqrt{A_e + B_e V_e^2/2} \right] \tag{59}$$

The integral will be :

$$-A_2\sqrt{B_e/2}\;x = \frac{-1}{\sqrt{2A_e/B_e}}\ln\left[\frac{\sqrt{2A_e/B_e}+\sqrt{(2A_e/B_e)+V_e^2}}{V_e}\right]+\ln(\text{constant}) \quad (60)$$

The constant of the integration is found by using the condition :

$V_e = V_{applied}$ *at* $x=0.$

$$\text{Const.} = \left[\frac{\sqrt{2A_e/B_e}+\sqrt{(2A_e/B_e)+V_{applied}^2}}{V_{applied}}\right]^{1/\sqrt{2A_e/B_e}} \equiv K^{1/\sqrt{2A_e/B_e}} \quad (61)$$

Substituting the above equation (61) into (60) and rearrange, it is found that :

$$V_e(x) = \frac{2K\sqrt{2A_e/B_e}\;e^{\sqrt{A_2B_2}\,x}}{\left(K\,e^{\sqrt{A_2B_2}\,x}\right)^2 - 1} \quad (62)$$

In order to find the voltage on each line at any point along the line, we make use of equations (44) to get :

$$V_1(x) = [V_e(x)+V_o(x)]/2 \quad (63\text{-a})$$

and

$$V_2(x) = [V_e(x)-V_o(x)]/2 \quad (63\text{-b})$$

The power as a function of the position along line k (k=1,2) can be calculated by using :

$$P_k = \text{Real}[V_k I_k^*]/2 \quad (64)$$

Where I_k^* *is the complex conjugate of the current on line k;*

$$I_k = \frac{V_k}{Z_k} \qquad \text{and} \qquad Z_k = \sqrt{\frac{Z_{k\text{-series}}}{Y_{k\text{-shunt}}}} \quad (65)$$

6.3 : THE RESULTS AND DISCUSSION :

6.3.1 : Linearized Schottky Lines :

For the case of loosely coupled Schottky lines, it is not feasible to satisfy the ideal contra-directional coupling condition. The capacitance required to match the capacitive and inductive coupling factors is 0.04113214 pF/mm. Since the depletion region capacitance is a weak function of the reverse bias voltage when this voltage is far from the built-in voltage (as shown in Fig. 6-4) this capacitance would require a prohibitive large voltage of 32449.7 volts. The result of this hypothetical case is plotted in Fig. 6-5.

The codirectional coupler response is shown in Fig. 6-6. For a given Schottky line length and for specific frequencies, the power is transferred to the receiving terminal of either line. This is also true if the frequency is chosen and the line length is made variable. Then, the power is transferred back and forth at specific points along the two lines.

Due to the mismatch of the termination impedances, a small fraction of the power is reflected back to the sending ends as shown in the figure. The effect of this reflection can be seen in the curves representing the receiving ends where the maximum power is less than 100%. The shift in the power curves with the different bias conditions is due to the change in the depletion layer capacitance which modifies the phase constant, and therefore the electrical length of the line. This shift can be utilized to design switches by varying the bias voltage.

As an example, we used the same structure to show the behavior of the switch at 15 GHz. One of the two bias voltages has been chosen to be -5.0 volts. It is found that the line length and the second bias voltage required to satisfy the switching conditions, as stated in the theoretical section, are 2489.263 μm and +0.401058 volts. The coupling factor and the Schottky junction capacitance are a nonlinear function of the bias voltage as shown in Fig. 6-7. This nonlinearity governs the power transferred to various coupled line ports as the bias voltage applied to the Schottky lines is varied.

In Fig. 6-8, the termination impedances of the switch are made variable, i.e., their values are equal to the characteristic impedances of the lines, which depend on the self capacitance, and therefore upon the voltage across the junction. This is an ideal case because it is impractical to terminate a line with real voltage-dependent impedances. Therefore, proper termination impedances have to be found. The impedances we have chosen to terminate the lines are obtained by evaluating the line characteristic impedances at a bias voltage where the junction capacitance is equal to the arithmetic average of the junction capacitances evaluated at the switching voltages V_1 and V_2. The voltage at which the line characteristic impedances, and hence the termination impedances are evaluated , is found to be -0.20154 volts. The results for this case are shown in Fig. 6-9. The effect of the mismatch at the output terminals is quite clear. When the dc-bias is 0.4 volts, about 100% of the power is transferred to the receiving end of the first line (port 4). However, when the dc-bias is switched to -5.0 volts, port 4 is isolated, but

some of the power is reflected back to the port where the signal is applied and more than 83% of the power is transferred to the receiving terminal of the second line. For practical applications, this is still a useful switching device.

6.3.2 : Nonlinear Quasi-Harmonic Analysis :

The results of the nonlinear quasi-harmonic analysis of the Schottky coupled lines are shown in Fig. 6-10. The power on both lines as a function of the position along the lines is presented for different dc-biases.

The applied voltage swing is limited on the positive cycle by the built-in voltage of the Schottky junction. Therefore, for a small dc-bias, the allowed input signal has to be small. On the other hand, if the magnitude of the reverse dc-bias is large, the change in the junction capacitance due to the applied voltage is small, even if the voltage amplitude is large. The applied signal itself has to be much smaller than the magnitude of the dc-bias and the built-in voltage combined for the quasi-harmonic analysis to be applicable. These restrictions on the input signal yield a very small nonlinear term, so that it is hard to notice its effect in Fig. 6-10 for V_{dc}=2 volts. If the dc-bias is small and the signal amplitude is made comparable to the magnitude of the dc-bias and the built-in voltage together, the nonlinear term effect becomes clear as shown in the same figure for V_{dc}=0. The power increases due to the reduction in the line impedance, which results from the self capacitance increase. The power function

is no longer symmetric about the vertical axis through the peak as compared with the linear system, i.e., when the nonlinear term is neglected.

Applying the nonlinear analysis to a system of two coupled transmission lines on a nonlinear substrate shows the effect of the nonlinearity on the power along the lines. Fig. 6-11 shows a shift in the position of the power peak along the lines. This shift is expected and it is attributed to the increase in the self capacitance and, therefore, in the phase constant. The increase in the self capacitance of the line results in a decrease in the line impedance. Due to the coupling between the lines, shifting of the power peak on one line to the left, shifts the power peak to the right on the other one.

Such analysis would be useful in designing a directional coupler if a nonlinear substrate is used. In this case, when the signal power is large so that the nonlinearty becomes significant, the line length at which the maximum power occurs can be calculated more accurately as compared to the results obtained by using the linear small-signal model.

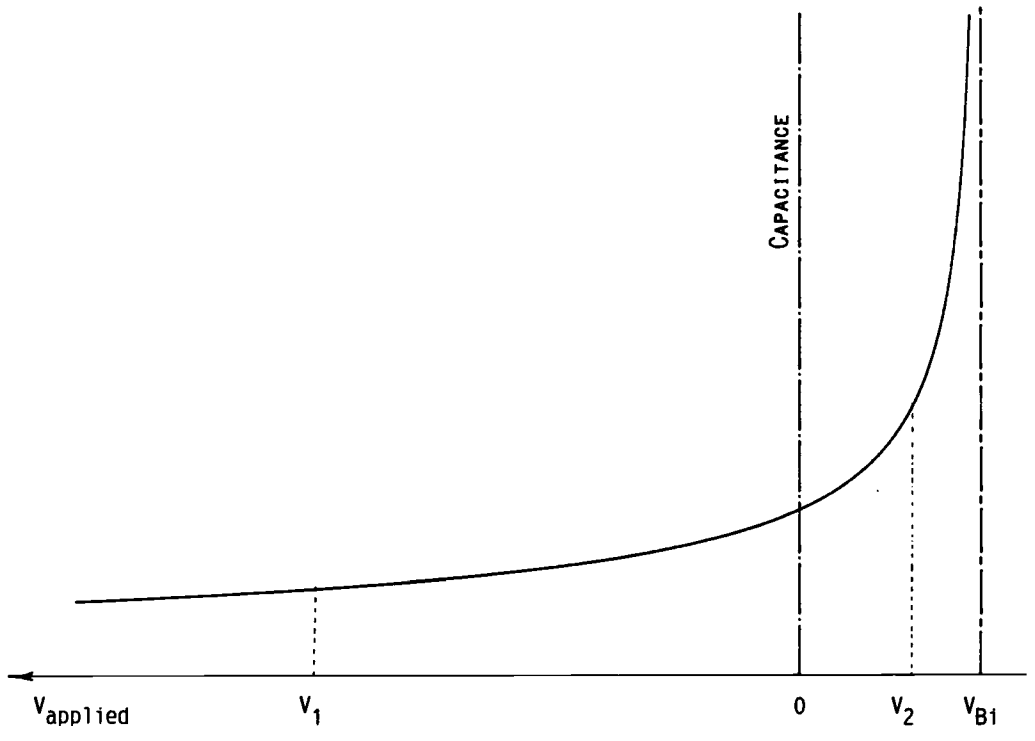

Fig. 6-4: The variation of the Schottky junction capacitance as a function of the bias voltage.

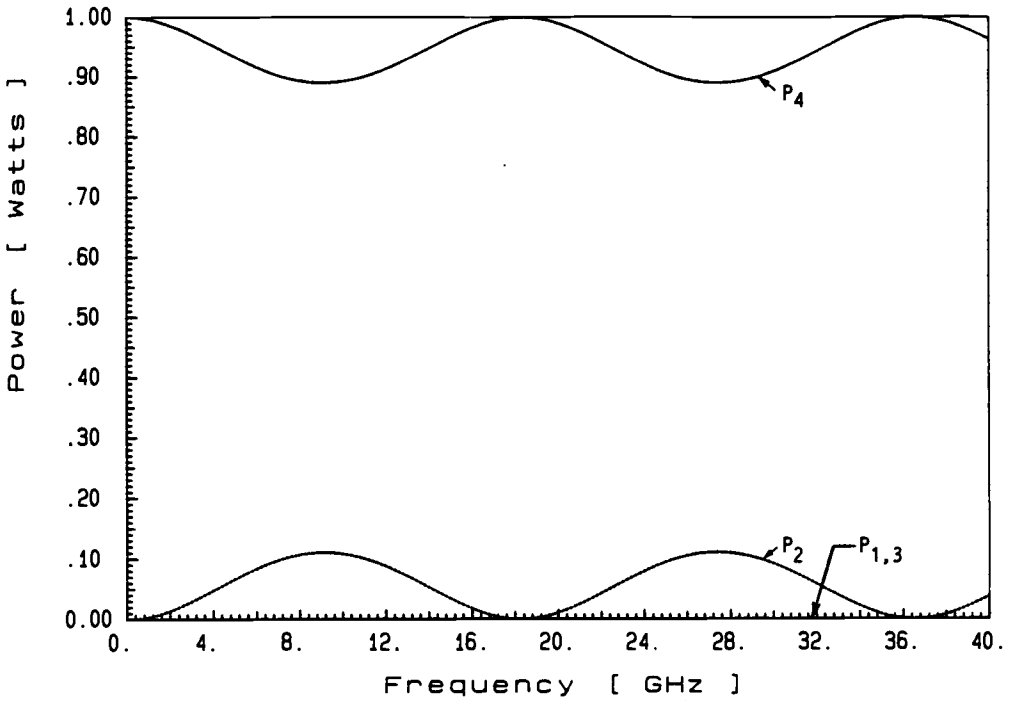

Fig. 6-5: Coupled Schottky lines as a contra-directional coupler.

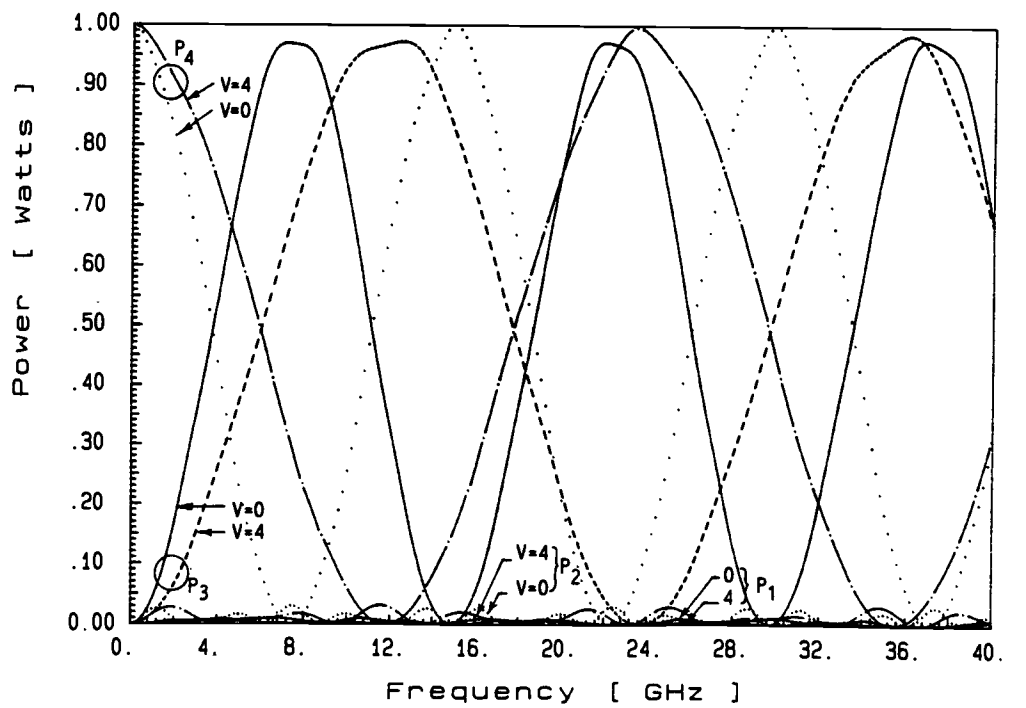

Fig. 6-6: Coupled Schottky lines as a co-directional coupler.

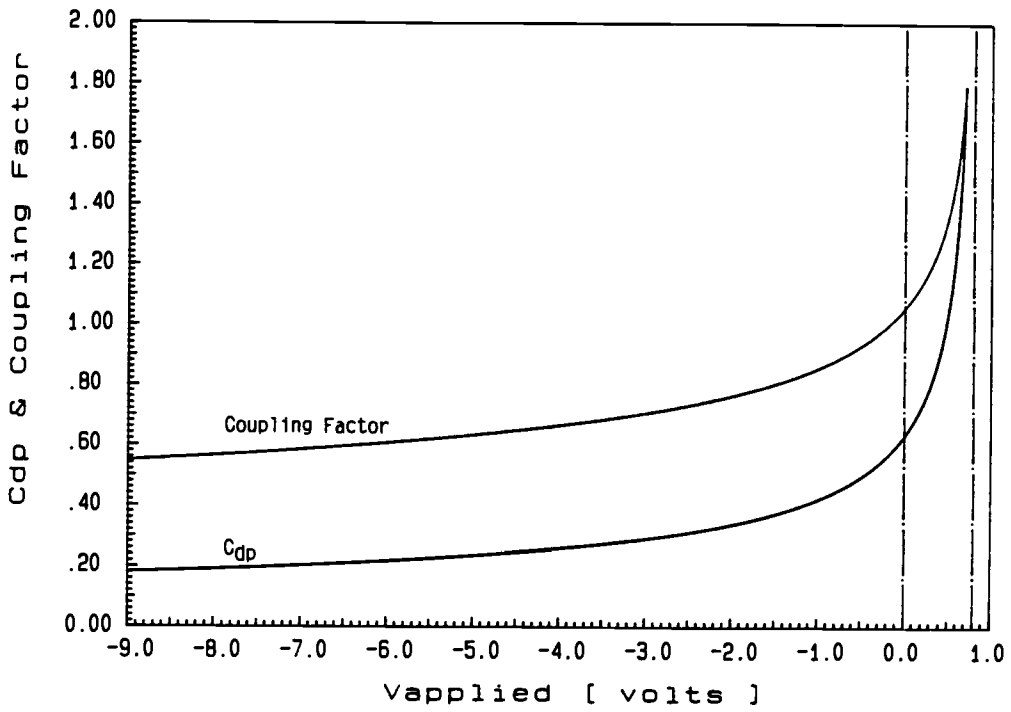

Fig. 6-7: The dependence of the coupling factor on the bias voltage.
The depletion layer capacitance is normalized by the coupling factor at $V_{applied}$ = 0.7 volts.

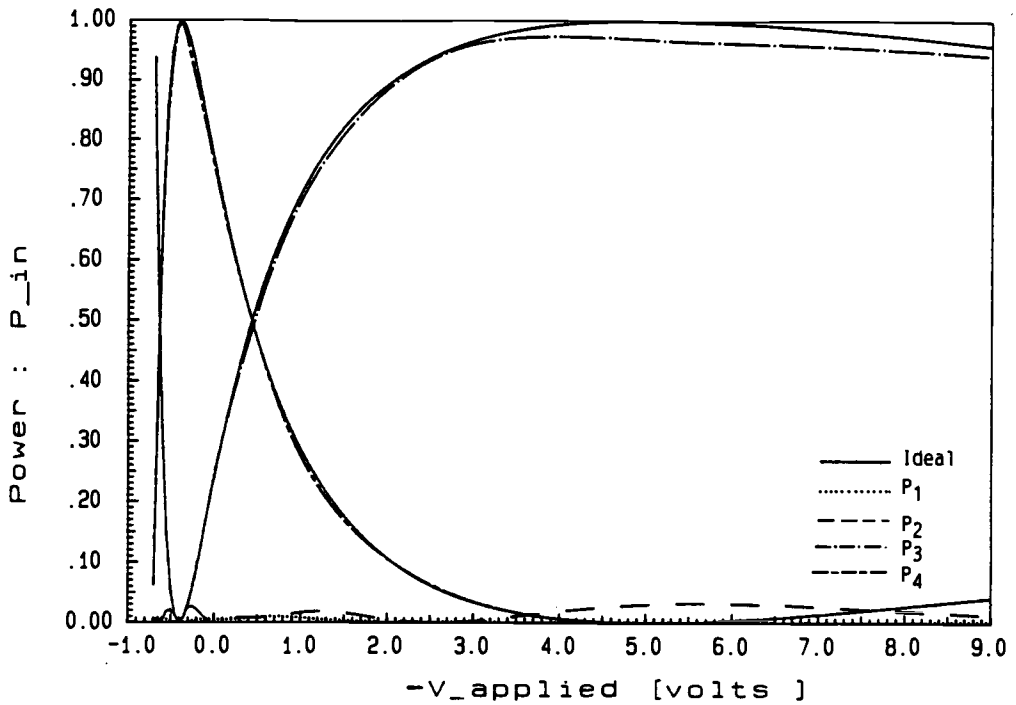

Fig.6-8: Schottky lines switch when the two lines are terminated by their characteristic impedance [ideal case].

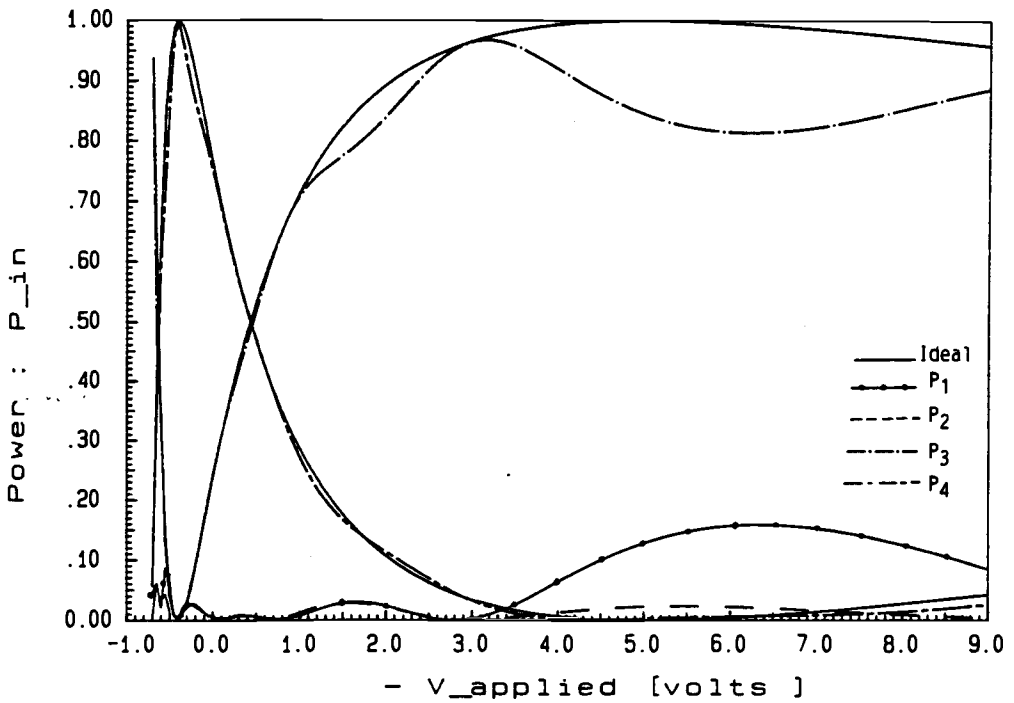

Fig.6-9: Schottky lines switch when the two lines are terminated by frequency and bias independent impedance [practical case].

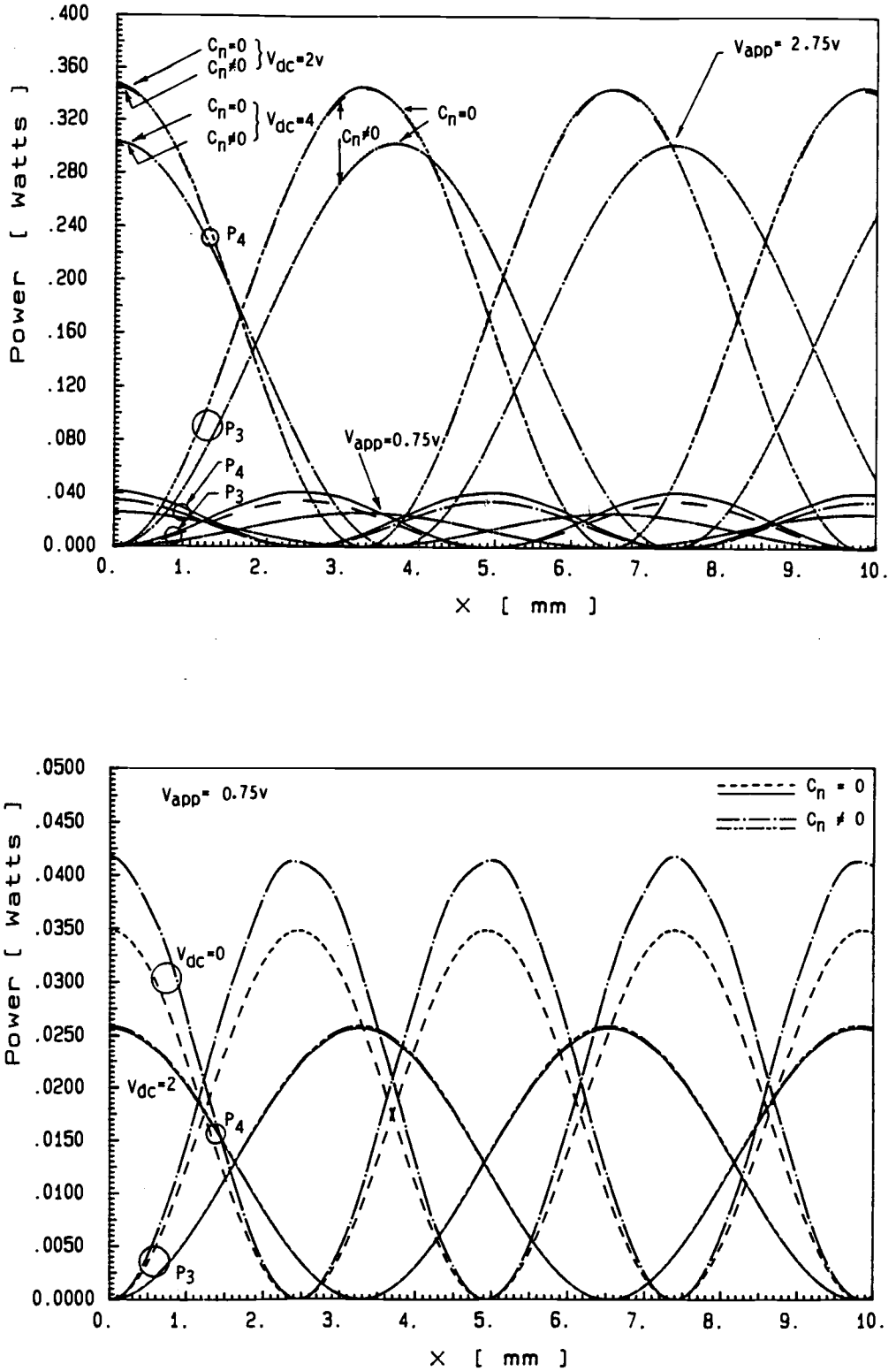

Fig. 6-10: Nonlinear quasi-harmonic analysis of coupled Schottky lines.

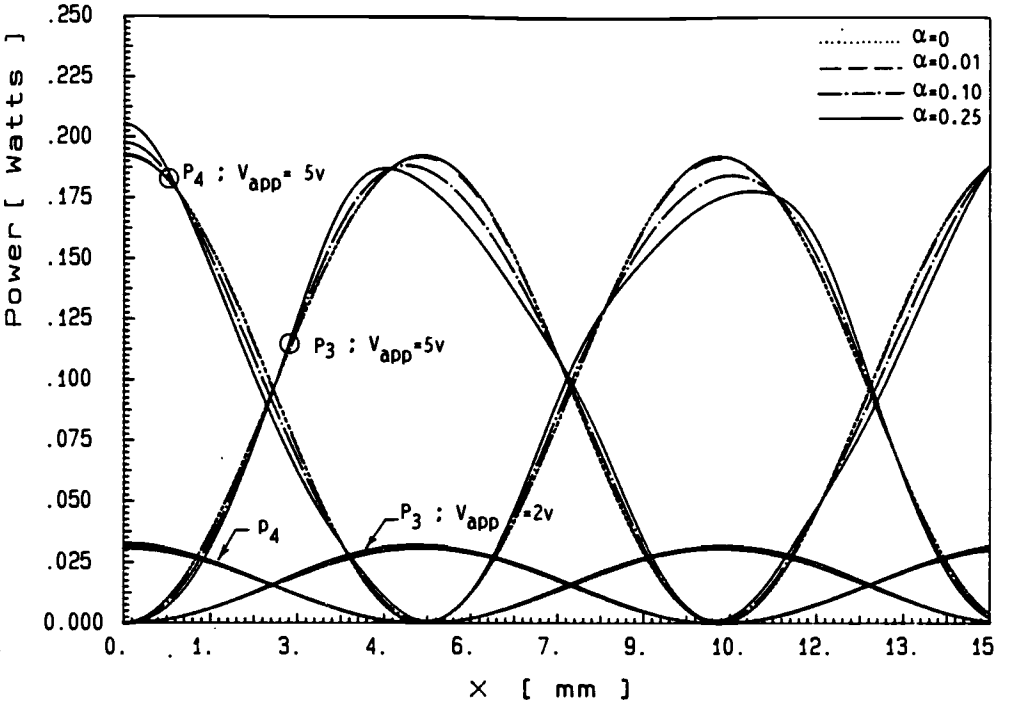

Fig. 6-11: Nonlinear quasi-harmonic analysis of coupled transmission lines on a nonlinear substrate.

CHAPTER 7

CONCLUSIONS AND SUGGESTIONS FOR FUTURE WORK

7.1 : THE OBJECTIVES AND ACHIEVEMENTS :

The objectives of the study described in this thesis were :

A. To model the GaAs MESFET by calculating the electrical parameters of the structure from its geometrical and material parameters.

B. To study the properties of the distributed parameter electrically long MESFET structures by applying the general normal mode analysis of the active coupled lines for possible applications as traveling-wave transistors, harmonic generators, and voltage tunable devices.

These objectives in general have been successfully fulfilled. Nevertheless, the main contributions made through out the course of this study can be summarized as follows :

1. Generalizing the normal mode coupled-line analysis of asymmetric lines in an inhomogeneous media to include the possible existence of active elements and the resulting asymmetric immittance matrices.

2. Developing a small-signal GaAs MESFET model based on the physical parameters of the structure. This includes the developing of a new accurate computer program to calculate the device distributed electrical parameters analytically. Empirical expressions were also implanted in the program to adjust the nonlinear circuit elements by considering their

dependence on the bias conditions.

3. *Developing an exact calculation of the interelectrode (mutual) capacitances of two and three asymmetric coplanar strips. Since the calculations utilize the conformal mapping technique, simple computer routines to calculate the exact values of the complete and incomplete elliptic integrals of the first kind were written. In addition, accurate and efficient closed-form expressions were also formulated for the computer aided design of coplanar strips to calculate these capacitances.*
4. *Application of rigorous coupled active distributed parameters theory to the traveling-wave transistor for application as broad-band power amplifier in microwave frequencies. This includes the calculation of the scattering parameters of a four-port network and the power gain by utilizing the electrical parameters of the GaAs MESFET.*
5. *Introducing the small-signal and quasi-harmonic analysis of coupled Schottky lines for applications as voltage tunable devices including directional couplers and electronic switches.*

7.2 : <u>THE CONCLUSIONS</u> :

Following are some of the conclusions one can deduce from the work described in this thesis :

1. *The general normal mode active coupled-line analysis can be applied to any uniformly coupled distributed parameter four-port circuit.*
2. *The small-signal model of GaAs MESFET is very useful as a design*

tool for many applications. It gives good results within the allowed range of the gate bias which is limited by the built-in potential on one side and the pinch-off voltage on the other. Still, the computer program OSUFET has some limitations as discussed in detail in chapter 3. The program can be improved to overcome these limitations, but the expected improvements are so small while the calculation time will be much longer especially if two-dimensional analysis is considered.

3. *The exact method and closed-form expressions for calculating the interelectrode (mutual) capacitances are very useful and efficient not only for MESFET structures considered here but also for many different structures of the same nature (i.e., consisting of coplanar strips) including interdigital planar devices such as photoconductive detectors, VLSI connections and MMICs (Microwave Monolithic Integrated Circuits).*
4. *The routines of complete and incomplete elliptic integrals of the first kind give very accurate results as compared to those derived by Legendre about two centuries ago[122]. These results are more accurate than those tabulated in some modern handbooks[125].*
5. *The power gain depends on the phase velocities and the characteristic impedances of the gate and drain electrodes. The maximum power gain requires equal phase velocities of the waves on both lines and a higher drain characteristic impedance.*
6. *The compensation element required to synchronize the phase velocities is a distributed inductance along the drain line. In*

the previous work, the compensation element was always a capacitance. However, distributing a shunt capacitance along the drain line will decrease its impedance and the power gain as well.

7. The gate line metalization resistance influences the device gain significantly. As the gate electrode resistance increases, input signal attenuation increases and the gain decreases. Such resistance has to be reduced to its minimum possible value by any means.
8. The nonlinearity of coupled Schottky lines due to the dependence of their junction capacitance on the applied voltage (ac and dc) can be utilized to build voltage tunable devices such as directional couplers and electronic switches. However, it is not feasible to satisfy the conditions for contra-directional coupler because the dc-bias required is very high.

7.3 : SUGGESTIONS FOR FUTURE WORK :

Within this subject of study are plenty of opportunities for improvement, development and innovation. For future work there are many areas which could be investigated. What follows are some suggestions for future research.

1. The analysis of active coupled-line in an inhomogeneous media can be generalized one step further to account for multi-line, multi-port circuits.
2. The empirical expressions used in the calculations of nonlinear electrical parameters of the GaAs MESFET can be improved to

achieve better fit between the calculated values and the measured data.

3. *Instead of two-region model and gradual channel approximation, the analysis of the GaAs MESFET device can be made more rigorous by including the region when the carrier velocity reaches its maximum value. This would mean three-region model approximation; constant mobility with positive differential resistance region, constant mobility with negative differential resistance region, and constant velocity region as shown in Fig. 7-1. The two-dimension analysis can also be used. The expected results are better than the results of the model used in this study. However, this will require longer time for computations.*

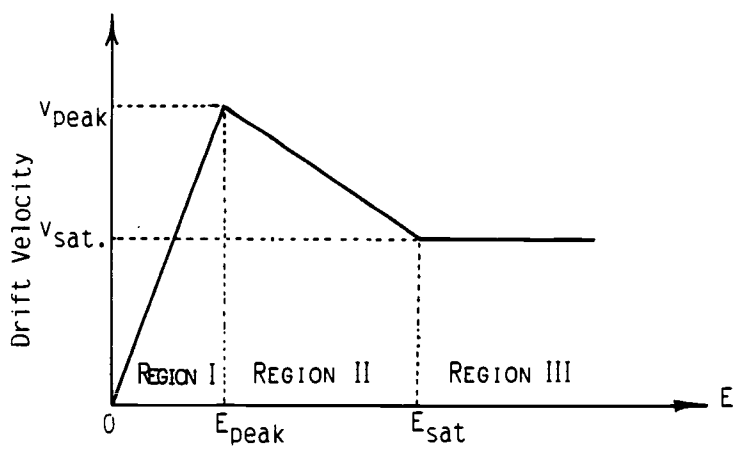

Fig. 7-1: The electron drift velocity versus the electric field in a GaAs MESFET, three-region model.

4. *Even today, there is no simple and exact analytical method to calculate the effect of the metalization thickness of the strips and the finite thickness of the substrate. With the advanced technology available these days the slot and strip widths become comparable to the metalization thickness of the strips and sometimes even smaller. As a result, the percentage of the electric field lines that end on the strip sides rather than on the top and bottom faces increases as the strip thickness increases. Therefore, the strip thickness has to be included in the calculation of the mutual capacitances. Although for thick substrate, i.e., when the substrate thickness is much larger than the slot widths, the semi-infinite substrate approximation is a very good one, in the thin substrate some of the electric field lines pass through the air under the substrate and this influences the mutual capacitance values. A general analysis considering the substrate thickness is important.*
5. *The analysis of three coplanar strips presented in chapter 4 is based on the assumption that the outer strips are symmetric about the central plane between them and the spacings between the strips and the central one are equal. This analysis can be generalized further by assuming three coplanar strips of different widths and separated by different slot widths. Furthermore, the analysis could include more than three strips.*
6. *In the traveling-wave amplifier (i.e., discrete cascaded active devices amplifier), the dual-gate devices were used and higher gain and better flatness were reported (as mentioned in*

chapter 5). The dual-gate GaAs MESFETs are already investigated for other applications but not for application as traveling-wave transistors for broad-band power amplifiers. Therefore, the dual-gate concept can be applied for single long device along with the analysis of linearized model (or quasi-harmonic analysis) of Schottky coupled lines.

7. *The quasi-harmonic analysis of coupled Schottky lines can be improved further to include the asymmetric non-identical lines. The general analysis of such nonlinear coupled lines should take in consideration the possible reflection at both the receiving and the sending ends due to the mismatch of the termination impedances of the finite length structures.*
8. *Experimental work including the fabrication and testing of the structure proposed and analyzed in this thesis should be undertaken. This includes the traveling-wave transistor with novel gate electrodes to reduce the series resistance and coupled Schottky lines designed for applications as directional couplers and electronic switches.*

REFERENCES

[1] W. S. Percival, " Thermionic Valve Circuits," British Patent Specifications, No. 460562, July 24, 1935 to April 22, 1937. (Applied for July 24,1936).

[2] E. L. Ginzton, W. Hewlett, J. Jasberg and J. Noe, "Distributed Amplification," Proc. IRE, vol. 36, PP. 956-969, Aug. 1948.

[3] H. G. Rudenberg and F. Kennedy, "200-MC Traveling-Wave", Electronics, vol. 22, pp.106-109, Dec. 1949.

[4] H. A. Wheeler, "Wide-Band Amplifiers For Television," Proc. IRE, vol. 27,pp. 429-438, July, 1939.

[5] A. J. Wahl, " Distributed Theory For Microwave Bipolar Transistors,"IEEE Trans. Electron Dev., vol. ED-21, pp.40-49, Jan.1974.

[6] G. W. McIver,"A Traveling-Wave Transistor," Proc. IEEE (Letters) vol. 53, pp 1747-1748, Nov. 1965.

[7] W. Jutzi, "A MESFET Distributed Amplifier With 2 GHz Bandwidth," Proc. IEEE(Letters), vol. 57, pp. 1195-1196, June 1969.

[8] Y. Ayasli, L. Reynolds, R. Mozzi and L. Hanes, " 2-20 GHz GaAs Traveling-Wave Power Amplifier," IEEE Trans. Microwave Theory Tech., vol. MTT-32, pp. 290-294, Mar. 1984.

[9] J. B. Beyer et al., " Wideband Monolithic Microwave Amplifier Study," ONR Report, NR243-033, Sept. 1983.

[10] A. J. Holden, D.R. Danial, I. Davies, C. H. Oxley and H.D. Ress, "Gallium Arsenide Traveling-Wave Field-Effect Transistor,", IEEE Trans. Electron Dev., vol. ED-61, pp. 61-66, Jan. 1985.

[11] Yu-an Ren, G. Ruan and H. Hartnagel, "Microwave Structuring of MESFET electrodes For Increased Power and Efficiency," IEEE-Int. Electron Device Meeting (IEDM), Tech. Digest, pp. 684-687, Washington, D.C., Dec. 1981.

[12] A. S. Podgorski and L. Y. Wei,"Theory of Traveling-Wave Transistors," IEEE Trans. Electron Dev., vol. ED-29, pp. 1845-1853, Dec. 1982.

[13] V. K. Tripathi, " Asymmetric Coupled Transmission lines in an Inhomogeneous Medium," IEEE Trans. Microwave Theory Tech., vol. MTT-23,pp. 734-739, Sept. 1975.

[14] R. A. Pucel, H. A. Haus, and H. Statz," Signal and Noise Properties of Gallium Arsenide Microwave Field-Effect Transistors," in Advances in Electronics and Electron Physics, by L. Marton,(Ed.)

vol. 38, pp. 195-265, Academic Press, New York, N.Y., 1975.

[15] M. S. Shur, " Analytical Model of GaAs MESFET's," IEEE Trans. Electron Dev., vol. ED-25, pp. 612-618,June 1978.

[16] H. A. Willing, C. Rauscher and D. de Santis, " A Technique For Predicting Large-Signal Performance of GaAs MESFET," IEEE Trans Microwave Theory Tech., vol. MTT-26, pp. 1017-1023, Dec. 1978.

[17] H. Fukui,"Determination of The Basic Device Parameters of a GaAs MESFET," Bell Syst. Tech. J., vol. 58, pp. 771-779, Mar. 1979.

[18] R. E. Neidert and C. J. Scott, Computer Program For Microwave GaAs MESFET's Modeling, NRL Report No. 8561, Feb. 1982.

[19] W. Shockley, " A Unipolar Field-Effect Transistor," Proc. IRE, vol. 40, pp. 1365-1376, Nov. 1952.

[20] A. B. Grebene and S. K. Ghandi, " General Theory For Pinched Operation of The Junction-Gate FET," Solid-State Electron., vol. 12, pp. 573-589, July 1969.

[21] W. R. Smythe, Static and Dynamic Electricity , 3rd Ed., pp. 100-104, McGraw-Hill, New York, N.Y., 1968.

[22] C. P. Wen, " Coplanar Waveguide : A Surface Strip Transmission Lines Suitable For Nonreciprocal Gyromagnetic Device Applications," IEEE Trans. Microwave Theory Tech. vol. MTT-17, pp.1087-1090, Dec. 1969.

[23] H. C. Lin, Integrated Electronics, Holden-Day, Inc., San-Francisco, CA 1967.

[24] M. E. Davis, E. W. Williams and A. C. Celestini,"Finite-Boundary Corrections to The Coplanar Waveguide Analysis," IEEE Trans. Microwave Theory Tech., vol. MTT-21, pp. 594-596, Sept. 1973.

[25] K. C. Gupta, R. Garg, and R. Chada, Computer Aided Design of Microwave Circuits, Artech House,Inc., Dedham, Mass. 1981.

[26] I.J. Bahl and R. Garg,"Simple and Accurate Formulas for a Microstrip With Finite Strip Thickness," Proc. IEEE, vol. 65, pp. 1611-1612, Nov. 1977.

[27] TOUCHSTONE, User's Manual, Version 1.3, EEsof, Westlake Village, CA, April 1985.

[28] H. Amemiya, " Time-Domain Analysis of Multiple Parallel Transmission Lines," RCA Rev., vol. 28, pp. 241-278, June 1967.

[29] D. C. Tiwari and H. L. Hartnagel,"Nonlinear Coupled Transmission Line Analysis For Second Harmonic Generation in Traveling-Wave

GaAs MESFET's," IEEE Trans. Electron Dev., vol. ED-33, pp. 366-372, March 1986.

[30] D. C. Tiwari and H. L. Hartnagel,"Coupled Transmission Line Analysis For Harmonic Generation in Traveling-Wave MESFETs," Int. J. Electron., vol. 58, pp. 687-692, April 1985.

[31] A. S. Podgorski, Modeling Analysis of Distributed Schottky-Barrier Field-Effect Transistors, Ph.D. Thesis, Dept. of Electrical Engineering, University of Waterloo, Ontario, Canada 1980.

[32] K. -H. Kretschmer, W. Heinrich and H. L. Hartnagel, " Active and Passive Coupling Between Electrodes on Semiconductor Surfaces," Arch. Elekt. Üebertrag. (AEÜ), vol. 37, pp. 229-235, July 1983.

[33] G. I. Zysman and A. K. Johnson, " Coupled Transmission Line Networks in an Inhomogeneous Dielectric Medium," IEEE Trans. Microwave Theory Tech., vol. MTT-17, pp. 753-759, Oct. 1969.

[34] E. M. T. Jones and J. T. Bolljahn, " Coupled-Strip-Transmission-Line Filters and Directional Couplers," IRE Trans. Microwave Theory Tech., vol. MTT-4, pp. 75-81, Apr. 1956.

[35] S. Yamamoto, T. Azakami and K. Itakuru, "Coupled Strip Transmission Line With Three Center Conductors," IEEE Trans. Microwave Theory Tech., vol. MTT-14, pp. 446-461, Oct. 1966.

[36] E. G. Vlostovoskiy, "Theory of Coupled Transmission Lines," Telcommun. Radio Eng., vol. 21, pp. 87-93, Apr. 1967.

[37] M. K. Krage and G. I. Haddad,"Characteristics of Coupled Microstrip Transmission Lines-I: Coupled-Mode Formulation of Inhomogeneous Lines," IEEE Trans. Microwave Theory Tech., vol. MTT-18, pp. 217-222, Apr. 1970.

[38] H. A. Willing and P. de Santis, "Modeling of Gunn-Domain Effect in GaAs MESFET's," Electron. Lett., vol. 13, pp. 537-539, 1st Sept. 1977.

[39] G. D. Vendelin, " Feedback Effect in the GaAs MESFET Model," IEEE Trans. Microwave Theory Tech., vol. MTT-24, pp. 383-385 (letters), June 1976.

[40] C. -J. Wei, " Novel Design of Travelling-Wave FET," Electron. Lett., vol. 19, pp. 461-462, 23rd June 1983.

[41] R. H. Dawson, " Equivalent Circuit of Schottky-Barrier Field-Effect Transistor at Microwave Frequencies," IEEE Trans. Microwave Theory Tech., vol. MTT-23, pp. 499-501 (short papers), June 1975.

[42] D. L. Peterson, A. M. Pavio and B. Kim, " A GaAs FET Model For Large-Signal Applications," IEEE Trans. Microwave Theory Tech., vol. MTT-32, pp. 276-281, Mar. 1984.

[43] H. Hartnagel, "Intermodulation Distortion of MESFET Amplifiers," Arch. Elekt. Üebertrag. (AEÜ), vol. 36, pp. 83-85, Feb. 1982.

[44] R. A. Larue, S. G. Bandy and G. A. Zdasiuk, "A 12-dB High-Gain Monolithic Distributed Amplifier," IEEE Trans. Microwave Theory Tech., vol. MTT-34, pp. 1542-1547, Dec. 1986.

[45] W. Yau et al., "A Four-Stage V-Band MOCVD HEMT Amplifier," IEEE MTT-S, Int. Microwave Symp. Dig., vol. I, pp.155-159,(Las Vegas, NV), June 9-11,1987.

[46] S. Asai, K. Joshin, Y. Hirachi and M. Abe,"Super Low-Noise HEMTs With a T-Shaped Gate Structure,"IEEE MTT-S, Int. Microwave Symp. Dig., vol. II, pp. 1019-1022, (Las Vegas, NV), June 9-11, 1987.

[47] C. Law and C. S. Aitchison, "Prediction of Wide-Band Power Performance of MESFET Distributed Amplifiers Using The Volterra Representation," IEEE Trans. Microwave Theory Tech., vol. MTT-34, pp. 1308-1317, Dec. 1986.

[48] A. Cappelo et al., "A High Performance, Quasi Monolithic 2 to 18 GHz Distributed GaAs FET Amplifier," IEEE MTT-S, Int. Microwave Symp. Dig., vol.II, pp. 833-836,(Las Vegas, NV), June 9-11,1987.

[49] L. C. Upadhyayula et al., " Passive GaAs FET Switch Models and Their Application in Phase Shifters," IEEE MTT-S, Int. Microwave Symp. Dig., vol.II, pp. 903-906(Las Vegas, NV), June 9-11, 1987.

[50] C. Camacho-Penalosa and C. S. Aitchison, " Modeling Frequency Dependence of Output Impedance of a Microwave MESFET at low Frequencies," Electron Lett., vol. 21, pp. 528-529, 6th June 1985.

[51] R. W. Engelmann and C. A. Liechti, "Bias Dependence of GaAs and InP MESFET Parameters," IEEE Trans. Electron Dev., vol. ED-24, pp. 1288-1296, Nov.1977.

[52] P. Gamand, Y. Crosnier and P. Gelin, "Large-Signal Capabilities and Analysis of Distributed Amplifier," Electron Lett., vol. 20, pp.317-319, 12th Apr.1984.

[53] J. M. Michael Golio and R. J. Trew, " Profile Studies of Ion-Implanted MESFETs," IEEE Trans. Microwave Theory Tech.,vol. MTT-31, pp. 1066-1071, Dec.1983.

[54] A. Gopinath and J. Bruce Rankin, "Single-gate MESFET Frequency Doublers," IEEE Trans. Microwave Theory., vol. MTT-30, pp. 869-875, June 1982.

[55] W. Heinrich,"Distributed Equivalent-Circuit Model For Traveling-Wave FET Design," IEEE Trans. Microwave Theory Tech., vol. MTT-35, pp. 484-491, May 1987.

[56] P. L. Hower and N. Bechtel, "Current Saturation and Small-Signal Characteristics of GaAs Field-Effect Transistors," IEEE Trans, Electron Dev., vol. ED-20, pp. 213-220, Mar. 1973.

[57] K.-H. Kretschmer and H. L. Hartnagel, "Some Microwave Properties of High-Speed Monolithic IC's," RCA Rev., vol. 44, pp. 525-536, Dec. 1983.

[58] R. L. Kuvas, " Equivalent Circuit Model of FET Including Distributed Gate Effects," IEEE Trans. Electron Dev., vol. ED-27, pp. 1193-1195, June 1980.

[59] T. McKay, J. Eisenberg and R. Williams, "A High-Performance 2-18.5 GHz Distributed Amplifier-Theory and Experiment," IEEE Trans. Microwave Theory Tech., vol. MTT-34, pp. 1559-1568, Dec. 1986.

[60] D. W. Kaki, J. M. Schellenberg, H. Yamasaki and L. C. T. Liu, "A 69 GHz Monolithic FET Oscillator," IEEE-1984 Microwave and Millimeter-Wave Monolithic Circuits Symp. Dig., pp. 63-66, (San Francisco, CA), May 28-June 1, 1984.

[61] M. Niori, T. Saito, K. Joshin and T. Mimura, " A 20 GHz High Electron Mobility Transistor Amplifier For Satellite Communications," IEEE-1983 Int. Solid-State Circuits Conf.(ISSCC) Dig.,pp. 198-199, Feb. 1983.

[62] A. M. Pavio, S. D. McCarter and P. Saunier,"A Monolithic Multi-Stage 6-18 GHz Feedback Amplifier," IEEE-1984 Microwave and Millimeter-Wave Monolithic Symp. Dig., pp. 45-48,(San Francisco, CA), May 28-June 1, 1984.

[63] T. Smith, "A Modeling System For Simulation of GaAs FET Performance," COMSAT Tech. Rev., vol. 15, pp. 237-258, Fall 1985.

[64] G. W. Rhyne and M. B. Steer, "Generalized Power Series Analysis of Intermodulation Distortion in a MESFET Amplifier: Simulation and Experiment," IEEE MTT-S, Int. Microwave Symp. Dig., vol. I, pp. 115- 118, (Las Vegas, NV), June 9-11, 1987.

[65] J. P. Wade, A Monolithic GaAs Distributed Multioctive Amplifier, MS Thesis, Dept. of Electrical and Computer Eng., M.I.T., Cambrdge, Mass., Jan. 1984.

[66] C. M. Krowne,"The Effect of Source Feedback on GaAs MESFET Circuit Models," Int. J. Electron., vol. 57, pp. 447-459, Oct. 1984.

[67] C. A. Liechti, E. Gowen and J. Cohn, " Microwave Transistors,

Modulators and Mixers,"IEEE-1972 Int. Solid-State Circuits Conf. (ISSCC) Dig., pp. 158-159, Feb. 1972.

[68] C. A. Liechti and R. B. Larrick, "Performance of GaAs MESFET's at Low Temperatures," IEEE Trans. Microwave Theory Tech., vol. vol. MTT-24, pp. 376-381, (Short Papers), June 1976.

[69] C. A. Liechti, " Microwave Field-Effect Transistor-1976," IEEE Trans. Microwave Theory Tech., vol. MTT-24, pp. 279-300, June 1976.

[70] W. R. Curtice, " A MESFET Model For Use in The Design of GaAs Integrated Circuits," IEEE Trans. Microwave Theory Tech., vol. MTT-28, pp. 448-456, May 1980.

[71] W. R. Curtice,"The Performance of Submicrometer Gate Length GaAs MESFET's," IEEE Trans. Electron Dev., vol. ED-30, pp. 1693-1699, Dec. 1983.

[72] W. R. Curtice and M. Ettenberg, "N-FET, a New Software Tool For Large-Signal GaAs FET Circuit Design," RCA Rev. vol. 46, pp.321-340, Sept. 1985.

[73] Y. Tajima, B. Wrona and K. Mishima, "GaAs FET Large-Signal Model and its Application to Circuit Designs," IEEE Trans. Electron Dev., vol. ED-28, pp. 171-175, Feb. 1981.

[74] Y. Tajima and P. D. Miller, "Design of Broad-Band Power GaAs FET Amplifiers," IEEE Trans. Microwave Theory Tech., vol. MTT-32, pp. 261-267, Mar. 1984.

[75] J. W. Bandler, S. H. Chen and S. Daijvad,"Microwave Device Modeling Using Efficient l_1 Optimization : A Novel Approach," IEEE Trans. Microwave Theory Tech., vol. MTT-34, pp. 1282-1293, Dec. 1986.

[76] J. W. Bandler and Q. J. Zhang, "An Automatic Decomposition Technique For Device Modeling and Large Circuit Design," IEEE MTT-S, Int. Microwave Symp. Dig., vol. II, pp. 709-712,(Las Vegas, NV), June 9-11, 1987.

[77] W. Baechtold, "Noise Behavior of GaAs Field-Effect Transistor With Short Gate Length," IEEE Trans. Electron Dev., vol. ED-19, pp. 674-680, May 1972.

[78] R. A. Minasian, "Simplified GaAs MESFET Model to 10 GHz," Electron. Lett., vol. 13, pp. 549-551, 1st Sept. 1977.

[79] K. B. Niclas et al., "Application of The Two-Way Balanced Amplifier Concept to Wide-Band Power Amplification Using GaAs MESFET's," IEEE Trans. Microwave Theory Tech., vol. MTT-28, pp. 172-179, Mar. 1980.

[80] K. B. Niclas et al, "The Matched Feedback Amplifier: Ultrawide-Band Microwave Amplification With GaAs MESFET's," IEEE Trans. Microwave Theory Tech., vol. MTT-28, pp. 285-294, Apr. 1980.

[81] M. L. Salib, D. E. Dawson and H. K. Hahn, "Load-Line Analysis in The Frequency Domain With Distributed Amplifier Design Examples," IEEE MTT-S, Int. Microwave Symp. Dig., vol. II, pp. 575-578,(Las Vegas, NV), June 9-11, 1987.

[82] E. W. Strid and K. R. Gleason, "A DC-12 GHz Monolithic GaAs FET Distributed Amplifier," IEEE Trans. Microwave Theory Tech., vol. MTT-30, pp. 969-975, July 1982.

[83] H. Fukui, "Channel Current Limitations in GaAs MESFETs," Solid-State Electron., vol. 22, pp. 507-515, May 1979.

[84] M.S. Shur,"Small-Signal Nonlinear Circuit Model of GaAs MESFET," Solid-State Electron. vol. 22, pp.723-728, Aug. 1979.

[85] H. Statz, H. A. Haus and R. A. Pucel, " Noise Characteristics of GaAs Field-Effect Transistors," IEEE Trans. Electron Dev., vol. ED-21, pp. 549-562, Sept. 1974.

[86] J. M. Golio, J. R. Hauser and P. A. Blakey, "A Large Signal GaAs MESFET Model Implemented on SPICE," IEEE Circuits and Devices Devices Magazine, vol. 1, pp. 21-30, Sept. 1985.

[87] K. Lehovec and R. Zuleeg, " Voltage-Current Characteristics of GaAs J-FET's in The Hot Electron Range," Solid-State Electron., vol. 13, pp. 1415-1426, Oct. 1970.

[88] T. Takada, K. Yokoyama, M. Ida and T. Sudo, "A MESFET Variable-Capacitive Model For GaAs Integrated Circuit Simulation," IEEE Trans. Microwave Theory Tech., vol.MTT-30, pp.719-723, May 1982.

[89] A. Madjar and F. J. Rosenbaum, " A Large-Signal Model For GaAs MESFET," IEEE Trans. Microwave Theory Tech., vol. MTT-29, pp. 781-788, Aug. 1981.

[90] K. Yamaguchi, S. Asai and H. Kodera, " Two-Dimensional Numerical Analysis of Stability Criteria of GaAs FET's,"IEEE Trans. Electron Dev., vol. ED-23, pp. 1283-1290, Dec. 1976.

[91] S. M. Sze, Physics of Semiconductor Devices, 2nd Ed., John Wiley & Sons, Inc., New York, N.Y., 1981.

[92] L. F. Eastman and M. Shur, "Substrate Current in GaAs MESFET's," IEEE Trans. Electron. Dev., vol. ED-26, pp.1359-1361, Sept.1979.

[93] P. N. Butcher, W. Fawcett and C. Hilsum, "A Simple Analysis of Stable Domain Propagation in The Gunn Effect," Brit. J. Appl. Phys., vol. 17, pp. 841-850, July 1966.

[94] P. N. Butcher and W. Fawcett, "Stable Domain Propagation in The Gunn Effect," Brit. J. Appl. Phys., vol. 17, pp.1425-1432, Nov. 1966.

[95] M. E. Levinstein and M. S. Shur, " Behavior of The High-Field Domains Below The Voltage of The Nucleation Threshold," Phys. Status Solidi, vol. 28, pp. 827-834, Aug. 1968.

[96] M. S. Levinstein and M. S. Shur,"Physical Investigations of The Gunn Effect (review)," Sov. Phys. Semicond. vol. 9, pp. 411-428, Apr. 1975.

[97] M. S. Levinstein and M. S. Shur, " Transient Processes in Gunn Diodes," Solid-State Electron., vol. 18, pp. 983-990, Nov. 1975.

[98] B. L. Gelmont and M.S. Shur,"Analytical Theory of Stable Domains in High-Doped Gunn Diodes," Electron Lett., vol. 6, pp. 385-387, 11th June 1970.

[99] M. S. Shur and L. F. Eastman, " Current-Voltage Characteristics, Small-Signal Parameters, and Switching Times of GaAs FET's," IEEE Trans. Electron Dev., vol. ED-25, pp. 606-611, July 1978.

[100] M. S. Shur,"Maximum Electric Field in High Field Domain," Electron. Lett., vol. 14, pp. 521-522, 3rd Aug. 1978.

[101] H. H. Berger, " Contact Resistance on Diffused Resistors," IEEE-1969 Int. Solid-State Circuits Conf. (ISSCC) Dig., pp. 160-161, Feb. 1969.

[102] H. Murrmann and D. Widmann,"Current Crowding on Metal Contact to to Planer Devices," IEEE-1969 Int. Solid-State Circuits Conf. (ISSCC) Dig., pp. 162-163, Feb. 1969.

[103] R. A. Pucel, D. J. Masse' and C. P. Hartwig, "Losses in Microstrip," IEEE Trans. Microwave Theory Tech., vol. MTT-16, pp.342-350, June 1968. (Correction: pp. 1064, Dec. 1968.)

[104] K. Lehovec and R. Zuleeg, " Direct-Coupled FET Logic (DCFL)," in GaAs FET Principles and Technology, by J. V. Dilorenzo and D. D. Khandelwal (Editors), Artech House, Inc., Dedham, Mass. 1982.

[105] A. Higashisaka and F. Hasegawa, " Estimation of Fringing Capacitance of Electrodes on S.I. GaAs Substrate,"Electron Lett., vol. 16, pp. 411-412, 22nd May 1980.

[106] C. P. Wen, "Coplanar-Waveguide Directional Couplers," IEEE Trans Microwave Theory Tech., vol. MTT-18, pp. 318-322, June 1970.

[107] T. Hatsuda, "Computation of Coplanar-Type Strip Line Characteristics by Relaxation Method and its Applications to Microwave Circuits," IEEE Trans. Microwave Theory Tech., vol. MTT-23, vol.

MTT-23, pp. 795-802, Oct. 1975.

[108] M. Houdart, "Coplanar Lines : Application to Broadband Microwave Circuits," Proc. 6th Europ. Microwave Conf., pp. 49-53, Rome, Italy, Sept. 1976.

[109] C. Veyres and V. F. Hanna, "Extension of The Application of Conformal Mapping Techniques to The Coplanar Lines With Finite Dimensions," Int. J. Electron., vol. 48, pp. 47-56, July 1980.

[110] V. F. Hanna and D. Thebault, "Theoretical and Experimental Investigation of Asymmetric Coplanar Waveguides," IEEE Trans. Microwave Theory Tech., vol. MTT-32, pp. 1649-1651, Dec. 1984.

[111] R. Garg and I. J. Bahl, " Characteristics of Coupled Microstriplines,"IEEE Trans. Microwave Theory Tech., vol. MTT-27, pp. 700-705, July 1979.

[112] Y. Fukuoka and T. Itoh, "Analysis of Slow-Wave Phenomena in Coplanar Waveguide on a Semiconductor Substrate," Electron. Lett., vol. 18, pp. 589-590, July 1982.

[113] Y. Fukuoka, Y. C. Shih and T. Itoh, " Analysis of Slow-Wave Coplanar Waveguide for Monolithic Integrated Circuits," IEEE Trans. Microwave Theory Tech., vol. MTT-31, pp. 567-573, July 1983.

[114] R.H. Jansen,"High-Speed Computation of Single and Coupled Microstrip Parameters Including Dispersion, High Order Modes, Loss Loss and Finite Strip Thickness," IEEE Trans. Microwave Theory Tech., vol. MTT-26, pp. 75-82, Feb. 1978.

[115] H. A. Wheeler, " Transmission-Line Properties of a Strip on a Dielectric Sheet on a Plane,"IEEE Trans. Microwave Theory Tech., vol. MTT-25, pp. 631-647, Aug. 1977.

[116] T. Kitazawa, Y. Hayashi and M. Suzuki, "A Coplanar Waveguide With Thick Metal-Coating," IEEE Trans. Microwave Theory Tech., vol. MTT-24, pp. 604-608, (Short Papers), Sept. 1976.

[117] K. C. Gupta, R. Garg, and I. J. Bahl, Microstrip Lines and Slot Lines, Artech House, Inc., Dadham, Mass., 1979.

[118] J. I. Smith, "The Even- and Odd-Mode Capacitance Parameters For Coupled Lines in Suspended Substrate," IEEE Trans. Microwave Theory Tech., vol. MTT-19, pp. 424-431, May 1971.

[119] W. Hilberg, "From Approximation to Exact Relation For Characteristic Impedances," IEEE Trans. Microwave Theory Tech., vol. MTT-17, pp. 259-265, May 1969.

[120] I. Kneppo and J. Gotzman, "Basic Parameters of Non-Symmetrical Coplanar Line," IEEE Trans. Microwave Theory Tech., vol. MTT-25,

pp. 718, Aug. 1977.

[121] V. F. Hanna and D. Thebault, "Analysis of Asymmetrical Coplanar Waveguides," Int. J. Electron., vol. 50, pp. 221-224, Mar. 1981.

[122] K. Pearson, Tables of The Complete and Incomplete Elliptic Integrals , Cambridge University Press, Cambridge, England, 1934.

[123] S. Ramo, J. Whinnery and T. Van Duzer,Fields and Waves in Communication Electronics, 2nd Ed., John Wiley & Sons, New York, N.Y., 1984.

[124] R. V. Churchill and J. W. Brown, Complex Variables and Applications, 4th Ed., McGraw-Hill, New York, N.Y., 1984.

[125] M. Abramowitz and I. Stegun, Handbook of Mathematical Functions With Formulas, Graphs, and Mathematical Tables, 10th Printing, National Bureau of Standards, Applied Mathematical Science-55, Washington, D.C., 1974.

[126] F. H. Boudebous, D. Pascal and S. Laval, "A Comparison of Interdigital and Straight Structures for a Photoconductive Detector," IEEE Trans. Electron Dev., vol. ED-32, pp. 836-837, Apr. 1985.

[127] H. R. Kaupp, "Characteristics of Microstrip Transmission Lines," IEEE Trans. Electron. Computers, vol. EC-16, pp. 185-193, April 1967.

[128] A. Schwarzmann, " Microstrip Plus Equations Add up to Fast Design," Electronics, vol. 40, pp. 109-112, Oct. 1967.

[129] R. F. G. Ross and M. J. Howes, "Simple Formulas For Microstrip Lines," Electron. Lett., vol. 12, pp. 410, Aug. 1976.

[130] M. A. R. Gunston and J. Weale, "The Transmission Characteristics of Microstrip," Marconi Rev., vol. 32, pp. 226-244, 3rd quarter, 1969.

[131] W. H. Horton, J.H. Jasberg and J.D. Noe,"Distributed Amplifiers: Practical Considerations and Experimental Results," Proc. IRE, vol. 38, pp. 748-753, July 1950.

[132] D. V. Payne, "Distributed Amplifier Theory," Proc. IRE, vol. 41, pp. 759-762, June 1953.

[133] P. W. Shackle, "An Experimental Study of Distributed Effects in Microwave Bipolar Transistor," IEEE Trans. Electron Dev., vol. 21, pp.32-40, Jan. 1974.

[134] F. Meyer, " Wide-Band Pulse Amplifier," IEEE J. Solid- State Circuits, vol. SC-13, pp.409-411, June 1978.

[135] L. F. Roeshot, " UHF broadband Transistor Amplifiers: Part II," Electrical Design News (EDN), vol. 8 - Part 1, pp. 24-28, FEb. 1963 and Part III, pp. 84-88, Mar. 1963.

[136] F. Schar, "Distributed MOSFET Amplifier Using Microstrip,", Int. J. Electron., vol. 34, pp. 721-730, June 1973.

[137] W. Jutzi, " Uniform Distributed Amplifier Analysis With Fast and Slow Waves," Proc. IEEE (Letters), vol. 56, pp.66-67, Jan. 1968.

[138] G. Kohn and R.W. Landauer,"Distributed Field-Effect Amplifiers," Proc. IEEE (Letters), vol. 56, pp. 1136-1137, June 1968.

[139] E. H. Kopp, " A Coupled Mode Analysis of The Traveling-Wave transistor," Proc. IEEE (Letters), vol. 54, pp. 1571-1572, Nov. 1966.

[140] P. N. Robson, G.S. Kino and B. Fay,"Two-Port Microwave Amplification in Long Samples of Gallium Arsenide," IEEE Trans. Electron Dev. (Corresp.), vol. ED-14, pp. 612-615, Sept. 1967.

[141] Y. Ayasli, J. L. Vorhaus, R.L. Mozzi and L. Reynolds,"Monolithic GaAs Traveling-Wave Amplifier," Electron. Lett., vol. 17, pp. 413-414, 11th June, 1981.

[142] Y. Ayasli, L. D. Reynolds, J. L. Vorhaus and L Hanes,"Monolithic 2-20 GHz Traveling-Wave Amplifier," Electron Lett., vol. 18, pp. 596-598, 8th July, 1982.

[143] Y. Ayasli, R.L. Mozzi, L. Vorhaus, L.D. Reynolds and R.A. Pucel, "A Monolithic GaAs 1-13 GHz Traveling-Wave Amplifier," IEEE Trans. Microwave Theory Tech., vol. MTT-30, pp. 976-981, July 1982.

[144] Y. Ayasli, L.D. Reynolds, J.L. Vorhaus and L.K. Hanes, "2-20 GHz GaAs Traveling-Wave Amplifier," IEEE Trans. Microwave Theory Tech., vol. MTT-32, pp. 71-77, Jan. 1984.

[145] J. A. Archer, F.A. Petz and H.P. Weidlich, "GaAs FET Distributed Amplifier," Electron Lett., vol. 17, p. 443, 25th June, 1981.

[146] B. Kim and H.Q. Tserng,"0.5W 2-21GHz Monolithic GaAs Distributed Amplifier,"Electron Lett., vol. 20, pp.288-289, 29th March 1984.

[147] Y. Ayasli, S. Miller, R. Mozzi and L. Hanes,"Capacitively Coupled Traveling-Wave Power Amplifier," IEEE Trans. Microwave Theory Tech., vol. MTT-32, pp.1704-1709, Dec. 1984.

[148] K. B. Niclas, W. Wilser, T. Kritzer and R. Pereira, "On Theory and Performance of Solid-State Microwave Distributed Amplifiers," IEEE Trans. Microwave Theory Tech., vol. MTT-31, pp. 447-456, June 1983.

[149] J. B. Beyer et al., " MESFET Distributed Amplifier Design Guidelines," IEEE Trans Microwave Theory Tech., vol. MTT-32, pp. 268-275, March 1984.

[150] C. L. Law and C. S. Aitchison, "2-18 GHz Distributed Amplifier in Hybrid Form," Electron Lett., vol. 12, pp. 684-685, 1st Aug. 1985.

[151] Y. Ayasli, "An Overview of Monolithic GaAs MESFET Traveling-Wave Amplifiers," Int. J. Electron., vol. 58, pp.531-541, April 1985.

[152] U. Christ, F. Arndt and S. Mem,"Optimized Traveling- Wave Amplifier With Two Parallel-Gate Transmission Lines," IEE Proc., vol. 132 Part I, pp. 140-142, June 1985.

[153] A. J. Holden and C. H. Oxley, "Computer Modeling of Traveling Wave Transistors," Proc. Int. Conf. Simulation of Semiconductor Devices and Process," Suansea, U.K., pp. 319-329, July 1984.

[154] Yu-an Ren, G. Ruan and H. Hartnagel, " Microwave Structuring For Traveling Wave FET," Arch. Elekt. Üebertrag. (AEÜ), vol. 36, pp. 245-251, June 1982.

[155] A. Higashisaka, Y. Takayama and F. Hasegawa, "A High-Power GaAs MESFET With an Experimentally Optimized Pattern," IEEE Trans. Electron Dev., vol. ED-27, pp. 1025-1029, June 1980.

[156] K. Fricke and H. L. Hartnagel, " Experimental Study of MESFET Traveling-Wave Structures," Int. J. Electron., vol. 58, pp. 629-638, April 1985.

[157] R. H. Dean and R. J. Matarese,"The GaAs Traveling-Wave Amplifier as a New Kind of Microwave Transistor," IEEE Proc., vol. 60, pp. 1486-1502, Dec. 1972.

[158] Yu-an Ren, G. Ruan and H. L. Hartnagel,"Traveling-Wave Power FET With Coplanar Slow-Wave Electrode Systems Modeling and Experimental Results," Arch. Elekt. Üebertrag. (AEÜ), vol. 11/12 , pp. 468-474, Nov./Dec. 1982.

[159] Y. A. Ren and H. L. Hartnagel, " Wave Propagation Studies on MESFET Electrodes," Int. J. Electron., vol. 51, pp.663-668, Nov. 1981.

[160] W. Heinrich and H.L. Hartnagel,"Field-Theoretic Analysis of Wave Propagation on FET Electrodes Including Losses and Small-Signal Amplification," Int.J. Electron., vol.58, pp.613-627, Apr. 1985.

[161] K.-H. Kretschmer, P. Grambow and T. Sigulla, "Coupled-Mode Analysis of Traveling-Wave MESFETs,"Int. J. Elect-ron., vol. 58, pp. pp. 639-648, April 1985.

[162] M. Fukuta, K. Suyama, H. Suzuki and H. Ishikawa, "GaAs Microwave Power FET," IEEE Trans. Electron Dev., vol. ED-23, pp. 388-394, April 1976.

[163] K. Fricke, H. L. Hartnagel and D. C. Tiwari, "High Efficiency Frequency Doubling by GaAs Traveling-Wave MESFET's," IEEE Trans. Electron Dev., vol. ED-34, pp. 742-745, April 1987.

[164] M. S. Gupta, R. W. Laton and T. T. Lee, "Performance and Design of Microwave FET Harmonic Generators," IEEE Trans. Microwave Theory Tech., vol. MTT-29(Short Papers),pp. 261-263, March 1981.

[165] V. K. Tripathi,"On The Analysis of Symmetrical Three-Line Microstrip Circuits,"IEEE Trans. Microwave Theory Tech., vol. MTT-25, pp. 726-729, Sept. 1977.

[166] B. M. Oliver, "Directional Electromagnetic Couplers," Proc. IRE, vol. 42, pp. 1686-1692, Nov. 1954.

[167] R. F. Schwartz, " Bibliography on Directional Couplers," IRE Trans Microwave Theory Tech., vol. MTT-2, pp.58-63 , July 1954.

[168] M. K. Krage and G. I. Haddad, " Characteristics of Coupled Transmission Lines-I: Coupled-Mode Formulation of Inhomogeneous Lines," IEEE Trans Microwave Theory Tech., vol. MTT-18, pp. 217-222, Apr. 1970.

[169] V.K. Tripathi,"Properties and Applications of Asymmetric Coupled Line Structures in an Inhomogeneous Medium," proc. 5th European Microwave Conf. , pp. 278-282, Hamburg, W. Germany 1975.

[170] H. Kogelink and R. V. Schmidt, "Switched Directional With Alternating $\Delta\beta$,"IEEE J. Quantum Electronics, vol. EQ-12, pp.396-401, July 1976.

[171] S. E. Miller, " Coupled Wave Theory and Waveguide Applications," Bell Syst. Tech. J., vol. 33, pp. 661-719, May 1954.

[172] S. S. Bedair and M. I. Sobhy, "Approximation Solution For Propagation Modes on Lossy Multiconductors Transmission Lines in Inhomogeneous Media," Elect. Lett., vol. 16, pp. 914-915, Nov. 1980.

[173] J. C. Isaacs,Jr. and N. A. Strakhov, " Crosstalk in Uniformly Coupled Lossy transmission Lines," Bell Syst. Tech. J., vol. 52, pp. 101-115, June 1973.

[174] V. K. Tripathi and R. J. Bucolo,"Analysis and Modeling of Multilevel Parallel and Crossing Interconnection Lines," IEEE Trans. Electron Dev., vol. ED-34, pp. 650-658, March 1987.

[175] W. H. Louisell, Coupled Mode and Parametric Electronic, John Wiley Co., New York, N.Y., 1960.

[176] B. Wedding and D. Jager, " Phase-Matched Second Harmonic Generation and Parametric Mixing on Nonlinear Transmission Lines," Electr. Lett., vol. 17, pp. 76-77, Jan. 1981.

[177] D. Jager, W. Rabus and W. Eickhoff, "Bias-Dependent Small-Signal parameters of Schottky Contact microstrip Lines," Solid-State Electron, vol. 17, pp. 777-783, Aug. 1974.

[178] D. Jager and W. Rabus, " Bias-Dependent Phase Delay of Schottky Contact Microstrip Line," Eelect. Lett., vol. 9, pp.201-203, May 1973.

[179] D. Jager, "Slow-Wave Propagation Along Variable Schottky Contact Microstrip Line," IEEE Trans. Microwave Theory Tech., vol. MTT-24, pp. 566-573, Sept. 1976.

[180] D. Jager, "Distributed Variable Capacitance Microstrip Line For Microwave Applications," Appl. Phys., vol. 12, pp. 203-207, Dec. 1977.

[181] A. Scott, Active and Nonlinear Wave Propagation in Electronics, Wiley-Interscience (John Wiley & Sons Co.), New York, N.Y. 1970.

[182] N. Kryloff and N. Bogoliuboff, Introduction to Nonlinear Mechanics, Princeton University Press, Princeton, New Jersey, 1947.

[183] H. Lee and V. K. Tripathi, "New Perspectives on The Green's Function For Quasi-TEM Planar Structures," IEEE MTT-S, Int. Microwave Symp. Dig., pp.571-573,(Boston, Mass.),May 31- June 3,1983.

[184] H. Lee and V. K. Tripathi, "Generalized Spectral Domain Analysis of Planar Structures Having Semi-infinite Ground Planes," IEEE MTT-S, Int. Microwave Symp. Dig., pp. 327-329, (San Francisco, CA), May 30- June 1, 1984.

[185] H. Lee, Computational Methods For The Quasi-TEM Characteristics of Fundamental MIC planar Structures, Ph.D. Thesis, Dept. of Electrical and Computer Engineering, Oregon State University, Corvallis, Feb. 22, 1983.

[186] A. R. Von Hippel,Dielectrics and Waves, John Wiley & Sons, Inc., New York, N. Y., 1954.

[187] I. P. Kaminow, An Introduction to Electrooptic Devices, Academic Press, New York, N.Y., 1974.